République Algérienne Démocratique et Populaire
Ministère de l'Enseignement Supérieur et de la Recherche Scientifique

Université Ferhat Abbas–Setif

THESE

Présenté à la Faculté des Sciences
Département de Physique

Pour l'obtention du diplôme de

DOCTORAT EN SCIENCES

Spécialité : Physique énergétique

Par

Azzouzi Ghania

THEME

STUDY OF SILICON SOLAR CELLS PERFORMANCES USING THE IMPURITY PHOTOVOLTAIC EFFECT

Soutenue Publiquement le 03/03 /2012
Devant la commission d'examen :

Président : Mr A. Layadi Professeur (Université Ferhat Abbas– Sétif)
Rapporteur: Mr M. Chegaar Professeur (Université Ferhat Abbas– Sétif)
Examinateur:M^{me} C. Azizi Professeur (Université Oum labouaghi)
Examinateur:Mr A. Bouabellou Professeur (Université Constantine)

Acknowledgements

It has been a long journey finishing this thesis and it would have been much harder without the aid of many excellent people.

First, I thank Pr Mohamed Chegaar for being my thesis supervisor all these years.

This thesis would not have been possible without the generous assistance of Pr Abdelhamid Layadi who has been a tireless source of encouragement, support and wisdom over these last years.

My gratitude also goes to the members of the jury who accepted to examine and evaluate my work. I thank heartily Mr A. Layadi Pr at Ferhat Abbas University who accepted to preside the jury. I thank greatly Mr A. Bouabellou, Pr at Mantouri (Constantine) university and many thank to M^{eme} C. Azizi Pr at Larbi ben Mhidi (Oum Labouaghi) University who honoured me by their acceptation to examine my thesis.

I must thank Mr Marc Burgelman from University of Gent (Belgium) for offering me the opportunity to use the Scaps Simulator and for email responses clarifying and explaining about details of IPV effect and SCAPS.

My thanks also go to Pr. Pierre Mialhe from Via Domitia University (Perpignan – France) for his kindness and patience given to me throughout the duration of my training period in France.

Finally, I thank my parents, my brothers , my sisters and my friends for their endless love and support that have made the hard times so much easier.

Table of contents

General Introduction

The very important goal nowadays is to find a new renewable form of energy. The renewable sources of energy derived from the sun are one of the promising options. Extensive studies on the photovoltaic cell as one of a renewable energy sources have been carried out in order to obtain cheap PV cells that are more efficient and safe.

The most important loss mechanisms in single band gap cells are the incapability to absorb photons with energy less than the band gap and thermalization of photon energy exceeding the band gap. The third generation solar cells have attracted wide attention in these last years, the concepts of this generation are still under fundamental investigation and are based on tackling one or both of the previous loss mechanisms in order to increase cell conversion efficiency. The impurity photovoltaic effect (IPV) is one of these concepts. It can, improve the conversion efficiency of a conventional single junction solar cell by the incorporation of optically active impurities into the device. These impurities permit electrons to be excited from the valence band to the conduction band via the defect level through the absorption of sub-band-gap photons.

The work presented in this thesis is focused on attempts to develop the efficiency of the silicon solar cell above the Shockley-Queisser efficiency limit through the *IPV* effect. We investigate numerically the potential of the *IPV* effect in silicon solar cell doped with sulphur as novel *IPV* impurity. The influences of light trapping and certain impurity parameters like impurity concentration and position in the gap on the silicon solar cell performances (Short circuit current density *Jsc*, open circuit voltage *Voc*, conversion efficiency η and quantum efficiency *QE*) were studied.

In chapter I, the essential principles of a solar cell, the main concepts and materials used for making solar cells, the efficiency loss mechanisms in *PV* cells and how to reduce or overcome these losses will be explicated. In the present day there are many attempts to invent and develop new concepts aimed to obtain high efficiency over the present limit. Chapter II will describe in detail many classes of these concepts and will further explain in more detail the impurity photovoltaic effect which is the purpose of our study. Chapter III comprises two parts: in the first part, a detailed description will be given of the Solar Cell Capacitance Simulator in one Dimension (SCAPS-1D) that is used in this work. In part two, the most significant results and discussion of the study will be presented.

Chapter One

Principles of Solar Cells

I.1 Introduction

This chapter lays out the theoretical foundations on which the analyses in this thesis are based. First, some notions about the sun as source of energy will be presented. Than, we will present the basic principles of a solar cell, the principal materials used in this field, the efficiency losses mechanisms in solar cells and the methods used to reduce these losses will be also analysed.

I.2 Solar Spectrum

The study of solar cells (progress, optimization and characterization….etc.) need some information about the source of energy used; the sun. This star is the biggest member of the solar system. The sun is a big sphere of plasma composed of *H* and *He* and some small amounts of other elements, it has an effective black-body temperature T_S of *5777 K*. The diameter of the sun is around 1.39×10^9 m and the distance between it and the earth is about 1.5×10^{11} m. The solar radiation is partially absorbed and scattered by its passage through the atmosphere. The absorption of the *X*–rays and extreme ultraviolet radiations of the sun is principally caused by nitrogen and oxygen while the absorption of the ultraviolet ($\lambda<0.40\ \mu m$) and infrared radiations ($\lambda>2.3\ \mu m$) is mainly caused by the ozone and water vapors. The atmosphere of the earth absorbs the ultraviolet (*UV*) and far infrared radiation and allows only short wavelength radiation (i.e. between *0.29* μm and *2.3* μm). It does not permit radiation having wavelength $\lambda>2.3\ \mu m$, (i.e. long wavelength radiation) [1]. Figure **(I-1)** shows the solar spectrum as a function of photon energy. The terms *AM0* and *AM1.5* used in this figure are the designations of a particular radiation conditions. The concept 'Air Mass *(AM)*' represents the amount of atmosphere through which the solar radiation has travelled and is correlated to the amount of absorption.

$$AM = 1/\cos(\theta) \qquad \textbf{(I–1)}$$

The θ represents the angle of the sun to the vertical. Outside the atmosphere the spectrum is *AM0* and that on the surface of the earth for normal incidence is *AM1*. The spectrum *AM1.5* corresponds to an angle of incidence of solar radiation of *48°* relative to the surface normal.

This energy spectrum is regarded as the standard spectrum for measuring the efficiency of *PV* cells used for terrestrial applications.

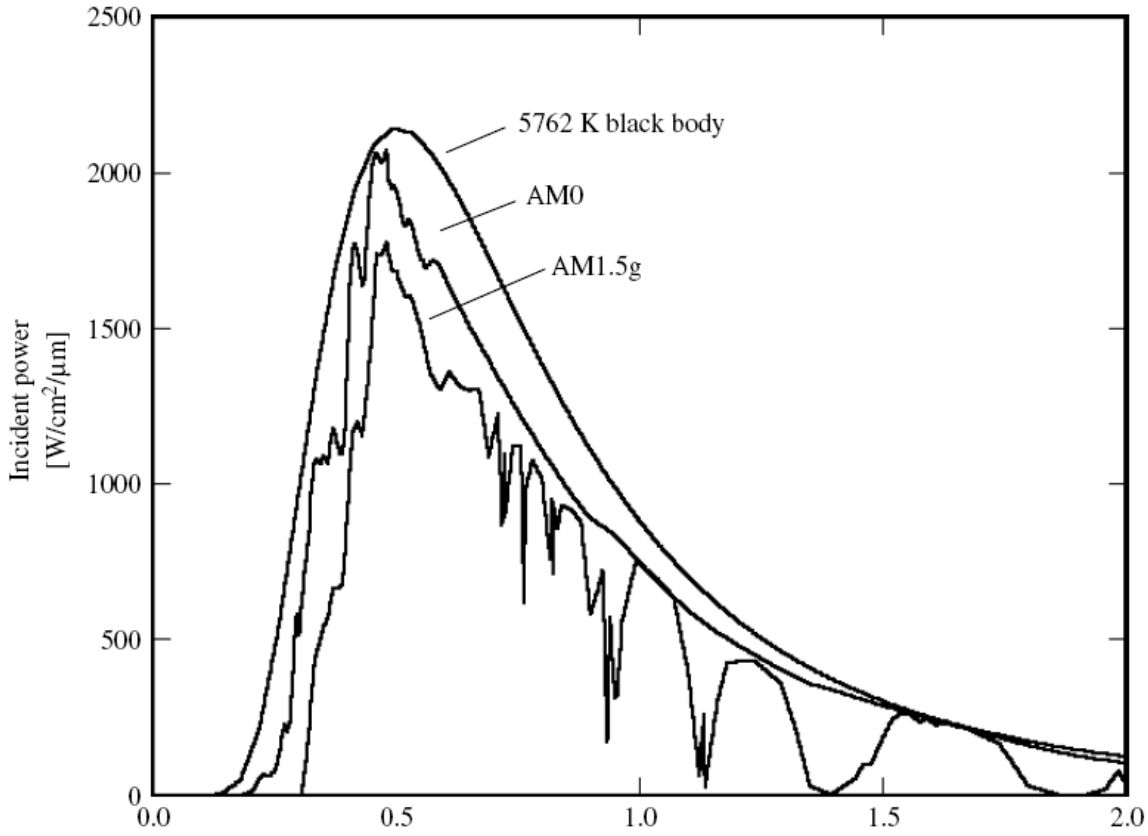

Figure I-1: Solar spectrum for different Air Mass and blackbody radiation corresponding to the sun.

I.3 Basic Principles of a Solar Cell

The photovoltaic effect was first observed by Henri Becquerel [2] in 1839**.** This phenomenon is the basic physical process in which a solar cell converts solar energy to electricity. In a global sense, the device intended to capture solar and non solar radiation is usually known as solar cell. Verily, this device require to realise two steps: the first, is the photogeneration of charge carriers (electrons and holes) and secondly the separation of these carriers to a conductive contact that will transmit the electricity. Currently, the majority of solar cells in use are silicon semi-conductor junction devices. Therefore, in order to study the photovoltaic cells we must have an understanding of the basics of the semi-conductor materials and particularly the *PN* junction, although, *PN* junctions and semiconductors are not

the only principles and materials to understand photovoltaic cell. Many materials, mechanisms and new concepts have been studied in the last years (see chapter 2)**.**

To recognize the function of semiconductor devices and therefore, of solar cells, it necessary to understand deeply, the processes within a p-n junction is important. The semiconductor junction is generally the base unit of many PV cells, in which two different dopants directly adjoin one another. This is called a p-n junction if a p-doped layer merges into an n-doped layer within the same lattice. In a simple example, we assume that – in silicon – both dopants are of the same magnitude and merge together abruptly. Figure **I-2** may clarify this behaviour. The left-hand side $x < 0$ would, for example, be doped with boron atoms with a concentration of $N_A = 10^{16}$ atoms per cm^{-3}, making it p-conductive. The right-hand side $x > 0$, on the other hand, could be doped with phosphorus atoms, at $N_D = 10^{16}\ cm^{-3}$, making it n-conductive. The freely moving charge carriers will not follow the abrupt change in concentration from N_A to N_D. Rather, the carriers will diffuse due to the difference in concentration, i.e., the holes from the p region will move into the n region, and the electrons from the n area will move into the p region. Diffusion currents will arise. The ionized acceptors and donors, which are no longer electrically compensated, remain behind as fixed space charges (Figure **I-2**). Negative space charges will arise on the left-hand side in the p region, and positive space charges arise on the right-hand side in the n region. Correspondingly – as occurs in a plate capacitor – an electric field is created at the p-n junction, which is directed so that it drives the diffusing charge carriers in the opposite direction to the diffusion. This process continues until equilibrium is created or, in other words, until the diffusion flow is compensated by a field current of equal magnitude. An (extremely large) internal electric field exists – even if both sides of the semiconductor are grounded. When the p-n junction is illuminated, charge carrier pairs will be generated wherever light is absorbed. The strong field at the junction pulls minority carriers across the junction and a current flow results. The semiconductor device is not in thermal equilibrium, which means that electric power can be delivered to a load. This is the basic mechanism of a solar cell**[3]**. A typical such solar cell according to Figure **I-3** consists of a *p-n* junction, which has a diode characteristic. This characteristic can be derived from standard solid state physics. It is:

$$I = I_0\left(e^{\frac{V_A}{V_T}} - 1\right) \qquad \textbf{(I-2)}$$

The I is the current through the diode at applied voltage V_A. V_T is a constant, the so-called thermal voltage. I_0 is the diode saturation current, which depends on the type, doping density,

and quality of the semiconductor material and the quality of the p-n junction. If this junction is illuminated, a supplementary current, the light-generated current I_{ph} is added: than the equation I-2 becomes

$$I = I_0\left(e^{\frac{V_A}{V_T}} - 1\right) - I_{ph}$$

Or $$I = I_{ph} - I_0\left(e^{\frac{qV}{k_B T}} - 1\right) \qquad \textbf{(I-3)}$$

The k_B is the Boltzmann constant, T is the absolute temperature, q (>0) is the electron charge, and V is the voltage at the terminals of the cell. I_0 is well known to electronic device engineers as the diode saturation current serving as a reminder that a solar cell in the dark is simply a semiconductor current rectifier, or diode. The photogenerated current I_{ph} is closely related to the photon flux incident on the cell and its dependence on the wavelength of light is frequently discussed in terms of the quantum efficiency or spectral response. The photogenerated current is usually independent of the applied voltage with possible exceptions in the case of a-Si and some other thin film materials **[4-6].**

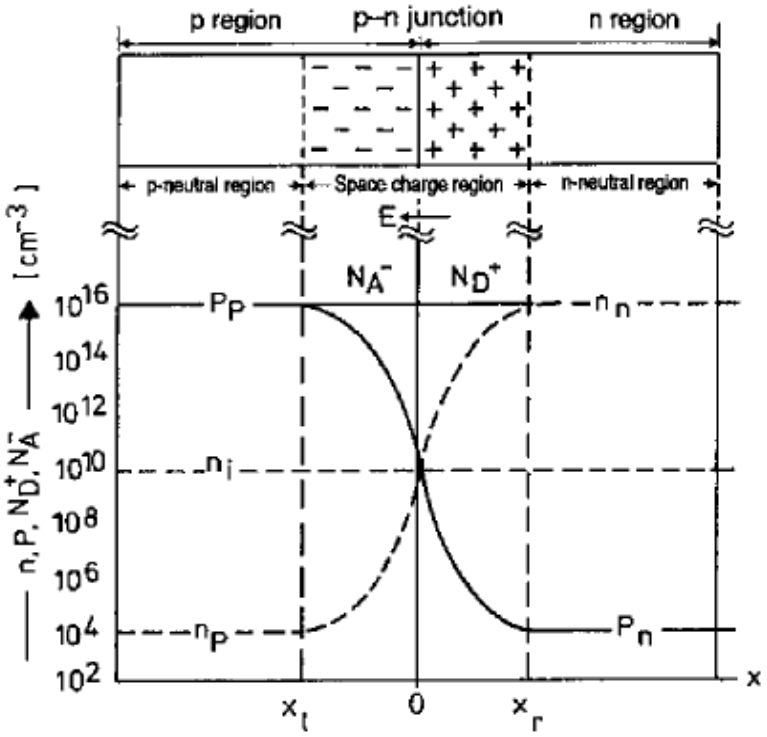

Figure I-2: Doping and concentration distribution of a symmetrical *p-n* junction in thermal equilibrium.

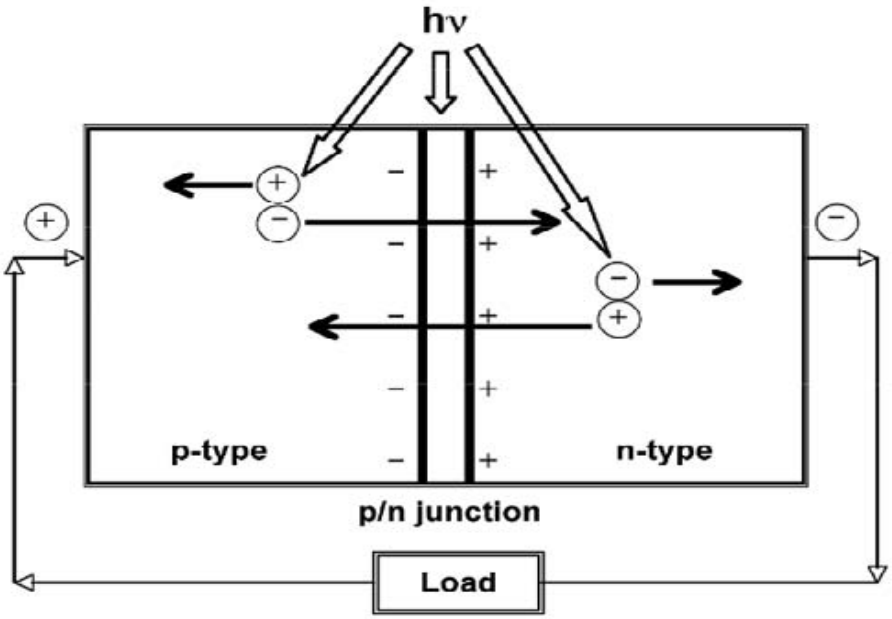

Figure (I-3) Operation mechanism of single-crystal silicon *p-n* junction solar cell.

The negative sign in equation **(I-3)** results from polarity conventions. Now the current *I* is no longer zero at zero voltage but is shifted to I_{ph}. Power can be delivered to an electric load. The *I-V* characteristic with and without illumination is shown in Figure **I-4**.

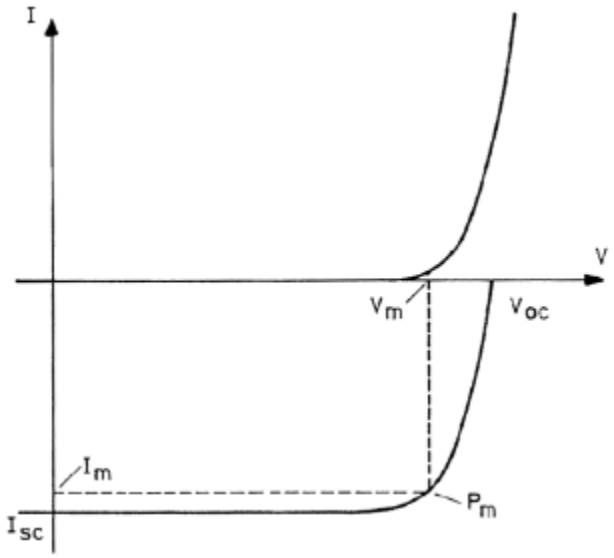

Figure (I-4) I–V characteristic of a solar cell with and without illumination.

I.4 Solar Cell Characteristics

*PV*cells are usually characterised with four performances: short circuit current I_{sc}, open circuit voltage V_{oc}, fill factor *FF*, and conversion efficiency η. These parameters can be represented using Figure **(I-5)**. The curve drawn in figure **(I-5)** is same as illuminated curve shown in figure **(I-4)**, but negative current axis is shown as positive, this signification is done for the sake of convenience.

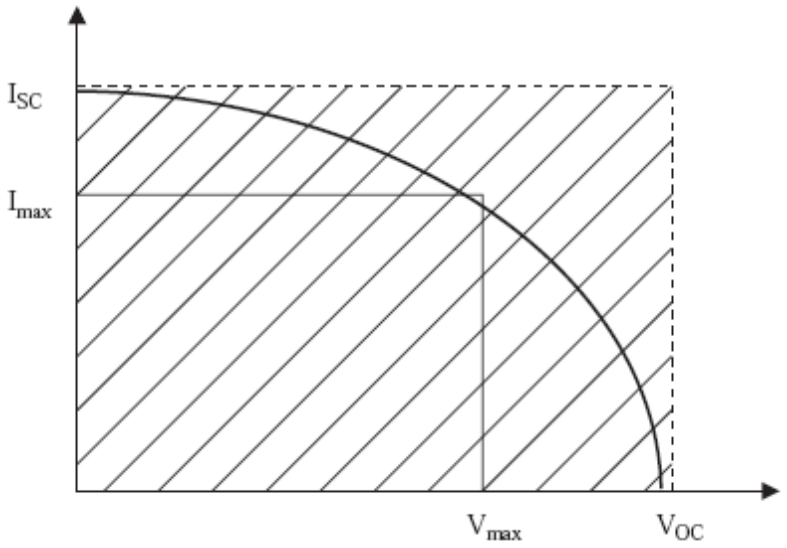

Figure I-5 Typical plot of a solar cell's I-V curve and its parameters.

I.4.1 Short Circuit Current Isc

The short-circuit current is the current through the solar cell when the voltage across the solar cell is zero (i.e., *V=0*). When we put V=0 in equation *I-3* we obtain the short circuit current as *Jsc =-Iph*. The I_{sc} is usually represented in terms of current density and current per unit area in terms of mA/cm^2.

I.4.2 Open Circuit Voltage

The open circuit voltage is the maximum possible voltage generated across the terminals of a solar cell when they are kept open, i.e., *I=0* **(**Figure **I-5).**

I.4.3 Fill Factor FF

The fill factor is defined as the ratio of maximum power $P_m = V_m.I_m$ that can be extracted from a solar cell to the ideal power $P_0 = V_{oc}.I_{sc}$. So,

$$FF = \frac{V_m.I_m}{V_{oc}.I_{sc}} \qquad \textbf{(I-4)}$$

The FF is a key parameter in evaluating the performance of solar cells. It is represented in terms of percentage.

I.4.4 Efficiency

The conversion efficiency is the most important property of a solar cell. It is defined as the ratio between the generated maximum power, P_m, generated by a solar cell and the incident power, P_{in}.

$$\eta = \frac{P_m}{P_{in}} = \frac{I_m V_m}{P_{in}} = \frac{FF.I_{sc}.V_{oc}}{P_{in}} \qquad \textbf{(I-5)}$$

I.5 Losses in Solar Cells

The conversion efficiency of a real solar cell is generally lower than that of an ideal solar cell due to the various loss factors, some of these are avoidable but others are intrinsic to the system. Schematic presentation of the important loss mechanisms in solar cells is presented in Figure **I-6** and these factors are:

I.5.1 Loss of Low Energy Photons:

In the solar cell a significant part of the solar spectrum is not utilised because of the incapability of the material to absorb the photons which have energy less than the band gap energy. Therefore, these photons do not contribute to the generation of electron hole pairs. This is referred to as “transmission loss”, and is almost equal to 23% for a single junction solar cell.

I.5.2 Thermalization Loss (loss due to excess energy of photons)

A photon which have energy equal to that of the band gap energy is needed to excite an electron from valance band to conduction band. If the energy of the absorbed photons E is

larger than the band gap energy *Eg*, the excess energy *E-Eg* is dissipated into lattice vibrations within a picoseconds. This loss is referred to as thermalization loss. For a single junction solar cell, this loss is equal to about 33%.

I.5.3 Voltage loss

The voltage factor is the ratio of the maximum voltage V_{oc} developed by the cell to the band gap voltage *Eg/q*. This loss happens due to the unavoidable intrinsic Auger recombination. The ration *Voc/ (Eg/q)* lies in the range of 0.65 to 0.72 for a thick silicon solar cell.

I.5.4 Fill Factor Loss

The fill factor *FF* describes the squareness of the *IV* curve. If the *FF* is equal to one, the *(I-V)* curve of an ideal solar cell is square. In reality, the cell *I-V* curve is given by the exponential behaviour. This form of loss appears from the parasitic resistances (series and shunt resistance) of the cell.

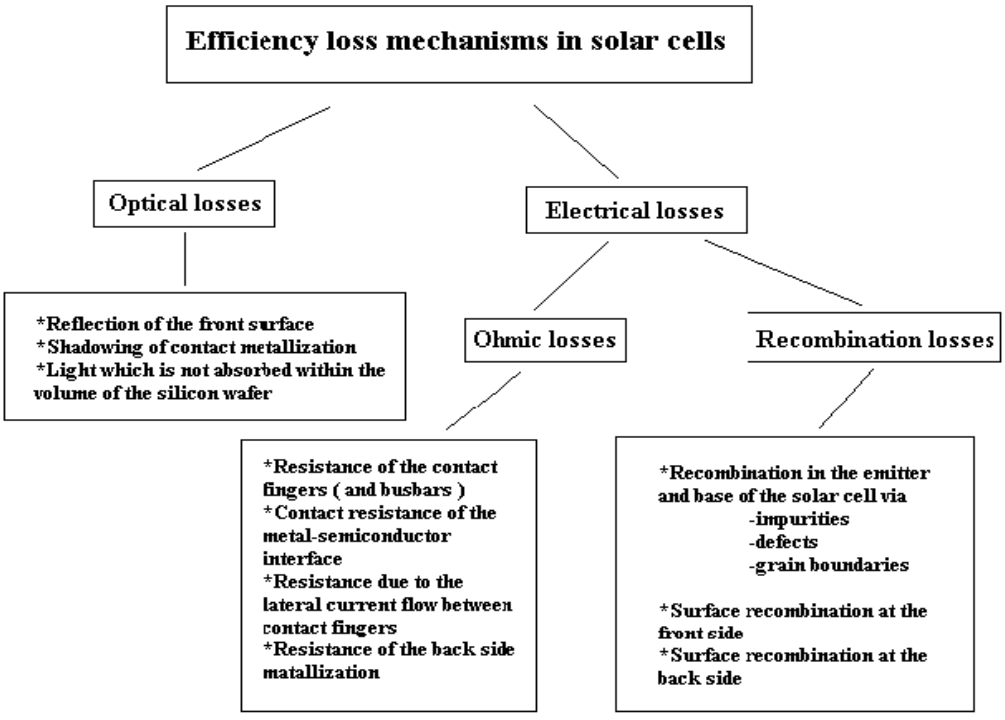

Figure I-6 Efficiency loss mechanisms in solar cells

I.5.5 Reflection losses:

The reflection loss occurs from the top surface of the *PV* cells. A part of incident photons are reflected from this surface and not absorbed.

I.5.6 Loss by Incomplete Absorption due to the Finite Thickness

Incomplete absorption in the absorber due to its limited thickness is an additional loss that reduces the efficiency of the energy conversion. It refers to the loss of photons which has enough energy to be absorbed in the cell, but can not absorbed in the cell by reason of limited solar cell thickness. The incomplete absorption is becoming important in the current when the wafer becomes thinner in order to save the active material for cost reduction purpose. Light trapping methods are generally used to reduce this loss.

I.5.7 Loss Due to Metal Coverage

The front contact of the solar cell is made by the form of finger, and busbar. This metal contact shadows some light. This loss is equal to about 10%.

I.5.8 Recombination losses

Not all the generated (electron – hole) pairs contribute to solar cell current and voltage due to recombination. The carriers recombine in the bulk, at the interfaces, and/or at the surfaces of the junction. Many techniques are used to minimize several recombination problems including passivation techniques.

The optical and electrical losses mentioned above should be minimized in order to get high solar cell characteristics. Many methods and techniques can be used for reducing efficiency losses. In the last two sections, these methods will be described in detail.

I.6 Model of a Solar Cell

I.6.1 Ideal Solar Cell

An ideal solar cell can be considered as current source connected in parallel with a rectifying diode, as shown in the equivalent circuit of Figure **I-7**. The *I-V* characteristic is described by the Shockley solar cell equation (equation (I-3)):

$$I = I_{ph} - I_0\left(e^{\frac{qV}{k_B T}} - 1\right)$$

The term I_0 represents the the diode saturation current. k_B represents the Boltzmann constant, T is the absolute temperature, q : is the electron charge, and V is the voltage at the terminals of the cell and I_{ph} is the photogenertated current.

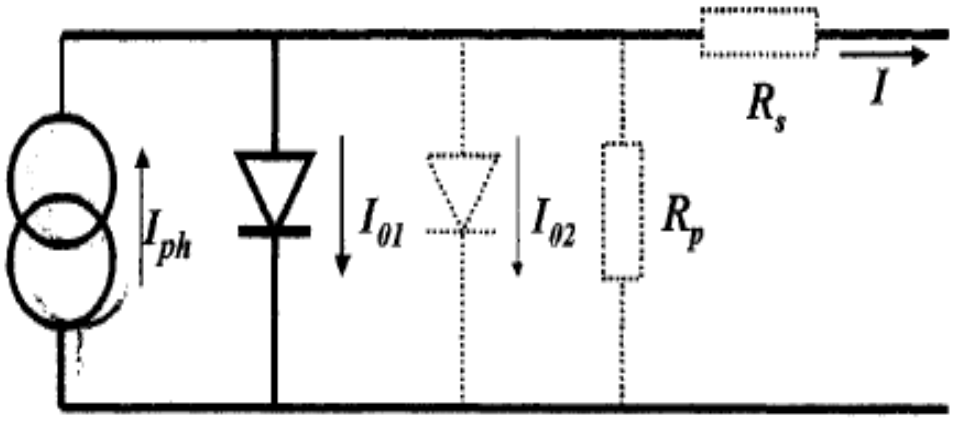

Figure I-7: The equivalent circuit of an ideal solar cell (full lines). Non-ideal components are shown by the dotted line.

Figure **I-8(a)** shows the *I-V* characteristic (Equation **(I-3)**). For the ideal solar cell, the short circuit current I_{sc} is equal to the photogenerated current I_{ph},

Open circuit voltage is obtained by setting I=0 in the expression for overall current i.e. *I=0* when $V=V_{oc}$. Therefore, the open circuit voltage V_{oc} is given by equation

$$V_{oc} = \frac{K_B T}{q}\ln\left(1 + \frac{I_{ph}}{I_0}\right) \qquad \textbf{(I-6)}$$

The power P = *I V* produced by the cell is shown in Figure **I-8 (b).** The cell generates the maximum power P_{max} at a voltage V_m and current I_m, and it is convenient to define the fill factor FF by

$$FF = \frac{I_m V_m}{I_{sc} V_{oc}} = \frac{P_{\max}}{I_{sc} V_{oc}} \qquad \textbf{(I-7)}$$

The fill factor *FF* of a solar cell with the ideal characteristic will be furnished by the subscript *0*(i.e. $FF=FF_0$ in the absence of any parasitic resistance) as given by the approximate expression [7]

$$FF_0 = \frac{v_{oc} - \ln(v_{oc} + 0.72)}{v_{oc} + 1} \qquad \textbf{(I-8)}$$

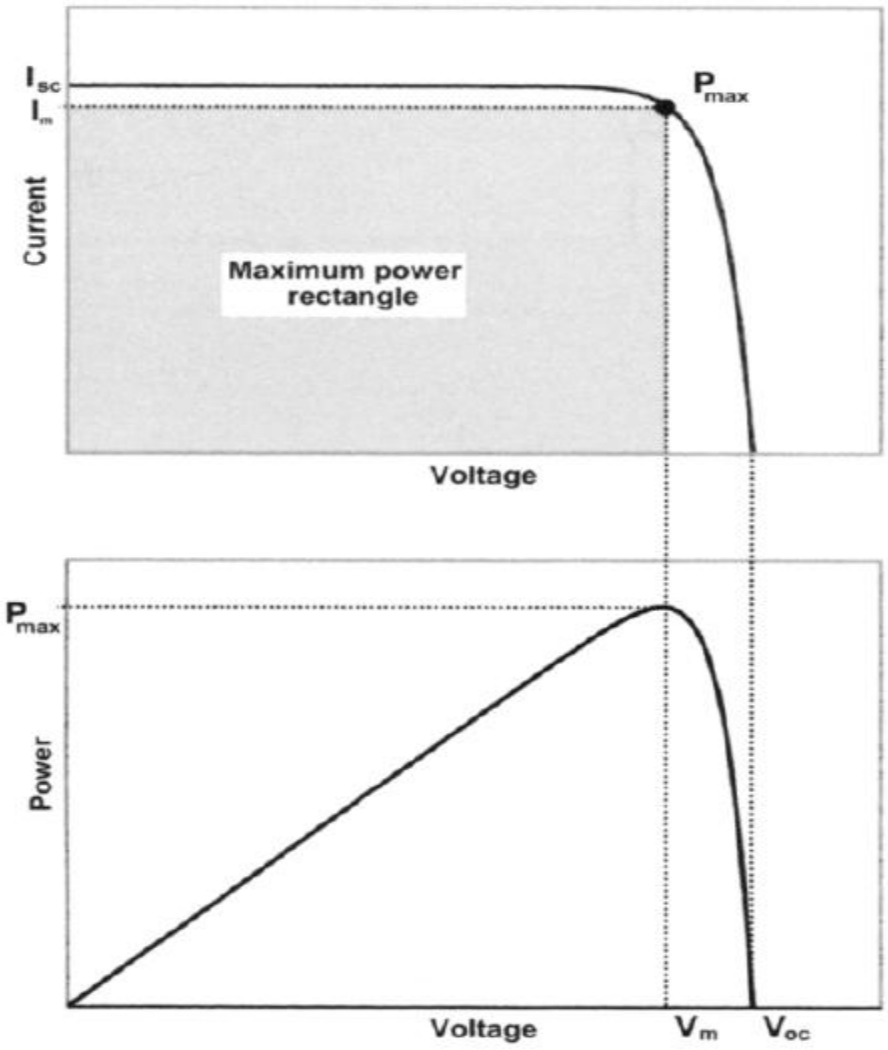

a

b

Figure I-8. The I-V characteristic of an ideal solar cell **(a)** and the power produced by the cell **(b).** The power generated at the maximum power point is equal to the shaded rectangle in **(a).**

I.6.2 Real Solar Cell

The behaviour of a real solar cell is deviated from the ideal due to electrical and optical losses. The *I-V* equation of equivalent circuit **(**Figure **I-7)** of real solar cell can be written in the form of the following equation.

$$I = I_{ph} - I_{01}\left\{\exp\left(\frac{V + IRs}{K_B T}\right) - 1\right\} - I_{02}\left\{\exp\left(\frac{V + RsI}{2K_B T} - 1\right) - 1\right\} - \frac{V + IRs}{Rp} \qquad \textbf{(I-9)}$$

The form of this equation is called "two-diode model". The term I_{01} and I_{02} represent the saturation current densities. The first term represents the recombination in the base and emitter of the cell. While I_{02} represents the recombination in the space charge region of the cell. The real solar cell (or circuit) may also contain series (*Rs*) and parallel (or shunt, R_p *or* (R_{sh})) resistances. The series resistance arises from the bulk resistance of the silicon wafer, the resistance of the metallic contacts of the front- and back surface and further circuit resistances from connections and terminals. The parallel resistance is principally caused by leakage currents by reason of *p-n* junction non-idealities and impurities near the junction, which cause partial shorting of the junction, particularly near the cell edges. These parameters are shown in the equivalent circuit of Figure **(I-7)** by the dotted lines.

Influence of Shunt and Series Resistances on Solar cell Efficiency

The effect of the series and parallel resistances, on the *I-V* characteristic of the solar cell is shown in Figures **I-9** (a and b). The series and shunt resistances affect mainly the fill factor and therefore affect the efficiency of the solar cell. The influence of these parameters on the fill factor can be written as

$$FF = FF_0\left(1 - r_s\right) \qquad \textbf{(I-10)}$$

Where, $r_s = Rs.\frac{I_{sc}}{V_{oc}}$.

And $$FF = FF_0\left(1 - \frac{1}{r_{sh}}\right) \qquad \textbf{(I-11)}$$

Where, $r_{sh} = R_{sh} \cdot \frac{I_{sc}}{V_{oc}}$

The fill factor indicates how well a junction was made in the cell and how low the series resistance was. Preferably the value of R_{sh} must be very large, in range of hundred *Ohms*. Only larger series resistances reduce the short-circuit current but very small shunt resistances reduce the open-circuit voltage. However, their effect reduces mainly the value of the Fill factor. Therefore, the maximum power output is decreased.

It must also be taken into consideration, other parameters such as radiation intensity and temperature which also affect the efficiency of a solar cell.

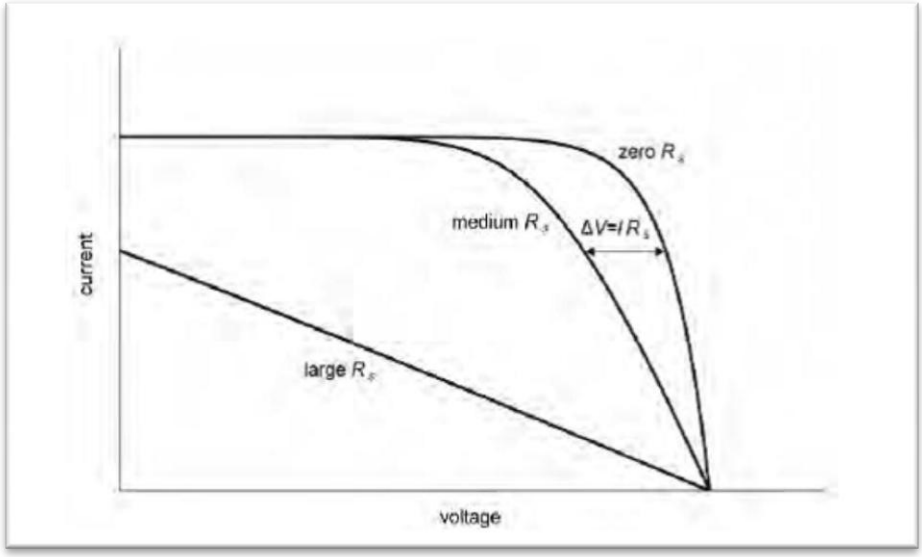

a

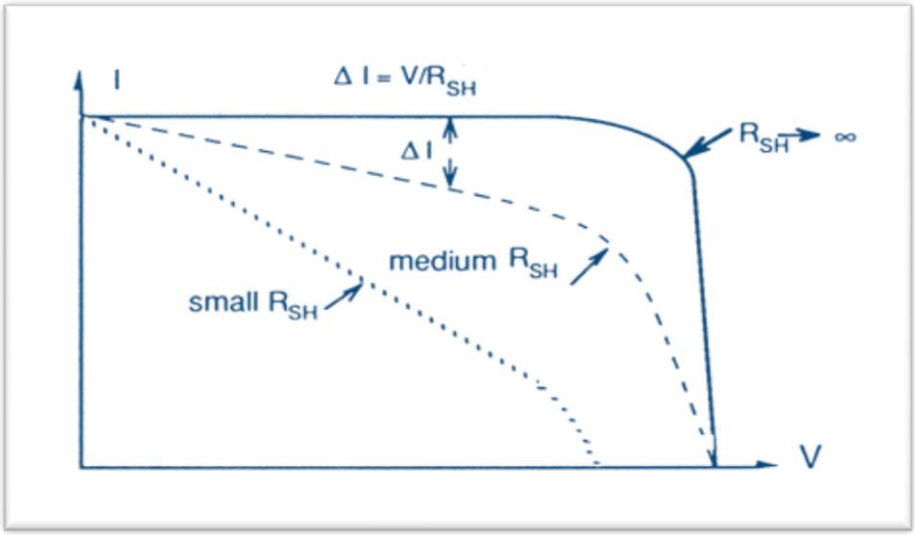

b

Figure I-9 The effect of series (**a**) and parallel ***(b)*** resistance on the *I-V* characteristic of the solar cell.

Temperature and Insolation Effects

For practical uses, solar cells do not operate under standard conditions (*1000w/m*^{2}, *AM1.5*global spectrum, *25°C*). Two important effects that must be taken into account are due to the variable temperature and insolation level.

The *I-V* characteristic of the solar cell, presented in Figure **I-8(a)**, is only for a certain irradiance, *Gt*, and cell temperature T. The *I-V* curve in figure *I-10*, is plotted to demonstrate the influence of these two parameters on the cell characteristic. As shown in Figure **I-10(a)**, the open circuit voltage increases logarithmically by increasing the solar radiation, while the short circuit current increases linearly. The influence of cell temperature on the cell characteristics is shown in the Figure **I-10(b).** The most significant effect of the increase in cell temperature is on open circuit voltage, which decreases with increasing temperature; thus the cell efficiency decreases. The temperature variation of the current is less marked.

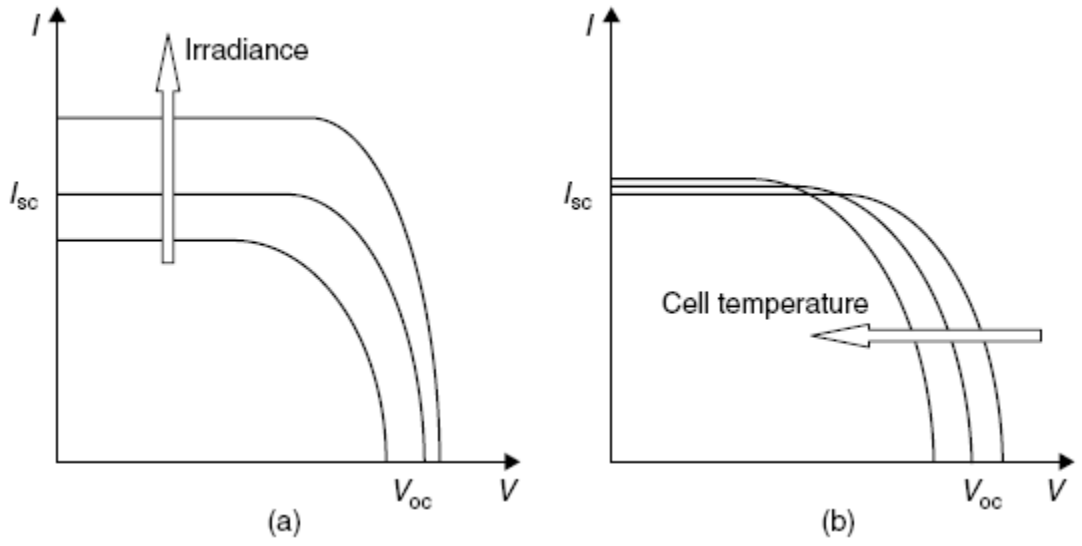

Figure I-10 influence of irradiation and cell temperature on PV cell characteristics **(a)** Effect of increased irradiation. (**b)** Effect of increased cell temperature.

I.7 Quantum Efficiency and Spectral Response

The quantum efficiency of a solar cell is defined as the ratio of the number of carriers collected by the *PV* cell to the number of photons of a given energy incident on the solar cell. One can define external and internal quantum efficiencies (designated by *EQE(λ)* and *IQE(λ),* respectively). They are different in the treatment of photons reflected from the cell: For the value of EQE all photons impinging on the cell surface are taken into account, however, for the value of IQE just photons that are not reflected are considered. The QE is given as a function of either wavelength or energy. If the internal quantum efficiency is identified, the total photogenerated current is given by

$$I_{ph} = q\int_{(\lambda)} \phi(\lambda)\{1 - R(\lambda)\}IQE(\lambda)d\lambda \qquad \textbf{(I-12)}$$

The *Φ(λ)* represents the photon flux incident on the cell at wavelength *λ*, *R(λ)* is the reflection coefficient from the top surface**.** In an ideal case, Quantum efficiency has a square shape, in which the QE value is fairly constant across the entire spectrum of wavelengths measured. In general, the QE of solar cells is reduced due to some factors like the effect of recombination, in which charge carriers are not capable of move into an external circuit. The same mechanisms that affect the collection probability also affect the QE. For example, modifying the front surface of a PV cell can affect carriers generated near the surface. A quantum efficiency curve for silicon solar cell is shown in Figure **I-11 [8].**

The spectral response *SR(λ)* of a solar cell permits an examination of how photons of different wavelengths contribute to the short circuit current. The SR *(λ)* is defined as the ratio of the photocurrent generated by a solar cell under monochromatic illumination of a given wavelength, to the value of the spectral irradiance at the same wavelength. The *SR (λ)* is given by [**9]:**

$$SR(\lambda) = \frac{q\lambda}{hc}QE(\lambda) = 0.808.\lambda.QE(\lambda) \qquad \textbf{(I-13)}$$

Spectral response in equation (**I-13**) can be either internal or external, depending on which value is used for the quantum efficiency.

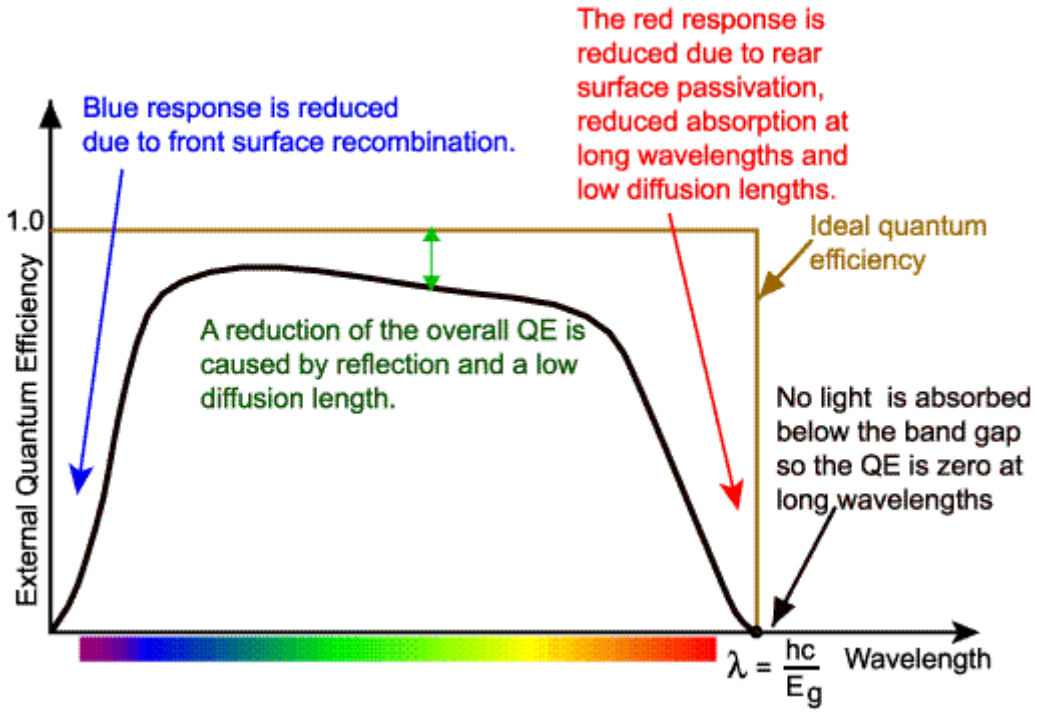

Figure I-11 The quantum efficiency of a silicon solar cell.

I.8 Solar Cell Materials and Different Generations

I.8.1 Technology Generation

According to M. A. Green's classification there are three major classes of solar cells (first, second and third generation). His classification is based on the nature of the material, the maximum efficiency reachable, and the cost of each type. There are a lot of researches into all these types but the first-generation technologies are dominant in the commercial production, accounting for 89.6% of 2007 production **[10]**.

I.8.1.1 First Generation

First-generation cells consist of large-area, high-quality and single junction devices. These cells are usually made using a silicon wafer. The highest conversion efficiencies

obtained up to now are in first generation *PV* cells. Single junction silicon devices are approaching the theoretical limiting efficiency of 33, 2%.

I.8.1.2 Second Generation

This generation is considerably cheaper to produce than first generation cells; low cost is associated with the use of such though they have lower efficiencies. The most successful second-generation materials are cadmium telluride (CdTe), copper indium gallium selenide, amorphous silicon and micromorphous silicon. These technologies do hold promise of higher efficiencies and offer cheaper production costs.

I.8.1.3 Third Generation

Principally, Third-generation technologies aim to improve poor electrical performance of second-generation thin-film technologies and keep the low production costs. Recent research has marked conversion efficiencies of *30–60%* while retaining low cost materials and manufacturing techniques **[11].** In order to achieve these high efficiencies, many concepts have studied in this last years such as intermediate solar cell, tandem solar cell, up and down conversion, impurity photovoltaic effect….etc (each of these approaches will be described in detail in chapter 2).

I.8.2 Photovoltaic Materials

The previous generations of technologies are made of various materials and with different structures in order to diminish the cost and reach maximum efficiency. Many types of solar cell material can be distinguished; single crystal, polycrystalline and amorphous silicon, compound thin-film materials and other semi-conductor absorbing layers.

The most popular type of Photovoltaic cells is made of crystalline silicon, while this type is expensive. The amorphous silicon thin-film solar cells are less expensive. The efficiency of an a-Si module is about 6–8% **[12].** A variety of compound semi-conductors can furthermore be used to fabricate thin-film solar cells. These compound materials are $CuInSe_2$, CdS, CdTe, Cu_2S and InP. In this part it will be explained in some detail these materials.

I.8.2.1 Silicon

After oxygen, the silicon is the most abundant element in the earth's crust; it constitutes about 26% of this crust. It is never occurs free in nature, but in combination with oxygen forming oxides and silicates. In addition to the previous properties, silicon is a non toxic and stable element. It has dominated the majority semi-conductor applications for a long period. Elemental silicon is used in photovoltaic as the main semiconductor material converting light to electricity. The most prevalent bulk material for solar cells is crystalline silicon. Crystalline silicon panels are the most expensive. Bulk silicon is classified into several categories according to crystallinity and crystal size in the resulting ingot, ribbon or wafer **[12].**

1. Monocrystalline silicon (c-Si): Often made using the Czochralski process. Single-crystal wafer cells tend to be expensive and, because they are cut from cylindrical ingots, do not completely cover a square solar-cell module without a substantial waste of refined silicon. Therefore, generally mono-crystalline panels have uncovered gaps at the four corners of the cells.
2. Poly- or multicrystalline silicon (poly-Si or mc-Si): is produced using of cast square ingots – large blocks of molten silicon carefully cooled and solidified. Mc-silicon cells are cheaper to produce than single-crystal cells but are less efficient (around *12%*). Polycrystalline silicon wafers are made by wire-sawing block-cast silicon ingots into very thin (*180* to *350* micrometre) slices or wafers. The wafers are usually lightly *p*-type doped. To make a solar cell from the wafer, a surface diffusion of n-type dopants is performed on the front side of the wafer. This forms a *p-n* junction a few hundred nanometres below the surface.
3. Ribbon silicon: formed by drawing flat thin-films from molten silicon and having a multicrystalline structure. These cells have lower efficiencies than poly-Si, but save on production costs due to a great reduction in silicon waste, as this approach does not require sawing from ingots.

Silicon thin-films are mainly deposited by chemical vapour deposition (typically plasma-enhanced (*PE-CVD*)) from silane gas and hydrogen gas. Depending on the deposition's parameters, this can yield:

1. amorphous silicon (*a-Si* or *a-Si:H*)
2. protocrystalline silicon or
3. Nanocrystalline silicon (*nc-Si* or *nc-Si:H*).

These types of silicon present dangling and twisted bonds, which results in deep defects as well as deformation of the valence and conduction bands. The solar cells made from these materials tend to have lower energy conversion efficiency than bulk silicon, but are also less expensive to produce. The quantum efficiency of thin-film solar cells is also lower due to the reduced number of collected charge carriers per incident photon. Amorphous silicon has a higher band gap (*1.7 eV*) than crystalline silicon (*c-Si*) (1.1 eV), which means it absorbs the visible part of the solar spectrum more strongly than the infrared portion of the spectrum. As *nc-Si* has about the same band gap as *c-Si*, the two materials can be combined in thin layers, creating a layered cell called a tandem cell. The top cell in a-Si absorbs the visible light and leaves the infrared part of the spectrum for the bottom cell in Nanocrystalline *Si*.

Recently, solutions to overcome the limitations of thin-film crystalline silicon have been developed. Light trapping schemes, where the incoming light is obliquely coupled into the silicon and the light traverses the film several times, enhance the absorption of sunlight in the films. Thermal processing techniques enhance the crystallinity of the silicon and pacify electronic defects. Despite the several attempts at making better solar cells by using new materials, the reality is that the photovoltaic market is still dominated by solar cells based on silicon wafer.

I.8.2.2 Cadmium Telluride (CdTe)

Cadmium telluride has a direct band gap (about *1.45eV*) which enables it to convert solar energy into electricity more efficiently than the indirect band gap semiconductors. It is an efficient light-absorbing material for thin-film solar cells. CdTe is easier to deposit and more appropriate for large-scale production. In *2008, CdTe* modules accounted for over 6% of the word production, more than any other thin film technology. In addition their conversion efficiencies of around 11% look set to advance towards *15%* in the next few years **[13].** Despite the toxicity of *CdTe*-based solar cells, this is the only technology (except for amorphous silicon) that can be delivered on a large scale.

The toxicity of *CdTe* is derived from the toxicity of elemental cadmium, a heavy metal that is a cumulative poison. Many studies, principally by researchers of the National Renewable Energy Laboratories (*NREL*) in the *USA*, have shown that the release of cadmium to the atmosphere is lower with *CdTe*-based solar cells than with silicon photovoltaics and other thin-film solar cell technologies **[14].**

The main layers in these thin films solar cells are a transparent top contact, a *CdS/CdTe* heterojunction and absorber, and a metallic back contact as shown in **Figure (I-12).** A suitable supporting substrate of glass, metal or plastic depending on the rigidity or flexibility of the cell is necessary.

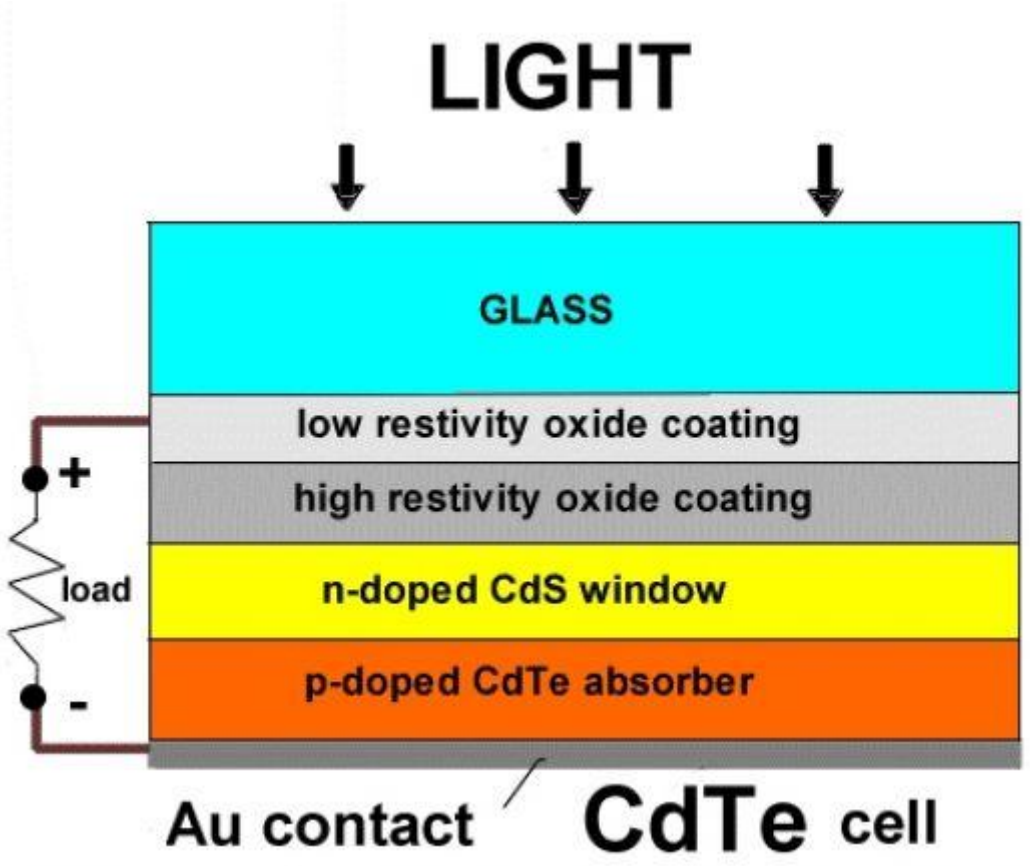

Figure I-12 CdTe solar cell structure.

I.8.2.3 Copper-Indium Selenide (CuInSe2)

The materials based on CuInSe2 that are of interest for photovoltaic applications take into account several elements from Groups *I, III* and *VI* in the periodic table. These semi-conductors are particularly attractive for thin-film solar cell applications because of their high optical absorption coefficients and versatile optical and electrical characteristics.

The basic structure of a *Cu(In,Ga)Se2* thin-film solar cell is shown in Figure**(I-13)**. The most common substrate is soda-lime glass of 1–3 mm thickness. This is coated on one

side with molybdenum (*Mo*) that serves as metal back contact. The *Cu(InGa)Se2* is deposited on top of the molybdenum back electrode as a PV absorber material. The heterojunction is then completed by chemical bath deposition of *CdS* and by the sputter deposition of a nominally undoped *ZnO* as an intrinsic layer and then a heavy doped *ZnO* layer. *ZnO* layer acts as the window layer of the solar cell. Efficiencies approaching 19% have been reported for laboratory scale service **[15]**.

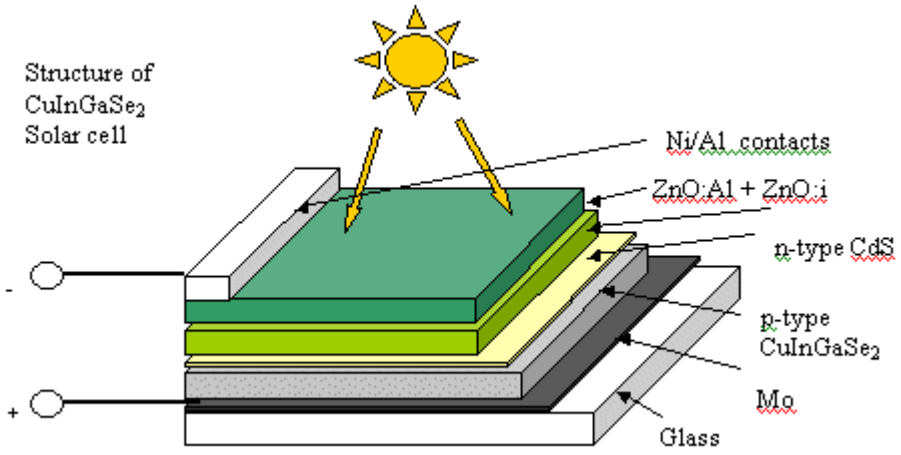

Figure I-13 Cross section of CIGS solar cell structure

.

I.8.2.4 Gallium Arsenide (GaAs)

Gallium is one of the elements in Group III of the periodic table while arsenic is in Group V. For this reason, gallium arsenide *(GaAs)* is referred to as a Group III- V semiconductor. The GaAs semiconductor has been used in photovoltaic field in space thanks to its higher efficiency than silicon. Its high efficiency is partly as a result of its direct band gap which means that light is absorbed much more efficiently than it is by silicon. The total active thickness is only a few micrometers. Other advantages for the current interest in GaAs space solar cells are its high radiation tolerance and high conversion efficiency. But there are some notable disadvantages of *GaAs* solar cell compared to silicon are its high cost, heavy weight and weak nature.

High-efficiency cells, especially multijunction cells have been developed for satellites application and space discovery. These cells consist of multiple thin films produced using

molecular beam epitaxy. A triple-junction cell, for example, may consist of the semi-conductors *GaAs, Ge* and *GaInP2* **[16].**

A multijunction photovoltaic cell is a cell which has several layers of film, all of which operate to absorb energy from the sun. Each layer (semi-conductor) will have a characteristic band-gap energy which causes it to absorb light most well at a certain colour or, more precisely, to absorb electromagnetic radiation over a portion of the spectrum. The semi-conductors are carefully chosen to absorb nearly the entire solar spectrum, thus generating electricity from as much of the solar energy as possible.

Up to now, GaAs multijunction devices are the most efficient solar cells. This type of solar cell reaches about *40.7%* efficiency under solar concentration and laboratory conditions [**17]**. These devices use *20* to *30* different layers in series. This will be explained in more detail in chapter II.

I.8.2.5 Light-absorbing Dyes

Dye sensitized solar cells were discovered by the Michael Greatzel et al in 1991, these cells also called 'greatzel cells'. They are photoelectrochimical cells that use photo-sensization of large band gap mesoporous oxide semiconductors. Figure **(I-14**) represents a Schematic representation of a dye-sensitized solar cell.

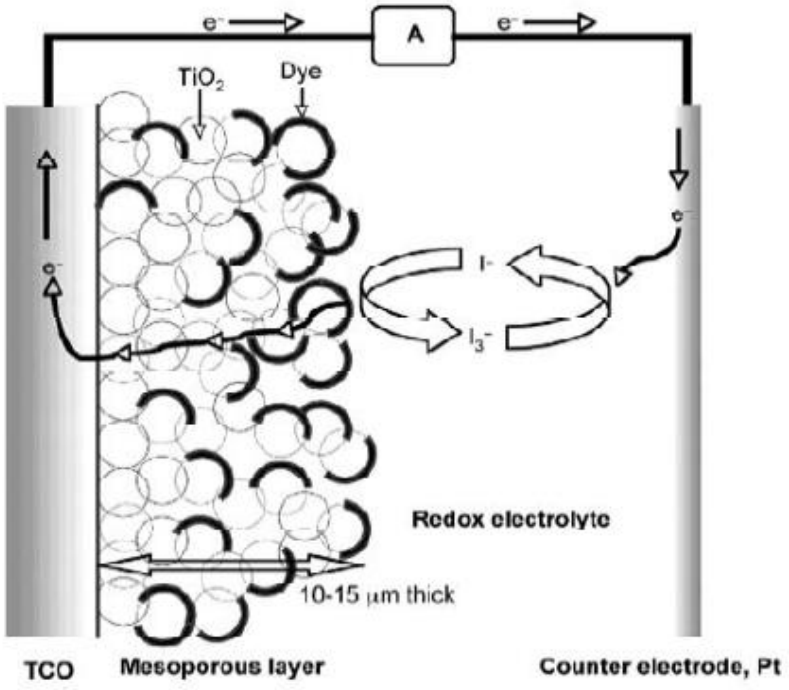

Figure I-14 Schematic representation of a dye-sensitized solar cell (*DSSC*).

Typically a ruthenium metal organic dye (*Ru*-centred) is used as a monolayer of light-absorbing material. The dye-sensitized solar cell *(DSSC*) depends on a mesoporous layer of nanoparticulate titanium dioxide to greatly amplify the surface area (*200–300*m^2/g TiO_2, as compared to approximately *10*m^2/g of flat single crystal). The photogenerated electrons from the light-absorbing dye are passed on to the n-type TiO2, and the holes are passed to an electrolyte on the other side of the dye[12]. The circuit is completed by a redox couple in the electrolyte, which can be liquid or solid **[18].** This type of cell permit a more flexible use of materials, and is in general manufactured by screen printing, with the potential for lower processing costs than those used for bulk solar cells. However, the dyes in this type of cells also suffer from degradation under heat and *UV* light. Furthermore, the cell casing is difficult to seal due to the solvents used in assembly. These cells are extremely promising due to their make-up of low cost materials.

I.8.2.6 Organic/Polymer Solar Cells

Organic solar cells are studied extensively for their potential as solution-processable, light-weight, low-cost, and large-area energy generators. Organic solar cells and polymer solar cells are built from thin films (typically *100 nm*) of organic semi-conductors such as polymers and small-molecule compounds like polyphenylene vinylene, copper phthalocyanine (a blue or green organic pigment) and carbon fullerenes. [**19].** The organic materials like conjugated polymer, dyes or molecular organic glasses can offer the possibility for the production of thin solar cells due to their high optical absorption coefficients. Energy conversion efficiencies achieved up to now using conductive polymers are low compared to inorganic materials, with the highest reported efficiency of *6.5%* [**17]** for tandem cell architecture.

I.8.2.7 Nano-crystalline Solar Cells

These structures make use of some of the same thin-film light absorbing materials but are overlain as an extremely thin absorber on a supporting matrix of conductive polymer or mesoporous metal oxide having a very high surface area to increase internal reflections (and hence increase the probability of light absorption). Using nanocrystals allows one to design architectures on the length scale of nanometres, the typical exciton diffusion length. In particular, single-nanocrystal (channel) devices, an array of single *p-n* junctions between the

electrodes and separated by a period of about a diffusion length, represent a new architecture for solar cells and potentially high efficiency **[12].**

Table 1 provides a summary of the state of the art conversion efficiency reported for various semiconductors based solar cells (sources adapted from MA Green **[20].**

Table I. Confirmed terrestrial cell and submodule efficiencies measured under the global AM1.5 spectrum (1000W/m2) at 25°C

Classification[a]	Effic.[b] (%)	Area[c] (cm^2)	V_{oc} (V)	J_{sc} (mA/cm^2)	FF[d] (%)	Test centre[e] (and date)
Silicon						
Si (crystalline)	**25.0 ± 0.5**	4.00 (da)	0.705	**42.7**	82.8	Sandia (3/99)[f]
Si (multicrystalline)	**20.4 ± 0.5**	1.002 (ap)	0.664	**38.0**	80.9	NREL (5/04)[f]
Si (thin film transfer)	**16.7 ± 0.4**	4.017 (ap)	0.645	**33.0**	78.2	FhG-ISE (7/01)[f]
Si (thin film submodule)	**10.5 ± 0.3**	94.0 (ap)	0.492[g]	**29.7**[g]	72.1	FhG-ISE (8/07)[f]
III-V cells						
GaAs (crystalline)	**26.1 ± 0.8**	0.998 (ap)	1.038	**29.7**	84.7	FhG-ISE (12/07)[f]
GaAs (thin film)	**26.1 ± 0.8**	**1.001 (ap)**	**1.045**	**29.5**	**84.6**	**FhG-ISE (07/08)[f]**
GaAs (multicrystalline)	**18.4 ± 0.5**	4.011 (t)	0.994	**23.2**	79.7	NREL (11/95)[f]
InP (crystalline)	**22.1 ± 0.7**	4.02 (t)	0.878	**29.5**	85.4	NREL (4/90)[f]
Thin film chalcogenide						
CIGS (cell)	**19.4 ± 0.6**[h]	0.994 (ap)	0.716	**33.7**	80.3	NREL (1/08)[f]
CIGS (submodule)	**16.7 ± 0.4**	16.0 (ap)	0.661[g]	**33.6**[g]	75.1	FhG-ISE (3/00)[f]
CdTe (cell)	**16.7 ± 0.5**[h]	1.032 (ap)	0.845	**26.1**	75.5	NREL (9/01)[f]
Amorphous/nanocrystalline Si						
Si (amorphous)	9.5 ± 0.3[i]	1.070 (ap)	0.859	17.5	63.0	NREL (4/03)[f]
Si (nanocrystalline)	10.1 ± 0.2[j]	1.199 (ap)	0.539	24.4	76.6	JQA (12/97)
Photochemical						
Dye sensitised	10.4 ± 0.3[k]	1.004 (ap)	0.729	**22.0**	65.2	AIST (8/05)[f]
Dye sensitised (submodule)	8.2 ± 0.3[k]	25.45 (ap)	**0.705**[g]	**19.1**[g]	61.1	AIST (12/07)[f]
Dye sensitised (submodule)	8.2 ± 0.3[k]	18.50	0.659[g]	**19.9**[g]	62.9	AIST (6/08)[f]
Organic						
Organic polymer	5.15 ± 0.3[k]	1.021 (ap)	0.876	**9.39**	62.5	NREL (12/06)[f]
Organic (submodule)	1.1 ± 0.3[k]	232.8 (ap)	29.3	0.072	51.2	NREL (3/08)[f]
Multijunction devices						
GaInP/GaAs/Ge	32.0 ± 1.5[j]	3.989 (t)	2.622	14.37	85.0	NREL (1/03)
GaInP/GaAs	30.3[j]	4.0 (t)	2.488	14.22	85.6	JQA (4/96)
GaAs/CIS (thin film)	25.8 ± 1.3[j]	4.00 (t)	—	—	—	NREL (11/89)
a-Si/μc-Si (thin submodule)[j,l]	11.7 ± 0.4[j,l]	14.23 (ap)	5.462	2.99	71.3	AIST (9/04)

[a]CIGS=CuInGaSe2; a-Si=amorphous silicon/hydrogen alloy.

[b]Effic.=efficiency.

[c](ap)=aperture area; (t)=total area; (da)=designated illumination area.

[d]FF=fill factor.

[e]FhG-ISE=Fraunhofer Institut fu¨r Solare Energie systeme; JQA=Japan Quality Assurance; AIST=Japanese National Institute of Advanced Industrial Science and Technology.

[f]Recalibrated from original measurement.

[g]Reported on a 'per cell' basis.

[h]Not measured at an external laboratory.

[i]Stabilised by 800 h, 1 sun AM1.5 illumination at a cell temperature of 50°C.

[j]Measured under IEC 60904-3 Ed. 1: 1989 reference spectrum.

[k]Stability not investigated.

[l]Stabilised by 174 h, 1 sun illumination after 20 h, 5 sun illumination at a sample temperature of 50°C.

Table II. Confirmed terrestrial module efficiencies measured under the global AM1.5 spectrum (1000 W/m2) at a cell temperature of 25°C

Classification[a]	Effic.[b] (%)	Area[c] (cm^2)	*Voc* (V)	*Isc* (A)	FF[d] (%)	Test centre (and date)
Si (crystalline)	**22.9 ± 0.6**	778 (da)	5.60	**3.97**	80.3	Sandia (9/96)[e]
Si (large crystalline)	**20.3 ± 0.6**	16300 (ap)	66.1	**6.35**	78.7	Sandia (8/07)[e]
Si (multicrystalline)	**15.5 ± 0.4**[f]	1017 (ap)	14.6	**1.37**	78.6	Sandia (10/94)[e]
Si (thin-film polycrystalline)	8.2 ± 0.2	661 (ap)	25.0	**0.320**	68.0	Sandia (7/02)[e]
CIGSS	**13.5 ± 0.7**	3459 (ap)	31.2	**2.18**	68.9	NREL (8/02)[e]
CdTe	**10.9 ± 0.5**	4874 (ap)	26.21	**3.24**	62.3	NREL (4/00)[e]
a-Si/a-SiGe/a-SiGe (tandem)[g]	10.4 ± 0.5[h]	905 (ap)	4.353	3.285	66.0	NREL (10/98)[e]

[a]CIGS=CuInGaSe2; a-Si=amorphous silicon/hydrogen alloy.

[b]Effic.=efficiency.

[c](ap)=aperture area; (t)=total area; (da)=designated illumination area.

[d]FF=fill factor.

[e]Recalibrated from original measurement.

[h]Not measured at an external laboratory

[g]Light soaked at NREL for 1000 hours at 50°C, nominally 1-sun illumination.

[h]Measured under IEC 60904-3 Ed. 1: 1989 reference spectrum

I.9 Technologies for the Reduction of Efficiency Losses

A schematic representation of part of a conventional solar cell is depicted in Figure **(I-15).**

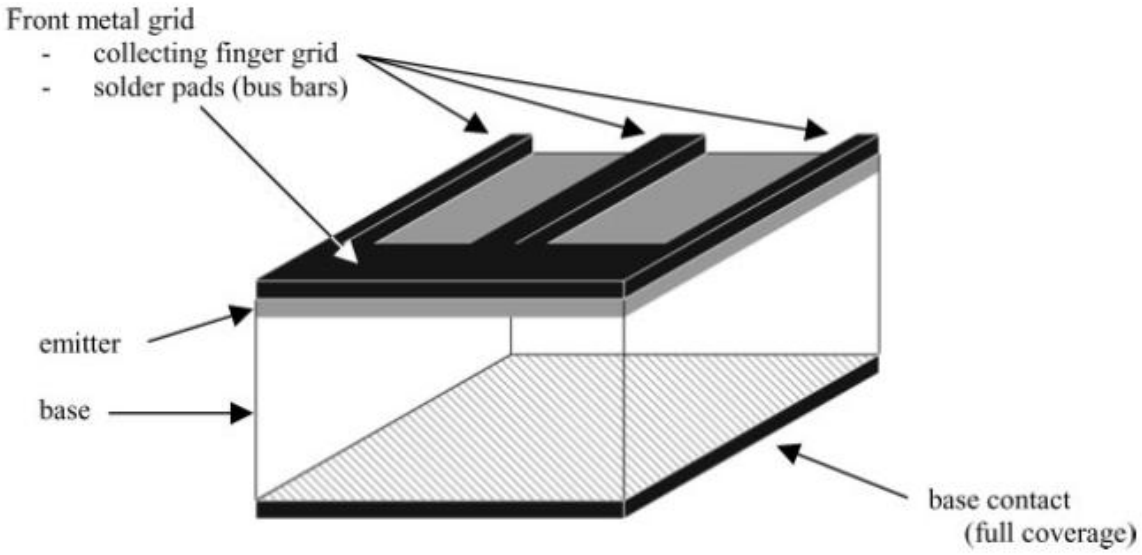

Figure I-15 Schematic representation of a conventional solar cell

The base is the main part of the mechanical structure. The emitter is located near the top or front surface. A metal grid to extract the carrier from the device, contacts each of these silicon regions. Whereas the rear surface is often fully covered (as in the drawing), on the front surface the metal grid is the result of a trade-off between having low coverage to limit optical losses and high coverage to limit resistive losses. Most manufactures apply a front grid consisting of thin parallel lines (fingers) that transport the current to centrally located bus bars. The bus bars are relatively wide and can be used as solder pads to connect to the external leads. In order to reduce the optical and electrical losses mentioned above, in this part, the optical and electrical technologies made for reducing efficiency losses will be described.

I.9.1 Technologies for the Reduction of Optical Losses (light confinement)

It is generally accepted that the cost of photovoltaic conversion has to diminish for *PV* to become of major importance as a renewable energy source. For crystalline silicon wafer technology, the silicon material is a major cost item. One decision to make more efficient use of the costly silicon material is the use of thinner silicon layers.

The current of a cell is directly related to the amount of light absorbed. One source of optical losses is that silicon (as indirect band gap material) absorbs infrared light in a rather weak way. Current wafers typically have a thickness of $300\ \mu m$. This is not enough to absorb the infrared light in one pass through the wafer. This effect becomes more important as wafers become thinner. Silicon however has a relatively large refractive index (around 3.5) **[21].** This high refractive index enables the use of total internal reflection as a powerful means to make light bounce up- and down many times in the silicon wafer, enhancing the path length of rays and hence increase the chance that an infrared photon is absorbed. Thinner silicon solar cells require light-trapping methods to be used in order to maintain good absorption of infrared light and hence maintain cell current and efficiency.

Light trapping technology is able to diffract and reflect the light inside the cell, such that the light bounces back and forth inside the cell, results in increase of optical path length. Front surface of cell is defined to be the surface where the incidence light comes. Back surface of cell is defined as the other side of front surface. Figure I-16 illustrates front and back surface.

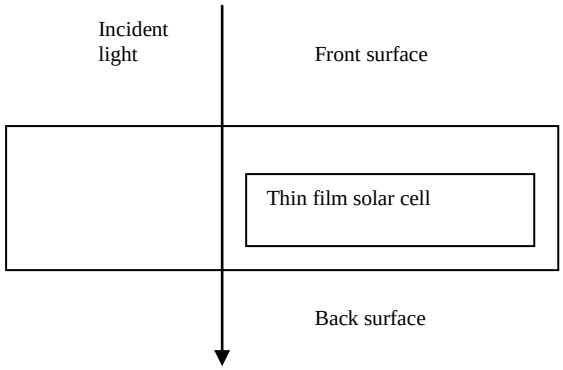

Figure I-16 thin film Si solar cell with front and back surface

There are three general methods to confine/ trap light inside a solar cell by using Antireflection Coating (*ARC*), surface texturing, and back reflector.

I.9.1.1 Antireflection Coating (*ARC*)

Anti-reflection coatings reduce the light loss by making use of phase changes and the dependence of the reflectivity on the refractive index. Antireflection Coating (*ARC*) by

depositing a layer of material that has lower refractive index (n_{ARC}) is used to reduce the amount of incident light that would normally be reflected (i.e. this layer reduces the light loss) . Single layer *ARC* has zero reflection at its center λc wavelength when the thickness of layer is t_{ARC}=0.13 $\lambda c/n_{ARC}$, where $\lambda c=576nm$ and $n_{ARC}=1.87$ [**22**].

There are many candidate of *ARC*, such as, *ZnO*, *SiOxNy*, *Si3N4*. *ZnO*, *SiOxNy*, and *Si3N4* can be deposited using *RF* sputtering [**21**], *LPCVD* [**23**]. Silicon nanowire can be used as antireflection coating too. For thin film solar cell with intergitated top contacts, the function of an *ARC* is to reduce the reflection of incoming light, passivize the surface, and provide insulation allowing selective plating of intergitated top contacts **[23]**.*Si3N4* is chosen since it can perform all three functions well.

I.9.1.2 Surface Texturing

Surface texturing, either in combination with an anti-reflection coating or by itself, can also be used to minimise reflection. Any "roughening" of the surface reduces reflection by increasing the chances of reflected light to bounce back onto the surface, rather than out to the surrounding air. Surface texturing of front or both front and back surface of a solar cell (based on silicon for example) is used to scatter the photon such that optical path length increases. Texturization is achieved by creating a topology of small, densely packed tetrahedral grooves, V-grooves or random pyramids that act as light traps on the solar cell's surface. When light impinges on this textured surface, reflection occurs at such an angle that it is deflected into a new point on the surface.

Multiple interactions occur with the silicon, thus reducing the amount of light normally lost through reflection. Together with an antireflection coating the reflection of sunlight can be kept well under 3%, making the cell appear black ("black cell"). The textured surface also provides a reduction in path length to the junction which is most pronounced for longer wavelength light, thereby increasing longer wavelength collection efficiency (an important factor for thin devices). As bulk region diffusion length is reduced by the effects of radiation, the reduced effective path length enables a contoured surface device to maintain more of the lower wavelength response than a comparable smooth cell. Texturization increases solar absorbance also in the wavelength region not contributing to the carrier generation. Figure **(I-16)** illustrates the pyramid surface texture.

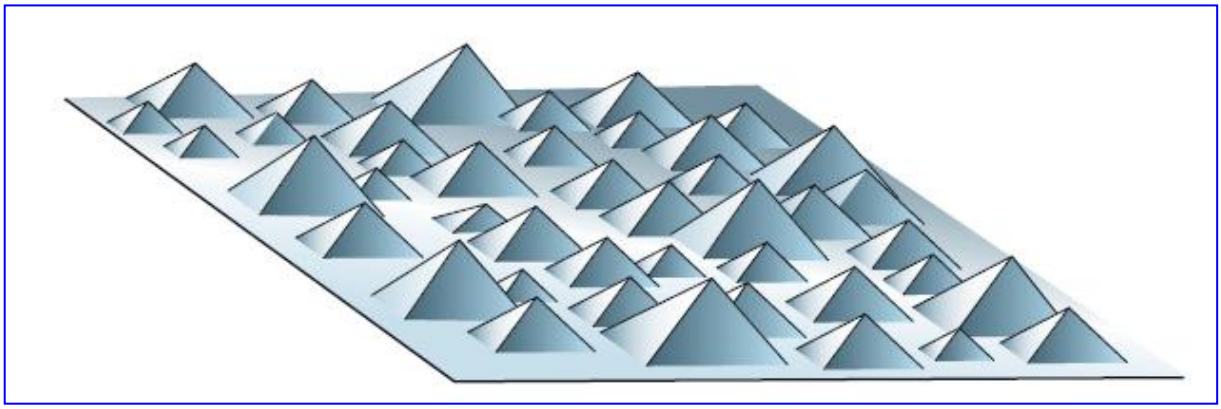

Figure I-16 Texturization by raised pyramids

I.9.1.3 Back Surface Reflector (BSR)

The absorption of photons from the incident sunlight depends on the absorption coefficient, which is high for short wavelengths and low for longer wavelengths. Accordingly red and infrared light penetrate deeper into the silicon material and a big portion is scattered or absorbed at the rear side contact. Polishing and coating the rear side with a thin aluminium reflector makes the back contact reflective give longer wavelengths a second chance at being absorbed and the energy which is not absorbed is re-emitted through the front surface leading to a reduction in cell absorbance.

Back reflector is used to reflect back the incident photon. Distributed back refractor (*BDR*) is proposed to replace current metal back refractor. The reflectivity of aluminium back reflector is typically > *95%* for normal incidence and <*80%* for oblique incidence, while the reflectivity of distributed brag reflector is much more superior of >*99.8%* over a wide range of wavelength (*800-1100nm*) and better for oblique incidence **[22].** The limitation of back reflector is that at most it can only enhance optical path length to twice of the cell thickness. To address this limitation, diffraction grating DG is used on back surface to diffract the light inside solar cell to certain angles based on different diffraction orders [**23**]. When only *BDR* is used, *70%* of light was lost due to low reflection; when *BDR* coupled with DG are used, they complement each other such that fewer light is lost [**23**].

DBR consists of pair of Si and SiO3 layers in 8 stacks, and deposited using *PECVD*. The *DBR* is deposited at temperature less than *450°C* but *DBR* performance is stable even after having a thermal history of as high as 1000°C for 3.5 hours [**23**].

I.9.2 Technologies for the Reduction of Losses Due to Recombination

I.9.2.1 Recombination Mechanism in Silicon Solar Cell

In a conventional silicon solar cell, recombination can occur in five regions:

• The front surface;

• The emitter region (N^+);

• The junction (the depletion region of the junction);

• The base region (P);

• The back surface

Therefore, there are principally two types of recombination: the recombination mechanisms in bulk (volume) and the surface recombination.

1. Recombination Mechanisms in the Bulk of the Silicon Solar Cell

There are three fundamental recombination mechanisms in a bulk semiconductor.

(a) Radiative or band-to-band recombination

(b) Auger recombination

(c) Recombination through defect or trap levels (often referred to as Shockley-Read-Hall recombination (*SRH* recombination))

These different processes are further illustrated with the Figure **(I-17)**

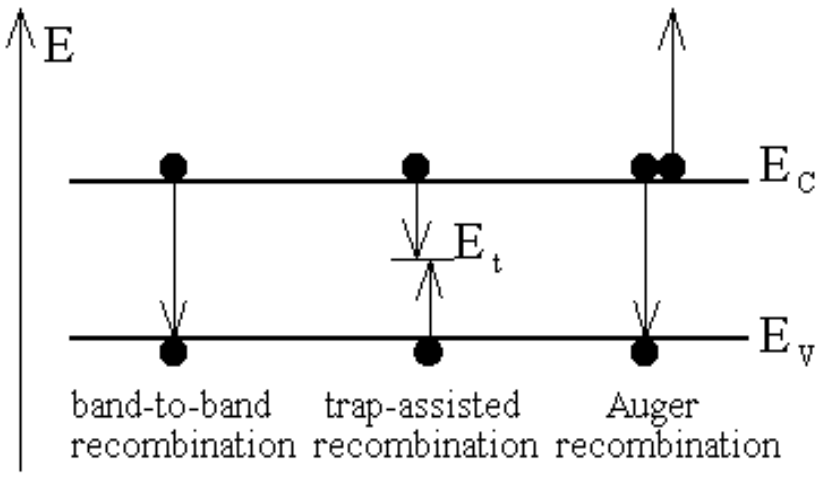

Figure I-17 Schematic representation of carrier recombination mechanisms in semiconductors

- **Radiative Recombination**

Radiative recombination (band-to-band recombination) corresponds to the recombination process where a free electron falls directly from the conduction band and recombines with a free hole in the valence band with all or most of the excess energy dissipated in the form of a photon. The radiative volume recombination rate, U_{BB}, is simply proportional to the electron concentration in the conduction band (the free-electron concentration) and the hole concentration in the valence band (the free-hole concentration):

$$U_{BB} = Bnp \qquad \textbf{(I-14)}$$

Where: B is the coefficient of radiative recombination, n is the free-electron concentration and p is the free-hole concentration. From detailed balance calculation, the value of B for Si was calculated to be $2\times10^{-15}\ cm^3\ s^{-1}$ **[24].** At thermal equilibrium ($\Delta n=0$), U_{BB} is equivalent to the thermal generation rate, G_{th}; the expression for U_{BB} at thermal equilibrium is

$$U_{BB} = G_{th} = Bn_0 p_0 = Bn_i^2 \qquad \textbf{(I-15)}$$

Where: n_0 and p_0 are the thermal equilibrium concentrations of free electrons and free holes and n_i is the intrinsic carrier concentration. From Equation **I-14** and **I-15**, the radiative recombination lifetime can readily be obtained as

$$\tau_{BB} = \frac{\Delta n}{B.(n_0 + \Delta n).(p_0 + \Delta n)} \qquad \textbf{(I-16)}$$

Consequently, the expressions for the radiative recombination lifetime under low and high injection are as follows:

$$\tau_{BB,lli} = \frac{1}{B.N_{doped}} \quad \text{and} \quad \tau_{BB,hli} = \frac{1}{B.\Delta n} \qquad \textbf{(I-17)}$$

N_{doped} is the donor (N_D) or the acceptor (N_A) concentration for n- or p-type semiconductors, respectively. Note that the radiative recombination lifetime stays constant at low injection and decreases with injection in intermediate and high injection regimes.

The radiative recombination in an indirect band gap semiconductor such as Si is considered to be small compared to other types of recombination. This is because the process

involves phonon as the fourth particle (apart from an electron, a hole, and a photon) to conserve the momentum (see Figure **I-18**).

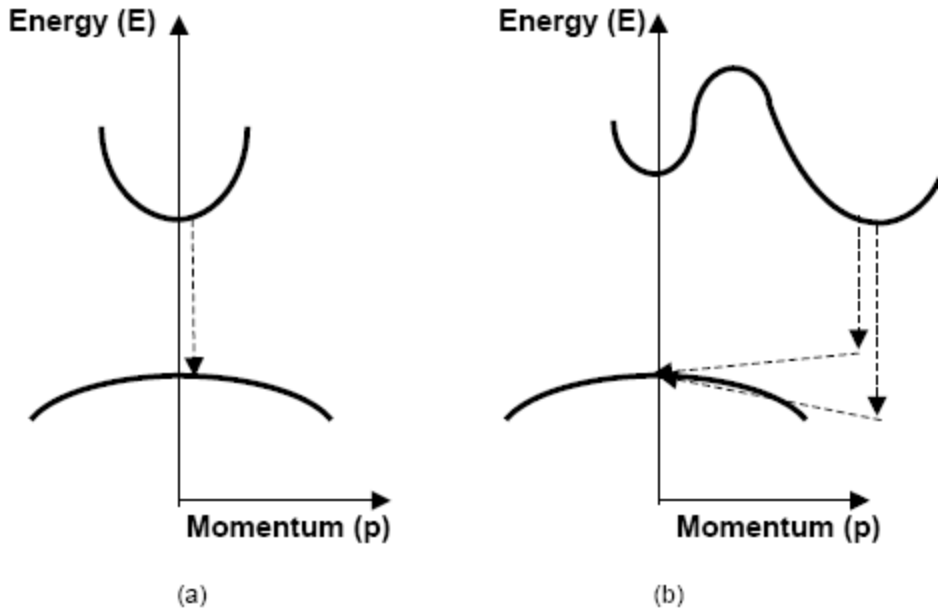

Figure I-18 Schematic representation of radiative recombination for (a) direct band gap (e.g. GaAs) and (b) indirect band gap (e.g. Si).

- **Auger Recombination**

Auger recombination is a three-particle interaction where an electron in the conduction band and a hole in the valence band recombine giving the excess energy to the third electron or hole. The *eeh* and *ehh* denote the cases where the excess energy is transferred to an electron and a hole, respectively. The Auger recombination rate, U_{Auger}, is given by

$$U_{Auger} = U_{ehh} + U_{eeh} \quad \text{Or} \quad U_{Auger} = C_n.n^2.p + C_p.n.p^2 \qquad \textbf{(I-18)}$$

The C_n and C_p are the Auger coefficients for electrons and holes, respectively. Consequently, the expressions for the Auger recombination lifetime under low and high injection are as follows:

N type Si $\tau_{Auger,lli} = \frac{1}{C_n . N_D^{\ 2}}$ and $\tau_{Auger,hli} = \frac{1}{(C_n + C_p).\Delta n^2}$ **(I-19)**

P-type Si $\tau_{Auger,lli} = \frac{1}{C_p . N_A^{\ 2}}$ and $\tau_{Auger,hli} = \frac{1}{(C_n + C_p).\Delta n^2}$ **(I-20)**

The most commonly used values for the Auger coefficients were determined by Dziewior and Schmid (C_n=2.8×10^{-31} cm^6 s^{-1} and C_p=0.99×10^{-31} cm^6 s^{-1}) for Si with a doping concentration greater than 5×10^{18} cm^{-3} **[25].**

The Auger recombination lifetime is, to the first order, a quadratic function of the carrier concentration, as opposed to a linear function in the case of the radiative recombination lifetime. As a result, Auger recombination dominates the lifetime at high doping or at high injection.

- **Shockley Read Hall Recombination (SRH)**

Defects in semiconductors can create energy levels within the band gap that can greatly enhance the recombination process. These trap levels form stepping stones whereby an electron falls from the conduction band to the defect level and then from the defect level to the valence band. This type of recombination normally dominates the net recombination rate in low quality materials with a high defect density. The dynamic of the recombination process via trap levels inside the band gap was first derived by Shockley and Read and Hall (so-called SRH recombination theory) **[26-27**]. Important assumptions made in the derivation of the SRH recombination rate are summarized in **[27]** and are listed below

(a) No radiative recombination or Auger recombination involves.

(b) The semiconductor is non-degenerate.

(c) The energy level of the defects does not change with their charging properties.

(d) The relaxation time of the charge carriers caught by the defects is negligibly small compared to the average time between two emission processes.

(e) Fermi-Dirac statistic applies.

(f) The defects do not interact with each other (i.e., an electron cannot make a transition from a defect level to another).

The SRH volume recombination rate, U_{SRH}, for single-energy level traps is then given by:

$$U_{SRH} = \frac{np - n_i^{\,2}}{\tau_{p0}(n + n_1) + \tau_{n0}(p + p_1)} \qquad \textbf{(I-21)}$$

The τ_{n0} and τ_{p0} are the characteristic electron and hole lifetimes, which are related to the thermal velocity of the charge carrier, υ_{th}, the defect concentration, N_t, and the capture cross-sections of electron and hole of the specific defect, σ_n and σ_p as

$$\tau_{n0} = \frac{1}{\sigma_n \nu_{th} N_t} \quad \text{And} \quad \tau_{p0} = \frac{1}{\sigma_p \nu_{th} N_t} \qquad \textbf{(I-22)}$$

$$n_1 = n_i \exp\left(\frac{E_t - E_i}{KT}\right) \quad \text{And} \quad p_1 = n_i \exp\left(\frac{E_i - E_t}{KT}\right) \qquad \textbf{(I-23)}$$

By definition, n_1 and p_1 are the free-electron and the free-hole concentrations in the case in which the Fermi level (E_F) lies at the trap energy level (E_t). The SRH recombination lifetime can then be obtained as follows:

$$\tau_{SRH} = \frac{\tau_{p0}(n + n_1) + \tau_{n0}(p + p_1)}{n_0 + p_0 + \Delta n} \qquad \textbf{(I-24)}$$

Consequently, the expressions for the SRH recombination lifetime under low and high injection are as follows:

N-type Si $\quad \tau_{SRH,lli} = \tau_{p0} + \dfrac{\tau_{n0}(\Delta n + p_1)}{N_D}$ and $\tau_{SRH,hli} = \tau_{n0} + \tau_{p0}$ **(I-25)**

P-type Si $\quad \tau_{SRH,lli} = \tau_{n0} + \dfrac{\tau_{p0}(\Delta n + n_1)}{N_A}$ and $\tau_{SRH,hli} = \tau_{n0} + \tau_{p0}$ **(I-26)**

For traps located at the middle of the band gap ($E_t \cong E_i$), both n_1 and p_1 become small and equal to n_i Consequently, the *SRH* lifetime under low injection can further be simplified as:

N-type Si $\quad \tau_{SRH,lli} = \tau_{p0}$ for mid-gap traps **(I-27)**

P-type Si $\quad \tau_{SRH,lli} = \tau_{n0}$ for mid gap traps. **(I-28)**

As can be seen from Equation **I-24** through **I-25**, with respect to the location of the traps in the band gap, the *SRH* lifetime becomes lowest when the traps lie at the middle of the band gap. Consequently, the mid-gap traps are considered to be the most damaging traps that can greatly enhance the overall recombination in the device.

In reality, all three recombination processes discussed above take place at the same time. The net volume recombination can be obtained simply by adding the three recombination rates as follows:

$$U_{net} = U_{BB} + U_{Auger} + U_{SRH} \qquad \textbf{(I-29)}$$

The net lifetime can therefore, be obtained as:

$$\frac{1}{\tau_{net}} = \frac{1}{\tau_{BB}} + \frac{1}{\tau_{Auger}} + \frac{1}{\tau_{SRH}} \qquad \textbf{(I-30)}$$

2. Surface Recombination

Surface recombination corresponds to a phenomenon where excited electrons in the conduction band recombine with holes in the valence band via defect levels at the surface, called surface states (**Figure I-19**). These surface states are the result of the abrupt discontinuity of a crystalline phase at the surface, which forms unsatisfied dangling Si bonds. The recombination via these surface states can be explained through minor modification of the volume SRH recombination theory.

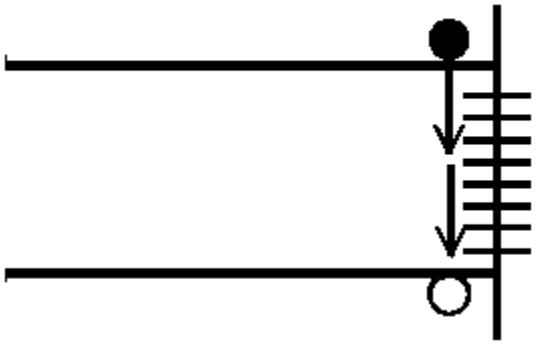

Figure I-19 Schematic representation of recombination via surface states.

It is useful to first introduce two main quantities that are used to quantify the surface recombination activity:

(a) Surface recombination rate, U_s *(cm^{-2} s^{-1}):* A recombination rate of carriers per unit area per unit time

(b) Surface recombination velocity, *S* or *SRV* (cm/s): A velocity of the excited carrier flowing to a surface.

These parameters are related to the surface recombination rate by the following equation:

$$S = \frac{Us}{\Delta n} \qquad \textbf{(I-31)}$$

With minor modifications to the expression of the volume *SRH* recombination (Equation I-21), the surface recombination rate, U_s, for single-energy level surface states can be obtained as

$$U_s = \frac{n_s.p_s - n_i^{\,2}}{\frac{n_s + n_1}{S_{p0}} + \frac{p_s + p_1}{S_{n0}}} \qquad \textbf{(I-32)}$$

Where n_s and p_s are the electron and the hole volume concentrations at the surface and S_{n0} and S_{p0} are the characteristic surface recombination velocities of the surface states, which are related the surface states density, N_{st} (cm^{-2}) as:

$$S_{p0} = \sigma_p.\nu_{th}.N_{st} \quad \text{and} \quad S_{n0} = \sigma_n.\nu_{th}.N_{st} \qquad \textbf{(I-33)}$$

Consequently, through the definition of the surface recombination velocity (Equation I-31), the *SRH* surface recombination velocity can be obtained as

$$S = \frac{n_{s0} + P_{s0} + \Delta n}{\frac{n_s + n_1}{S_{p0}} + \frac{p_s + p_1}{S_{n0}}} \qquad \textbf{(I-34)}$$

In reality, surface states are not localized at a single-energy level but are distributed across the band gap of a semiconductor. Here, the total surface recombination rate is obtained by integrating Equation **I-31** through the entire band gap of a semiconductor:

$$Us = \int_{E_v}^{E_c} \frac{n_s.p_s - n_i^{\,2}}{\frac{n_s + n_1(E)}{\sigma_p(E)} + \frac{p_s + p_1}{\sigma_n(E)}}.\nu_{th}.D_{it}.dE \qquad \textbf{(I-35)}$$

The E_v is the conduction band energy, E_c is the valence band energy, and D_{it} is the density of surface states per unit energy ($1/(eV \cdot cm^{2})$).

The parameter called the "surface recombination velocity", in units of cm/sec, is used to specify the recombination at a surface. In a surface with no recombination, the movement of carriers towards the surface is zero, and hence the surface recombination velocity is zero. In a surface with infinitely fast recombination, the movement of carriers towards this surface is limited by the maximum velocity they can attain, and for most semiconductors at the rate of 1×10^{7} cm/sec **[28].**

I.9.2.2 Minimisation of Recombination

As mentioned above, recombination of generated carriers is possible at the surface, in the depletion region and in the bulk of the semiconductor. In order to obtain high photocurrent and therefore high conversion efficiency all these recombination problems must be minimised.

a- Surface passivation

- **Front surface passivation**

In the crystalline materials, surface represents sudden discontinuity of the crystal arrangement, which gives rise to dangling or unfinished bonds. These bonds act as good recombination centres. In terms of energy band diagram, the dangling bands at the surface give rise to energy states in the middle of the band gap, which act as a good recombination centres. Thus, in order to avoid recombination, both front and rear surfaces should be passivated, i.e., the recombination properties of the surface should be nullified. This is known as surface passivation. At the front surface, the surface passivation is achieved by deposition of a dielectric layer such that it passivizes the unfinished bonds at the surface (removing energy states from the middle of the band gap). *SiO2* or *Si3N4* are used to pacify the crystalline Si surface. Both layers have high energy gap which prevents carriers reaching the surface deposited dielectric layer **[29].**

- **Back Surface Passivation – Back Surface Field**

In another method of surface passivation, high level doping, in a low doped semiconductor of similar impurities (for instance *Al* in *P* type silicon or *P* in *N* type silicon) is done. This is typically done at the rear side (usually *P* type) for crystalline Si solar cells. In this way, a PP^+ junction is obtained (P^+ represents heavy doping $10^{18}cm^{-3}$ or higher) as shown in Figure **I-20.** It gives rise to an electric field at a junction in the direction from *P* to P^+ side. This junction represents a potential energy barrier to the minority electrons. The electric field repels electrons back towards *P-N* junction and reduces the recombination at the surface. This field is known as back surface field (*BSF*).

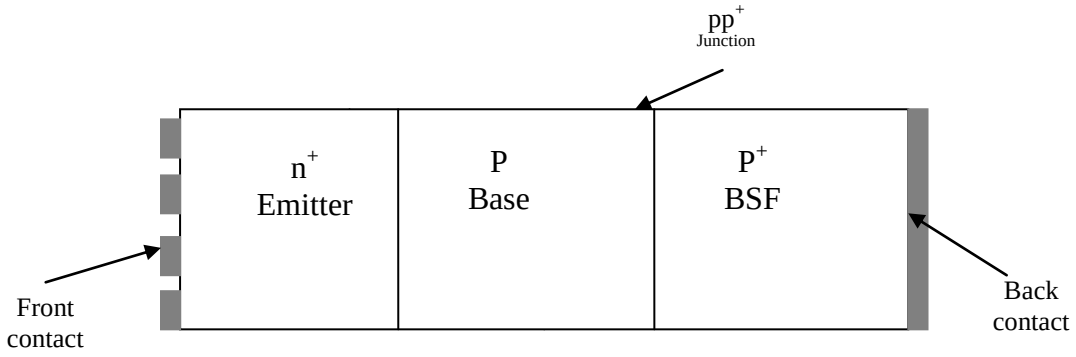

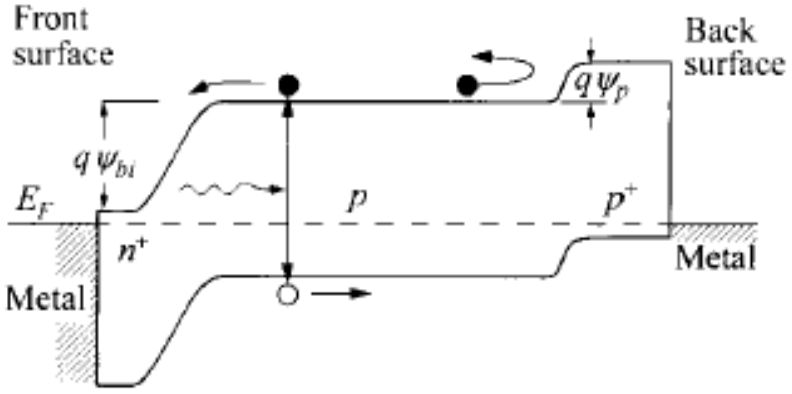

Figure I-20 Solar cell structure and Energy-band diagram for an *n+-p-p+* back-surface field junction solar cell

The effectiveness of the surface recombination is given in terms of surface recombination velocity (*SRV* or *S*). It is defined as the rate of recombination at the surface divided by the excess of carrier concentration at the surface. Mathematically:

$$S_n = \frac{R_{sur}}{\Delta n_{sur}}, S_p = \frac{R_{sur}}{\Delta p_{sur}} \qquad \textbf{(I-36)}$$

Here S_n and S_p are *SRVs* for electrons and holes, respectively. The lower is the *SRV* the better is the surface passivation. An *SRV* value of about *10cm/s* is corresponding to a well passivized surface while *SRV* of value more than $10^4 cm/s$ is corresponding to a poorly passivized surface.

b- Bulk Passivation

In general, a deposited thin film active material (in thin film solar cell technologies), multicrystalline silicon and most materials with a low degree of crystallization can contain crystallographic defects, grain boundaries, metallic impurities…etc. These defects affect the minority carrier lifetime of the bulk material and degrade the solar cell performances. To treat recombination problems in the bulk, specific treatments have been developed either by passivating the bulk crystallographic defects using hydrogen or by gettering a process for removing metallic impurities.

- **Bulk passivation: The Gettering**

It is well known that, commercial silicon solar cells are fabricated on low cost substrates that have high concentration of impurities and defects. Gettering techniques eliminate or reduce contaminant impurities in these substrates by localising and blocking them away from the active region or totally removing from the device. In commercial solar cells fabrication, gettering of impurities is obtained by Phosphorous or Aluminium diffusions. Aluminium is used to create back surface field and to make a back contact. This element not only does the Al layer produce a BSF it also helps in the passivation of defects in the back. The *Al-Si* alloy works well for effective gettering of metallic impurities **[29].** The effect of phosphorous gettering is used during the step of the emitter formation. In this case, gettering of metallic impurities takes place as a result of enhanced solubility of metallic impurities in *SiP* particles formed by heavy *P* diffusion in silicon these particles act as the gettering sites **[30].**

- **Bulk Passivation: Hydrogenation**

Hydrogen has received attention in various solar cell types. It was discovered that the incorporation of Hydrogen strongly improved the properties of amorphous *Si* (*a-Si:H)* [**31**]. This improvement is attributable to the ability of H to saturate Silicon dangling bonds which otherwise form defect states in the band gap of a- Si and act as recombination centers for the charge carriers [**32**]. A similar beneficial effect has also been found for grain-boundary passivation by *H* in poly-*Si* **[33-34**].

I.10 Conclusion

In this chapter, the fundamental principles of solar cell devices are discussed; attention is given to a description of the basics of the semi-conductor materials and particularly the PN junction, solar parameters influencing the operation of solar cells, main materials used in the PV technologies, efficiency loss mechanisms in PV cells and the different methods used to reduce these losses.

REFERENCES

[1] G. N. Tiwari, Solar Energy, Fundamentals, Design, Modelling and Applications, Narosa, Publishing House, New Delhi, India, 2004.

[2] A E. Becquerel, Comt Rend. Academie d. Sciences **9** (1839) p. 561.

[3] A. Goetzberger and Volker U. Hoffmann, Photovoltaic solar energy generation, Springer Verlag Berlin 2005.

[4] Y. Hishikawa, Y. Imura and T. Oshiro, Proc. 28th IEEE Photovoltaic Specialists Conf. *(*2000), Anchorage, pp. 1464-1467.

[5] J. E. Philips, J. Titus and D. Hofmann, Proc. 26th IEEE Photovoltaic Specialist Conf.(1997), Anaheim, pp. 463-466.

[6] S. S. Hegedus, Prog. Photovolt: Res. Appl.1997, Vol. 5, pp. 151-168.

[7] M. A. Green, Silicon Solar Cells: Advanced Principles and Practice. 1995, publisher: Centre for Photovoltaic Devices and Systems, University of New South Wales.

[8] C. Honsberg, S. Browden http://pveducation.org/pvcdrom.

[9] T. Markvart, L. Castaner, Solar Cells: Materials, Manufacture and Operation 2005, Hardcover, Elsevier Science & Technology.

[10] W. P. Hirshman, G. Hering and M. Schmela, Cell and Module Production 2007: Photon International, 2008, 152.

[11] M. A. Green, Physica E,2002, 14(1–2), 65–70.

[12] G. N. Tiwari and Swapnil Dubey, Fundamentals of Photovoltaic Modules and Their Applications, 2010 Royal Society of Christry.

[13] P. A. Lynn, Electricity from Sunlight: An Introduction to Photovoltaics, Wiley and Sons, first edition 2010.

[14] V. M. Fthenakis, Renew. Sustain. Energ. Rev., 2004, 8, 303–334.

[15] Gopal Nath Tiwari,Basant Agrawal, Building Integrated Photovoltaic Thermal Systems: For Sustainable Developments, RSC publishing,1st Edition., 2011

[16] J. AbuShama, S. Johnston, T. Moriarty, G. Teeter, K. Ramanathan and R. Noufi, Progress in Photovoltaics: Research and Applications, 2004, 12, 39.

[17] J. Y. Kim, K. Lee and N. E. Coates, Science J., 2007, 317(5835), 222

[18] S. A. McDonald, G. Konstantatos, S. Zhang, P. W. Cyr, E. J. Klem, L. Levina and E. H. Sargent, Nat. Mater., 2005, 4(2), 138.

[19] A. Mayer, Mater. Today, 2007, 10(11), 28.

[20] M.A. Green, K. Emery, Y. Hishikawa and W. Warta, Prog. Photovolt: Res. Appl. 2011; 19:84–92.

[21] S.M. Sze, K.Ng. Kwok, Physics of Semiconductor Devices, third edition, Wileyand Sons, 2007

[22] KP. Bhuvana et al, Journal of alloys and compounds, 2009 473(1-2): P 534-537.

[23] L. zeng, Design and processing. 2008; MIT.

[24] W. Michaelis and M. H. Pilkhun, Physica Status Solidi A, vol. 36, pp. 311-319, 1969**.**

[25] J. Dziewior and W. Schmid, Applied Physics Letters, vol. 31, pp. 346-348, 1977.

[26] W. Shockley and W. T. Read, Physical Review, vol. 87, pp. 835-842, 1952.

[27] R. N. Hall, Physical Review, vol. 87, pp. 387, 1952.

[28] A. G. Aberle, Advanced surface passivation and analysis: Centre for Photovoltaic Engineering, University of New South Wales, 1999.

[29] C.S. Solanski , Solar photovoltaics: Fundamentals, technologies and applications eastern Economy Edition, 2009.

[30] B. Sopori, L. Jastrzebski and T. Tan, 1996. Proc. 25th IEEE Photovoltaic Specialists Conf., Washington DC, 1996, pp. 625-628.

[31] W. Paul, A. Lewis, G. Connell, and T. Moustakas. Solid State Commun **20** (1976).

[32] J. I. Pankove. Applied Physics Letters **32**, 12 (1978).

[33] J. I. Pankove, M. A. Lampert, and M. L. Tarng. Applied Physics Letters **32**, 7 (1978).

[34] C. H. Seager and D. S. Ginley. Applied Physics Letters **34**, 5 (1979).

CHAPTER TWO

THIRD GENERATION SOLAR CELLS

II.1 Introduction

'Third Generation Photovoltaics' has recently become the latest term in the solar cell domain. Research in this new subject is continuously increasing, in order to manufacture high efficiency cells by means of low-cost materials and technologies. In a global sense, this generation try to overcome the two most important loss mechanisms in solar cells (thermalization and transmission), by the use of the following concepts – multiple gap tandem cells, intermediate band solar cells, impurity photovoltaic effect, hot carrier solar cells and spectrum conversion solar cells …..Etc. In this chapter, we will explain what is meant by Third Generation concepts, Shockley Queisser limit and we will discuss these concepts in detail and explain more particularly the IPV effect on which our study is based.

II.2 Shockley Queisser Limit

New concepts for photovoltaic conversion of solar energy, which aim to obtain a higher efficiency than Shockley Queisser limit, have largely studied during the last years and the term 'third generation' has been invented for this group of concepts. The term ''third generation' refer to any device that can exceed the theoretical solar conversion efficiency limit for a single energy threshold material. This limit was calculated by Shockley and Queisser as 31% under 1 sun illumination and 41% under maximal concentration of sunlight.

Shockley and Queisser in 1961 **[1]** used a number of idealising suppositions which give the maximum possible efficiencies from a solar cell. The basic factors to calculate this limit are the detailed balance formalism and plank's law. Among their suppositions are the perfect absorption with each photon creating one electron hole pair, perfect collection of carriers and radiative recombination as the only allowed recombination mechanism. They assumed zero contact resistance and infinite mobility. The band gap of their idealised cell was optimised to give a maximum efficiency. The band gap describes the threshold for absorption of light, which is assumed to be perfectly abrupt i.e. no light is absorbed below the band gap and every photon is absorbed above the band gap. Therefore the ways to exceeding the Shockley-Queisser limit concentrate on the below band gap and the thermalization loss mechanisms in figure **II-1**.

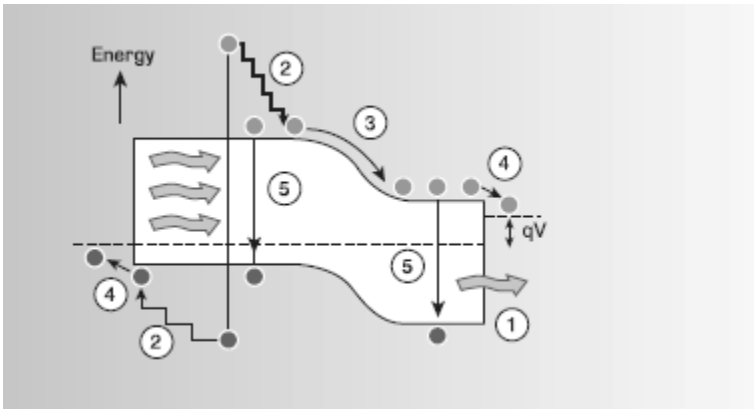

Figure II-1: Loss processes in a standard solar cell: (1) non-absorption of below band gap photons; (2) Lattice thermalization loss; (3) and (4) junction and contact voltage losses; (5) recombination loss.

II.3 Price and Efficiency Projections for Solar Cell Generations

The term third Generation obtains from the evolution of photovoltaic technologies. To know what is meant by the term 'third generation solar cells' we should understand the plot of the efficiency (%) as a function of PV module price (*US$/m*^{2}) and PV power price (*US$/Wp*) (see figure **II-2**). In this figure, the region I, II and III are related with the first, second and third generations PV modules respectively.

The first generation of solar cells have high-cost, high-efficiency, high quality and are approaching the limiting efficiencies for single band gap devices. From the figure **II-2**, we can notice that the efficiency varies between 15% and 20% and the module cost varies between US$180/m^2 and US$500/m^2 but the power cost is also high, between US$3.00/Wp and US$3.50/Wp. So, these devices are not likely to achieve lower costs than US$1/W. The second generation of solar cells are low-cost, low-efficiency cells. These are most frequently associated with thin film solar cells designs (*CdTe*, *CdS*, *CuInSe2*, amorphous silicon, and poly-silicon….etc) that use minimal materials and cheap manufacturing processes such as vapour deposition and electroplating. Such processes can bring costs down to a little under *US$0.50/W*, but as a result of the defects inherent in the lower quality processing methods, this generation has low efficiencies compared to first generation. The cost ranges between *US$50/m*^{2} and *US$120/m*^{2} while the power cost is between *US$0.50/Wp* and *U S$$3.50/Wp*. The efficiency is however low and ranges between 6% and 15%. Both the organic tandem solar cells with the maximum efficiency of 6.5% and the dye sensitized solar cells can be classified as second generation solar cells due to their low efficiency and cost of fabrication.

The idea for third generation solar cells is to attain efficiency > 31% (Queisser-Shockley limit) while maintaining the cost very low. The price of this generation is expected to be between *US$0.20/Wp* and *US$0.50/Wp*. The module power cost is targeted to be about *US$50/m2* and *US$200/m2*.

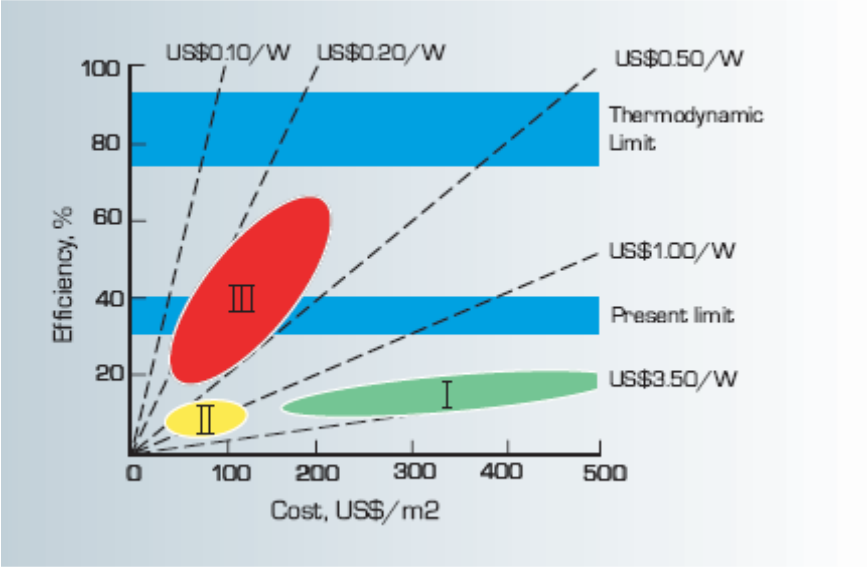

Figure II-2: PV efficiency against PV cost and PV power cost for the three photovoltaic generations **[2].**

II.4 Different Third Generation Solar Cells

Several new concepts to increase the conversion efficiency of solar cells have been presented over the last few years, from either a theoretical or experimental point of view **[3–6].** They incorporate new free carrier generation mechanisms not taken into consideration in the Shockley–Queisser theory. All these concepts (called third generation concepts) are based on tackling one or both of the "below band gap" or "thermalization" loss mechanisms. A critical goal for this generation is the development of high efficiency, low cost photovoltaic structures which can reach the thermodynamic limit of solar energy conversion. Different techniques and approaches are used to enhance the conversion efficiency in third generation photovoltaics, including multiple gap tandem cells, intermediate band solar cells, impurity photovoltaic effect, hot carrier solar cells, spectrum conversion solar cells and thermovoltaics…etc. Some of these technologies are already on the market whereas others are

currently under active research. We will explain in the following section many third generation solar cells with some of their advantages and disadvantages.

II.4.1 Multiple Junction (MJ) Solar Cells (Tandem Solar Cell)

The tandem cell approach has been the most successful approach to date in improving solar cell performance. Tandem solar cells allow higher conversion efficiencies thanks to their capability to absorb light across a wider spectrum than conventional single-junction cells. This type consists of a multiple, single junction solar cells stacked on one another, with each solar cell absorbing part of the solar spectrum closest to its band gap. The MJ solar cells were first deployed for satellite power applications. When this type combined with solar concentrators, it is expected that these cells will dominate in near future the terrestrial exploitation **[7–9**]. At present, triple junction solar cells are used to reach efficiencies of up to 41% and *InGaP/GaAs/Ge* is a very common triple junction solar cell with maximum efficiency of 40.7% **[10].** Multi-junction solar cells are capable of attain such high efficiencies by separating the absorption of the polychromatic solar spectrum into semiconductors with different bandgaps. So, the high energy photons are absorbed by the high bandgap material and low energy photons are absorbed by low band gap material. This way allows a large portion of the solar spectrum to be absorbed and avoids thermalization losses. By stacking an infinite number of junctions, theoretically, the efficiency increases at 86% under maximum solar irradiance **[11].**

There are two configurations in which solar cells can be stacked (parallel and series configuration). Figure **II-3** shows the difference between the two configurations. For the so-called parallel configuration or multi-terminals tandem (figure **II-3** Right), different p-n junctions are grown on individual substrates. Contacts are formed at each junction and later the different junctions are separated from the substrate and are stacked. For each p-n junction different contacts are used. In this configuration, there is no limitation on the maximum current generated by the solar cell and the arrangement of band gaps is less important. On the other hand, each cell grown requires its own substrate and the use of many substrates increases the cost of the solar cell and complicates its fabrication. The second configuration or monolithic multi-junction cells is mostly used, they integrates the cells monolithically with tunnel junctions joining them in series. As for thin film solar cells with heterojunction, it is important to keep the lattice mismatch between each successive layer to a minimum in order to avoid dislocations at the interface and therefore to reduce non radiative recombination

which can diminish the efficiency of solar cells. For these reason, *InGaP/GaAs/Ge* triple-junction cells have proven to be extremely efficient as all three layers are strictly lattice matched but *InGaP/GaAs/Ge* structures do not have the optimum arrangement of band gaps to maximize efficiencies. Monolithic multi-junction cells are limited as they are connected in series. Therefore, in this structure the total current output is limited by the lowest current producing junction and the excess current generated is wasted in this structure. In the case of *InGaP/GaAs/Ge*, the Ge subcell produces excess current that is wasted. Therefore it would be advantageous to have different combinations of band gaps in the three layers**.** With Ge as the bottom cell, the optimum middle and top bandgaps are 1.16 eV and 1.73 eV respectively. This structure could theoretically attain efficiencies more than 60% under 500 × concentrations **[12]**

Tandem cells are also used to develop the performance and reliability of terrestrial amorphous silicon cells with efficiency as high as 13% confirmed for triple junction cells based on the Si-Ge:H alloy **[13].**

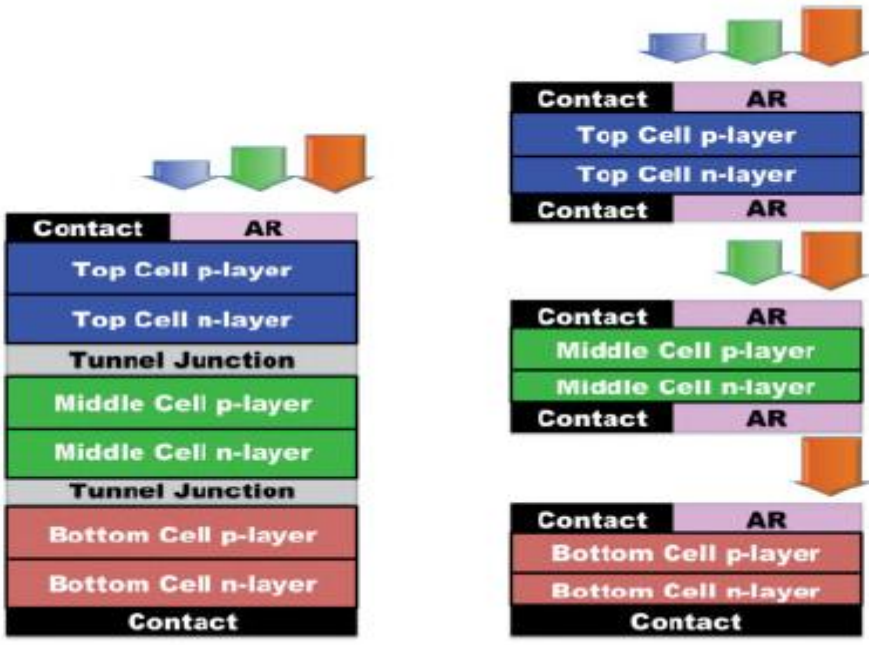

Figure II-3 Monolithic (two-terminal) multi-junction solar cell (left). Mechanically stacked (multi-terminal) multi-junction cell (right)**[14]**.

II.4.2 Spectrum Conversion Solar Cells: Down and Up Conversion

Some third generation techniques are focused on adjusting the bandgap of the solar material to match the spectrum of the sun. In the last years, research has been done to convert the spectrum from that of the sun to one more suitable for the solar cell. In this technique, the low bandgap photons are up-converted into high energy photons and high bandgap photons are down-converted into multiple low energy photons. These ideas are also well established as new third-generation-concepts within the PV community.

- **Up Conversion**

The up-conversion solar cell system is schematically represented in Figure **II-5**.

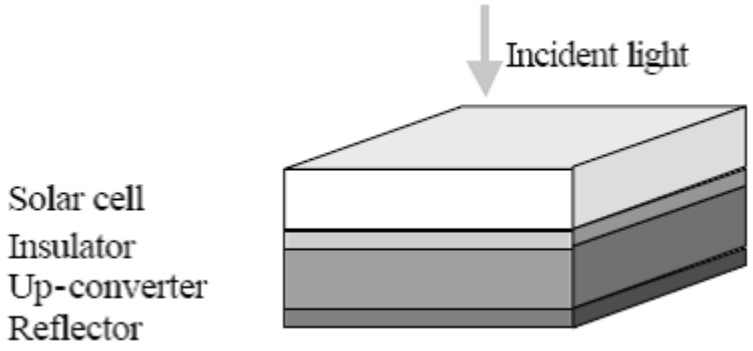

Figure II-5 Conventional solar cell in combination with an up converter

It is based on a conventional bifacial single junction solar cell and an up-converter, which partially transforms the sub-band-gap photons transmitted by the solar cell into high-energy photons. The up-converter is electronically isolated from the solar cell and located behind it. A perfect reflector is located at the rear surface of the up-converter.

Up conversion represents a new method to exploit subband gap photons and therefore diminish the transmission losses of a solar cell. Without the up converter the sub-band gap photons will pass throughout the material without being absorbed. Inside it the sub-band gap radiation is transferred to photons with energies above the band gap and these photons can then be absorbed in the solar cell. Up-conversion involves a sequential excitation of electrons

into an excited state via a real, lower-lying metastable excited state. A schematic energy-level diagram of such an up-converter is shown in Figure **(II-6).** It consists of a material with a band-gap equal to or larger than the band-gap of the solar cell and has intermediate levels (*IL*) with energy E_1 above the valence band edge.

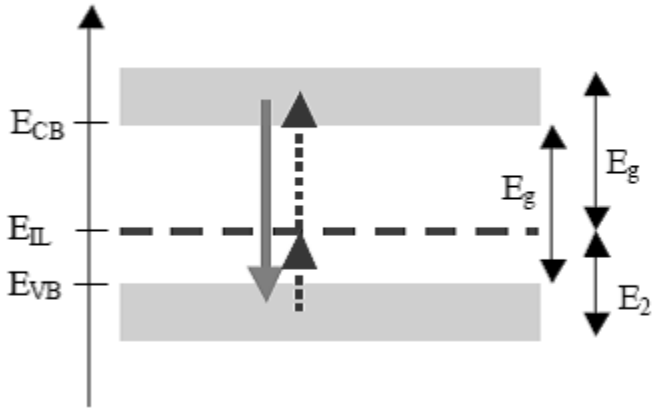

Figure II-6 Energy diagram for an up-converter.

The absorption of sub-band-gap photons in the up-converter leads to the generation of electron hole-pairs via transitions from the valence band into the *IL* and from the *IL* into the conduction band. A fraction of the excess electron hole pairs generated inside the up-converter recombines via radiative band to band-transitions (solid arrow in Fig.II-6), which is accompanied by the emission of photons with energies above the band-gap. The absorption of these photons leads to an additional generation rate of electron hole pairs in the solar cell.

In up conversion system, recombination of electrons and holes through the intermediate level is possible only inside the up-converter. In this system an additional advantage is that the materials of the up-converter and of the solar cell can be optimised independently **[15].**

Common up converter materials usually consist of a rare earth doped into inorganic host materials. These UC materials are usually in the form of phosphors, crystals or fibres. Phosphors would be the most practical morphology for solar cell applications since they are more versatile **[16].** Trivalent rare-earth-doped materials are usually used for potential UC devices. Ref. **[17]** explains the use of terbium-doped lanthanum fluoride and thulium-doped calcium tungstate materials for application with photovoltaic (PV) devices. A limiting

efficiency of 63.17% is found for maximum concentration of the sunlight with a luminescent up converter on the rear surface. Efficiencies of up to 47.6% are predicted for non-concentrated sunlight for a solar cell in combination with an improved up converter. However, these efficiencies require a semiconducting material with a band gap of about 2 eV **[15].**

- **Down Conversion**

For down-conversion DC, the luminescent converter is located on the front surface of a solar cell, which has a band-gap energy E_g. High-energy photons with energy $>2Eg$ are absorbed by the converter and well down-converted into two lower energy photons with energy $>E_g$, which can both be absorbed by the solar cell. Therefore, the *DC* can increase current by converting ultraviolet (*UV*) photons to a larger number of visible photons. Fig.**II-7a** shows a device schematic of a solar cell in combination with a down-converter. The down converter ideally transforms incident photons with energies exceeding n times the band-gap energy of the solar cell material into n lower energy photons, which can solar cell then be used for the generation of n e-h-pairs inside the solar cell. Down-conversion therefore represents a method for multiplying the e-h-pair generation per incident high-energy photon and can be used to reduce the thermalization losses. Because the absorption of high-energy photons in the solar cell must be avoided, the converter must be located on the front surface for semiconductor solar cells (Fig**.II-7a**).

The converter is modelled as a semiconductor with one intermediate level of energy Eg above the valence band edge. It is electronically isolated from the solar cell – the coupling between the converter and the solar cell is purely radiative. With a down-converter on a solar cell (Figure II-7 a), high-energy photons are absorbed by a band-to-band transition (green arrow, Figure II-7 b). The two-step recombination of the generated electron.hole pair via the intermediate level (red arrows Figure II-7) is accompanied by the emission of two lower-energy photons, which can both be used for the generation of electron-hole pairs. (Center for Third Generation Photovoltaics, University of New South Wales, Sydney, Australia). A maximum efficiency of 38.6% was found for non-concentrated sunlight and for a converter with one intermediate level **[18]**.

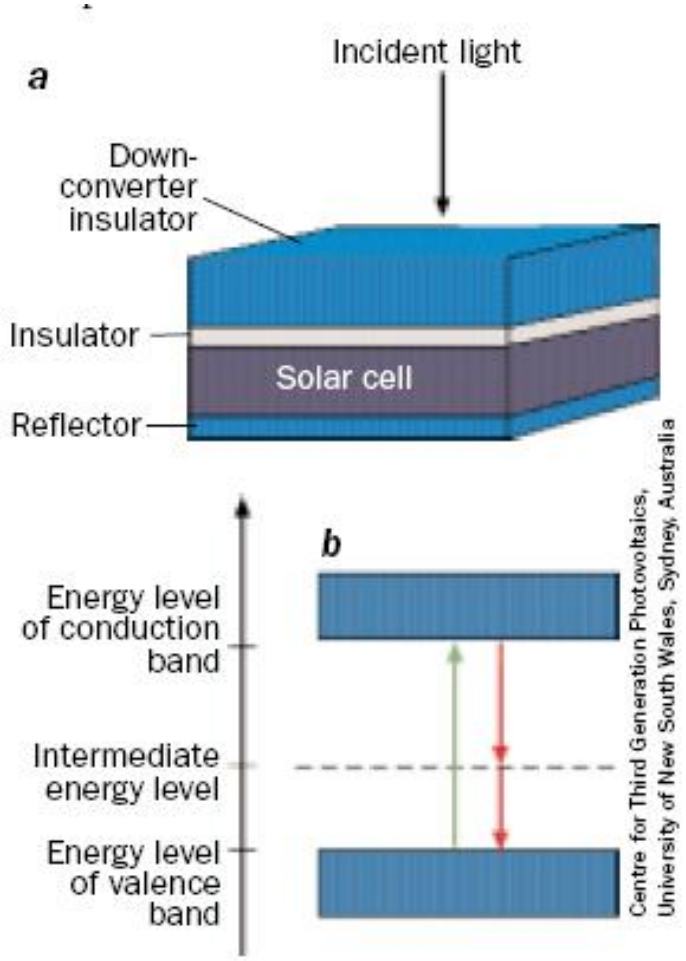

Figure II-7 a) Combination of an ordinary solar cell and a down converter, **b)** Energy diagram for a down-converter

II.4.3 Hot Carrier Solar Cells

Hot carrier cell has been studied theoretically as a mean of tackling the thermalization loss mechanism in a solar cell **[19-20]** and therefore it contributes to enhance cell efficiencies. Photons with elevated energies than the band gap energy of an absorbing material generate electron-hole pairs, and they are excited to the energy states far above conduction and valence band edge for electrons and holes, respectively. These high energy carriers first interact with each other and repopulate obeying the Fermi distribution function with a carrier temperature higher than that of the lattice. Then these hot carriers immediately loss (within a few picoseconds) their excess kinetic energy and relax to the band edge by thermalization, that is,

interaction between the hot carriers and phonons. This thermalization process is the principal limiting factor for the conversion efficiencies in the conventional single band gap solar cells. This idea permits thermalization within populations of hot carriers but does not permit thermalization of these populations with the lattice. If the lattice of the absorber material is at ambient temperature carrier collection has to arise before the average thermalization time of charge carriers within the absorber -of the order of a picosecond. Hence in order to be effective such a cell must ensure carriers are collected before they can interact with the lattice, either by doing so very quickly; or by slowing thermalization; or by substantially increasing the ratio of the rate of radiative recombination/emission to the thermalization rate (i.e. from the ratios for bulk materials of about for GaAs and for Si to values closer to 1, most likely in low dimensional structures). Figure **II-10** shows the band diagram of a hot carrier absorber with selective energy contacts for electrons and holes on opposite sides of the device. The device consists of the hot carrier absorber, at TH and selective energy contacts in which the carriers cool from TH to the ambient temperature, TA**.**

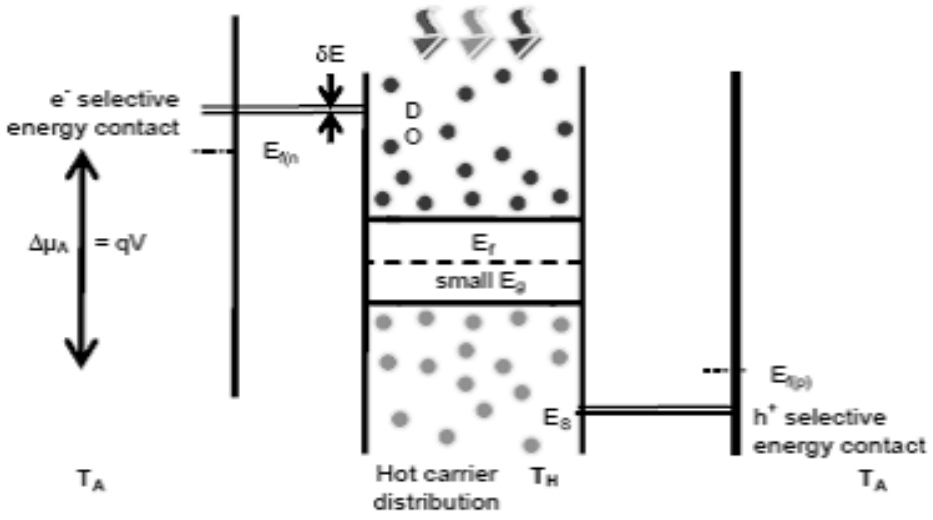

Fig II-10: Concept of a hot carrier solar cell

In ref **[19],** they proposed the idea of using hot carriers for photovoltaic devices and showed that the conversion efficiency of more than 60% is theoretically reachable under 1 sun illumination in such hot carrier solar cells. One practical structure of a hot carrier solar cell is to use a photon absorbing layer, in which hot carriers are slowly cooled, sandwiched between

two selective energy contacts (SEC) as schematically illustrated in Figure **II-10 [21-22].** A SEC is an energy filter allowing the carriers with specific energy to pass through and hot carriers are collected through the SEC from the absorber to the outer contacts. Double barrier resonant tunnelling diode (RTD) structures such as Si quantum dots embedded in SiO2 barrier layer are considered to be a promising candidate for SEC **[23,24].** until now, advancement on research of hot carrier solar cells have been presented theoretically and only few experiments particularly on exploring appropriate materials or structures for SEC have been reported. The limiting efficiency for the hot carrier cell is about 65% at 1 sun and 85% at maximum concentration **[2, 19, 21].**

II.4.4 Intermediate-band solar cells

An intermediate-band solar cell (*IBSC*) is a photovoltaic device conceived to exceed the limiting efficiency of single-gap solar cells thanks to the exploitation of the electrical and optical properties of intermediate-band (IB) materials. This type of material takes its name from the existence of an extra electronic band located in between what in ordinary semiconductors constitutes its bandgap, *E*g. The *IB* divides the bandgap *E*g into two forbidden energy intervals (sub bandgaps), E_L and E_H as drawn in figure **II-11.**

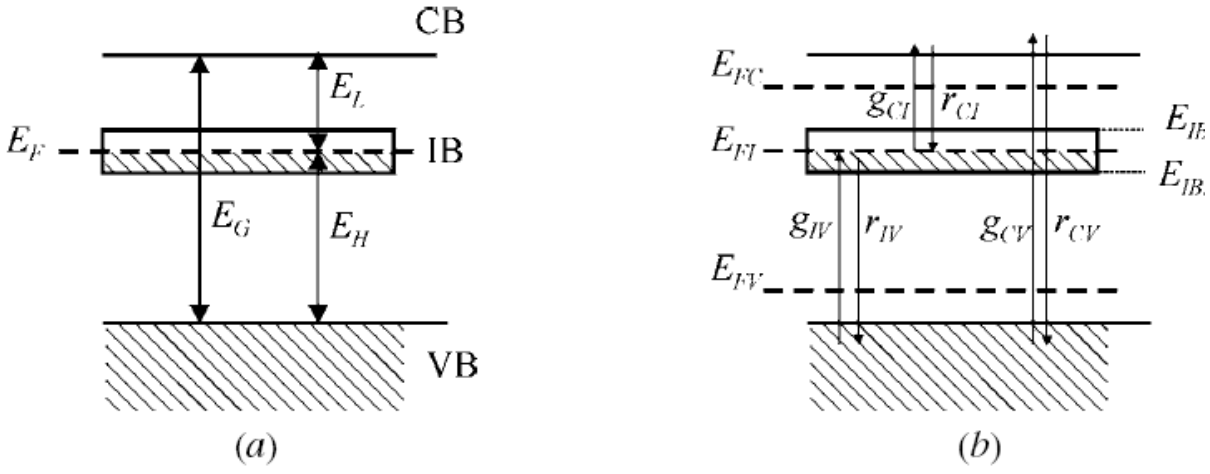

Figure II-11. Representation of the simplified band structure of an intermediate band material. (a) In equilibrium, with the IB half-filled with electrons and (b) out of equilibrium. (The hatched regions indicate energy states predominantly filled with electrons)

The fundamental concept in this solar cell type is that a narrow density of states within the bandgap of a semiconductor can allow sub-bandgap absorption while maintaining the same open-circuit voltage. The key is to have multiple quasi-Fermi levels present with the same system[14] as shown in Figure **II-11b [4, 20, 25].** Three different absorption processes are available in such a system: Valence Band (VB) → IB, IB →Conduction Band (CB) and VB→CB. These three absorption processes allow the creation of three quasi-Fermi levels corresponding to the population of holes in the VB, electrons/holes in the IB and electrons in the CB.

Introducing impurities into Silicon to extend the sub-bandgap response of these cells and therefore increase cell efficiency was the first experimental basis for this solar cell type **[26].** After that the researchers use the quantum dots [QDs] to form the intermediate band **[27, 28].** Fig.**II-12**. shows the basic concepts of such a structure. The QDs have a lower bandgap than the barrier regions and as a result of quantum confinement, the QDs form discrete energy levels. Due to the periodic arrangement and close proximity of the QDs, the discrete energy levels overlap and form mini-bands allowing for sub-bandgap absorption. One important requirement for the operation of IB solar cells is the IB Fermi level must reside within the IB **[29-30].** This allows sufficient numbers of electrons in the IB to be promoted into the CB. It is also beneficial to have no overlap in the absorption coefficients between the three transitions **[31].** If this is not the case, high energy photons that should transfer electrons between the VB and CB could be absorbed in a VB → IB transition, losing some of the energy in a similar way that a traditional single-junction cell experiences blue losses.

In ref. **[32-33]** the GaAs layers with imbedded InAs and GaSb QDs are used to fabricate a Test cells. All experimental cells of this type shown to date exhibit lower overall efficiencies than cells fabricated without QDs[14], due to lower open circuit voltages. This lower Voc is attributed to non-radiative recombination between the CB and VB suggesting that current growth techniques introduce defects lowering the efficiency of these cells. However, the experiments do suggest it is possible to have three separate quasi-Fermi levels.

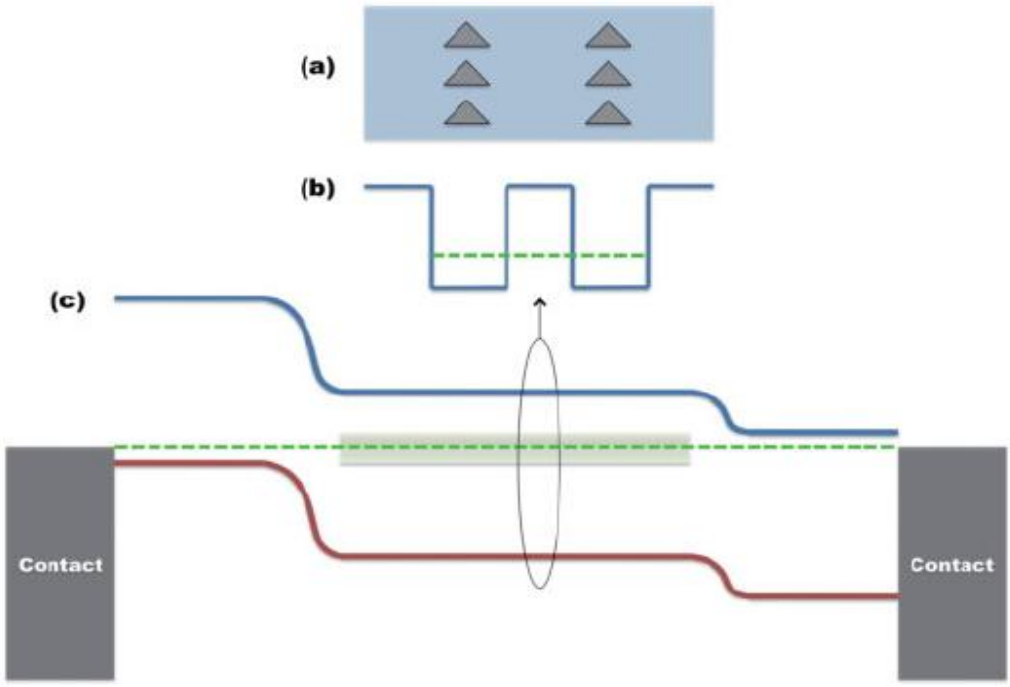

Figure II-12. (a) Periodic arrangements of quantum dots lead to the formation of mini-bands as seen in (b). The mini-band acts as the IB and allows the promotion of electrons from the quantum dot to the barrier material via photons. (c) The quantum dots are placed in-between a p- and n-type barrier layer.

The QDs are very small and therefore it does not absorb much light. In order to have enough QDs to significantly improve the photocurrent, it is necessary to have several layers of QDs. Unfortunately, the growth of multiple layers of QDs results in additional structural damage, which decreases efficiencies [34]. The lower efficiencies have been attributed to the creation of threading dislocations from the QDs in the intrinsic region **[35].** The origin of these dislocations is the lattice mismatch between the QDs and buffer material. Ref. **[36]** showed that the addition of strain compensating layers between each QD layer has been shown to improve performance and can also increase the short circuit current of QD IB solar cells.

In addition to QDs, there have been focused efforts in exploring alloys that may feature an IB using computational techniques. Certain alloys such as Ga3P4Ti **[37-38]** are expected to feature IBs. It is also predicted that CuGaS2 **[39]** can form an IB if transition metal impurities are added in which the impurity levels are located in the band gap. The

maximum efficiency of 63.2% is achieved for a cell of gap 1.95 eV with the IB Fermi level located at 0.71 eV from one of the bands. This efficiency is higher than the one corresponding to two series-connected ideal cells in tandem, of 54.5% (for band gaps of 0.8 and 1.54 eV).

II.4.5 Impurity Photovoltaic Effect

II.4.5.1 Introduction

It is well known that one of the efficiency losses present in solar photovoltaic energy conversion comes from the fact that the semiconductor material used to make the solar cell can not convert the long wave length photons; these photons do not excite carriers from the valence band to the conduction band. To improve cell infrared response and therefore solar cell conversion efficiency, several approaches have been studied in these last few years as we mentioned above. The impurity photovoltaic (IPV) effect is one of the approaches used to enhance cell infrared response whereby deliberate addition of an impurity into a solar cell provides a multi-step absorption mechanism for sub gap photons to create electron-hole pairs, enabling the infrared portion of the solar spectrum to contribute to solar cell efficiency**.**

In conventional solar cells only photons with energy higher than the band gap energy generate electron-hole pairs. Photon 1 and 2 will pass through the solar cell without being absorbed (Fig. II.13).

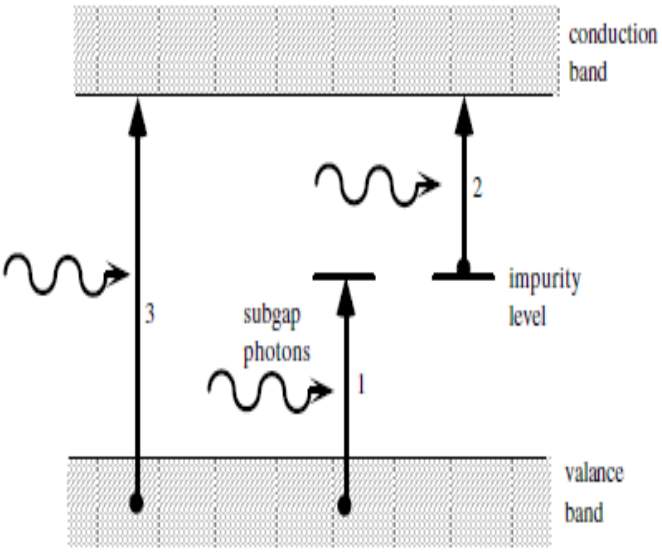

Figure II-13. The IPV effect: Sub gap photons create electron-hole pairs via impurity levels (1 and 2). Compare to intrinsic band-to-band absorption (3).

In solar cells based on the IPV effect, the defects create energy levels in the forbidden band of the semiconductor. The energy level in this case essentially functions as a relay point. Photon 1 will excite an electron from the VB into the Intermediate level (IL) and photon 2 will excite an electron from the IL into CB. Therefore, two sub-band gap photons are able to produce an electron-hole pair. At the same time, higher-energy photons are still able to excite electrons directly from the VB to the CB as usual. The IPV cells therefore offer theoretically higher conversion efficiencies than conventional cells because lower-energy photons can also be put to use.

The IPV concept was proposed by Wolf in 1960 **[40]** His idea was to use energy levels *Et* within the forbidden energy gap of the device to permit subband gap absorption by doping the material with suitable impurities. His results are very optimistic. Using defects to allow sub band gap absorption was studied also by Shockley and Queisser**[41],** they concluded that the presence of defects would augment the recombination in the device. Guttler and Queisser **[42]** confirmed these results for silicon doped with gold. Wurfel **[43]** showed theoretically that a midgap impurities could maybe increase the short-circuit current of a silicon solar cell, but at the same time lead to a degradation in the open-circuit voltage. In the begging of these studies (IPV studies) there was a considerable reservation over the benefit of the IPV effect. The IPV has been experimentally observed on silicon and other materials in several times. The impurity photovoltaic effect can, in principle, increase the conversion efficiency of a conventional single junction solar cell by the introduction of optically active impurities or defects into the device. These "defects" ideally allow electrons to be excited from the valence band to the conduction band via the deep defect level through the absorption of sub-band-gap photons. However, the existence of energy levels within the semiconductor band gap is considered as a source of non radiative recombination (Shockley–Read–Hall (SRH) recombination) at the same time. This recombination can negate any benefits. To overcome these problems and to tip the scale in favour of IPV, many studies have been presented recently. In 1994, Keevers and Green **[26]** presented a new treatment of the IPV effect, in which they use deep level impurities for changing the balance in favour of IPV cells. Their calculations, showed a small efficiency increase in silicon solar cell doped with indium. Schmeits and Mani **[44]** confirmed numerically an improvement in solar cell performances was theoretically possible if the correct device structure was selected. They proposed a new structure (p+-n-n+) , where the n layer close to the contact is essentially free

of deep defects safeguarding a reasonable value of the built-in voltage and the open circuit voltage.

One of the most important factors to improve solar cell efficiency due to the IPV effect is the location of energy levels of deep defects. Matsumura and Kasai **[45]** have studied the IPV effect theoretically in silicon solar cells as a function of energy level of deep defects. It was found that the deep defect level acts only to degrade cell efficiency markedly if its energy level is located near the middle of the band gap, because of electron-hole recombination through the defect. Many other authors **[46-47]** have studied the IPV effect on silicon doped with indium as optical doping. In last few years many studies have treated and described the IPV effect in large band gap materials such as the GaAs and the silicon carbide, they concluded that the choice of the host materials with large band gap can improve cell performances **[48-49].**

II.4.5.2 Theory of the IPV Effect

As we saw in chapter one, in the simple Shockley–Read–Hall (SRH) recombination model, electrons and holes are captured and excited thermally from an impurity with an energy level in the forbidden band gap of the semiconductor . To take account of the IPV effect, this model is extended with two impurity optical transitions as shown in Figure II-14.

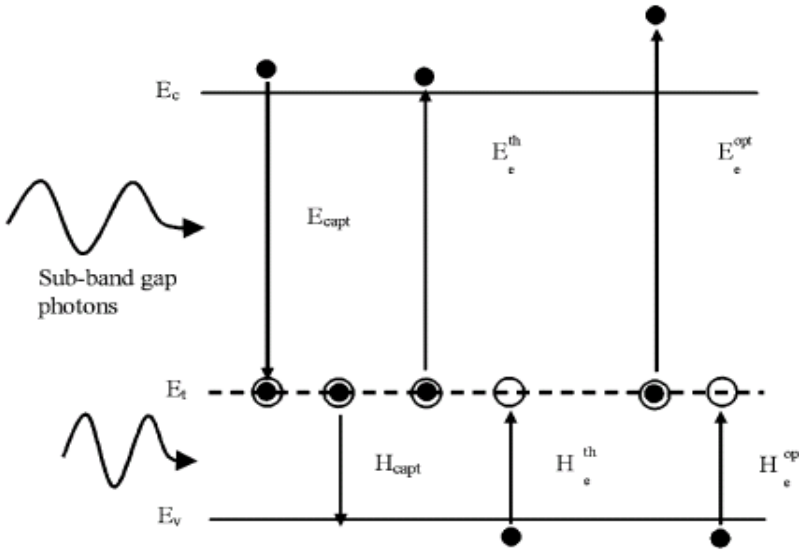

Figure II-14. Transitions between an IPV defect level and the conduction and valence bands: thermal capture (E_{capt} and H_{capt}), thermal emission (E^{e}_{th} and H^{e}_{th}) and the optical IPV emission (E^{e}_{opt} and H^{e}_{th}), where E stands for electrons and H for holes.

The modified SRH expression is then given by **[26]**

$$U = \frac{np - n_1^* p_1^*}{\tau_{n0}\left(p + p_1^*\right) + \tau_{p0}\left(n + n_1^*\right)} \qquad \textbf{(II-1)}$$

where n and p are the electron and hole concentrations respectively, and

$$n_1^* = n_1 + \tau_{n0} g_{nt} \quad \text{and} \quad p_1^* = p_1 + \tau_{p0} g_{pt} \qquad \textbf{(II-2)}$$

$$n_1 = N_c e^{\frac{-(E_c - E_t)}{KT}} \quad \text{and} \quad p_1 = N_v e^{-\left(\frac{E_t - E_v}{KT}\right)} \qquad \textbf{(II-3)}$$

n_1 and p_1 being the electron and hole concentrations after impurity doping. N_c and N_v are the effective densities of states in the conduction and valence bands. E_t is the impurity energy level, E_c and E_v are the conduction and valence band edge. In Eqs. (1) and (2), τ_n and τ_p are the Shokely Read Hall (SRH) lifetimes for electron and hole concentrations after illumination and are given by

$$\tau_{no} = \frac{1}{\sigma_n v_{th} N_t} \qquad \textbf{(II-4)}$$

and

$$\tau_{po} = \frac{1}{\sigma_p v_{th} N_t} \qquad \textbf{(II-5)}$$

where σ_n and σ_p are the electron and hole capture cross sections, v_{th} is the carrier thermal velocity and N_t is the impurity concentration. In Eq.(2), g_{nt}, g_{pt} are the electron and hole optical generation rates respectively and they are given by

$$g_{nt} = N_t \int_{\lambda_{n\min}}^{\lambda_{n\max}} \sigma_n^{opt}(x,\lambda)\phi_{ph}(x,\lambda)d\lambda \qquad \textbf{(II-6)}$$

and

$$g_{pt} = N_t \int_{\lambda_{p\min}}^{\lambda_{p\max}} \sigma_p^{opt}(x,\lambda)\phi_{ph}(x,\lambda)d\lambda \qquad \textbf{(II-7)}$$

Here, σ_n^{opt} and σ_p^{opt} are the electron and hole photoemission cross sections of the impurity, while $\phi_{ph}(x,\lambda)$ is the photon flux density at a depth x inside the lambartien cell and at wavelength λ. Moreover, $\phi_{ph}(x,\lambda)$ can be expressed as

$$\phi_{ph}(x,\lambda) = \phi_{ext}(\lambda)\frac{1+R_b e^{-2\alpha_{tot}(\lambda)(L-x)}}{1-R_b R_f e^{-2\alpha_{tot}(\lambda)L}} e^{-\alpha_{tot}(\lambda)x} \qquad \textbf{(II-8)}$$

where $\phi_{ext}(\lambda)$ is the external incident photon flux. L is the total length of the cell. R_b and R_f are the internal front and rear reflectances, respectively. $\alpha_{tot}(\lambda)$ is the total absorption coefficient. Finally, $\alpha_{tot}(\lambda)$ and R_f can be written as

$$\alpha_{tot}(\lambda) = \alpha_n(\lambda) + \alpha_p(\lambda) + \alpha_{fc}(\lambda) + \alpha_{e-h}(\lambda) \qquad \textbf{(II-9)}$$

and

$$R_f = 1 - \frac{1}{n^2} \qquad \textbf{(II-10)}$$

where α_n and α_p are the absorption coefficients for electron and hole photoemission from the impurity level. α_{fc} is the absorption coefficient for free carrier absorption, $\alpha_{e\text{-}h}$ is the band to band absorption coefficient and n is the refractive index of the semiconductor. and the parameters R_f and R_b describe the light trap of the solar cell.

II.4.5.3 Requirements for the IPV Effect

Many attempts of researchers to develop more efficient solar cells using the IR solar radiation based on the impurity photovoltaic effect have not yet been successful **[26, 44, 48, 50].** The main reason is the very strict requirements imposed either on the impurity atoms or on semiconductor host material. These limitations are:

- **Location of Energy Levels of Deep Defects**

One of the most key factors to improve solar cell efficiency using the IPV effect is the location of energy levels of deep defects. Matsumura and Kasai have studied the IPV effect theoretically in silicon solar cells as a function of energy level of deep defects **[45].** It was found that the deep defect level acts only to degrade cell efficiency noticeably if its energy level is located near the middle of the band gap, because of electron-hole recombination through the defect. The energy states created within the band gap act as additional recombination centers which can have severe influence on lowering the solar cell conversion efficiency. In this reference they also showed that if the energy level is carefully chosen far from the gap center, the IPV effect can contribute to improve the cell efficiency. The first work concerning the impurity photovoltaic effect has been first studied in silicon doped with gold **[42].** Gold has a donor level located in the middle of the band gap at 0.55 eV above the valence band. They confirmed that the incorporation of this midgap impurity in the silicon lead to a severe degradation in all solar cell performances. In the reference [26] it was shown that the non-mid-gap but deep level impurity atoms are more suitable. In addition, choosing such a deep level impurity allows at least one of the two transitions of the carriers (from the valence band to the impurity level and from there to the conduction band) to occur through strong thermal excitation rather than through weak optical absorption.

Indium is the most important optically active impurity used in the impurity photovoltaic effect studies and it was selected as one of the impurities that satisfy the previous condition. According to the calculations of the authors [26, 47], doping of silicon solar cells with an In impurity, creating an acceptor level of (0.157 eV), can lead to an increase in solar cell efficiency. It was proposed as a possible candidate for the IPV effect on the basis of optical modelling [26]. However, experimental attempts to use Indium to boost cell efficiency have failed because of the increased recombination described above, although improved absorption of infrared light was clearly observed **[44, 6, 26].**

In ref. **[51]** Johan Verschraegen et al observed that efficiency is maximal when the impurity is at 0.20 to 0.25 eV for the silicon solar cell and at 0.30 to 0.35 for GaAs solar cell above the valence band (see fig. **II-15**). (i.e. when the impurity located far from the middle of the band gap).

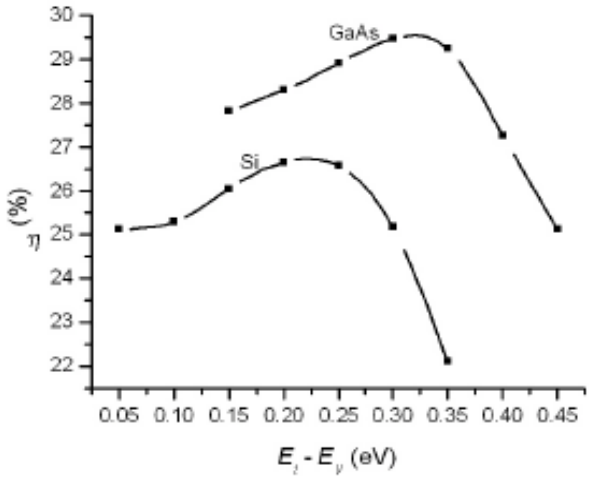

Figure II-15 : calculation of the conversion efficiency η as function of the energy level of the impurity $E_t - E_V$. Upper curve is for a GaAs solar cell, lower curve for a Si cell **[51].**

- **Impurity concentration factor**

The suitable impurity concentration value introduced in the semiconductor material is crucial for improving solar cell characteristics based on the IPV study. In the Ref. **[26,49],** where they introduced indium impurity into silicon lattice (in p^+-n-n^+ structure), they showed that both efficiency and short circuit current increase with increasing impurity concentration N_t when N_t is less than N_D (shallow acceptor concentration) and decrease above shallow concentration. An Indium concentration Nt lower than the base concentration N_D keeps the indium level fully occupied which allows sub-band gap photons to be absorbed by the electron photoemission process (from the In level to the conduction band). When indium concentration compensates the base doping $N_t>N_D$ (the semiconductor becomes P type), the hole photoemission process (from the In level to the valence band) is maximized. It competes with the first photoemission process and also with electron hole pair creation by intrinsic band-to-band absorption, which reduces the available photon flux and photocurrent of the cell. The open-circuit voltage decreases with increasing in impurity concentration. But it is still kept in moderate values before the impurity densities larger than the shallow doping density in the base (Nt>ND). This effect is due to the particular choice of the structure p–n–n+. This structure has an advantage to keep a high value for the built-in voltage and thereafter

keeps the impurity (In in previous work) level occupied. Therefore, the open-circuit voltage is safeguarded **[44].**

In practice, the maximum Impurity concentration that can be incorporated in silicon (or in other host material) is fixed by the solid solubility of each doping type in material. The solid solubility limit of impurities is defined as the maximum concentration of the impurity in the host semiconductor at which the impurity is homogeneously distributed in the host semiconductor without any precipitates. The presence of precipitates of a doping element in a semiconductor can therefore be used as an indicator that the solid solubility limit has been exceeded. So, to absorb maximum number of photons (through IPV effect) impurity concentration shouldn't be exceeded the solid solubility limit. Figure **II-16 and II- 17** show the influence of the impurity concentration on some silicon and silicon carbide solar cell performances according to ref **[48, 26]**

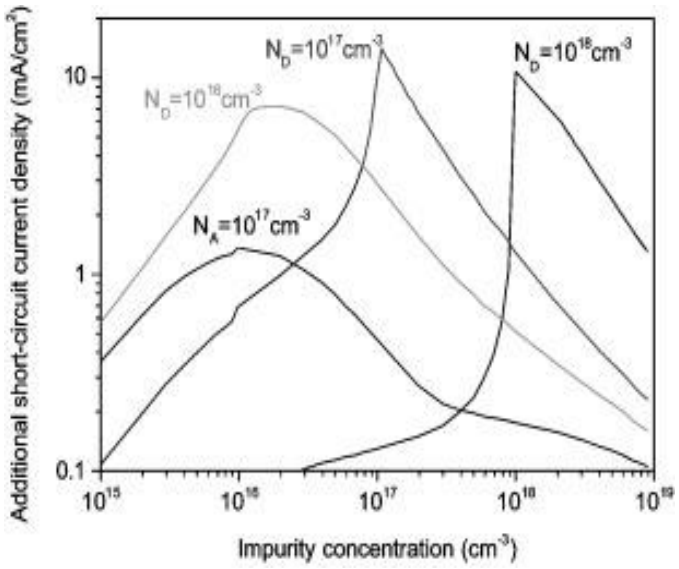

Figure II-16. Additional short-circuit current density as a function of the impurity concentration for ideal impurities in silicon carbide **[48].**

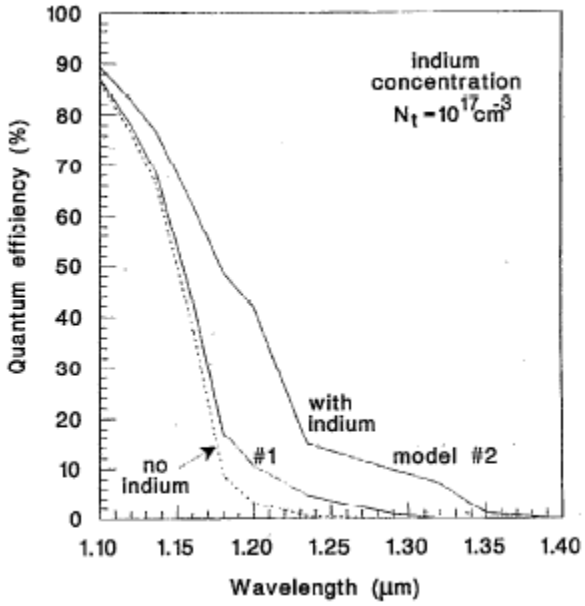

Figure II-17. Effect of indium incorporation on sub gaps spectral response **[26].**

- **Host material**

In the last few years many studies have been treated and described the IPV effect in large band gap materials, they concluded that the choice of the host materials with large band gap can improve cell performances. In ref. **[48]** Boron-doped cubic silicon carbide (3C-SiC:B) has been suggested as one possible candidate for the fabrication of an impurity photovoltaic (IPV) solar cell. The theoretical conversion efficiency predicted for a realistic IPV device based on 3C-SiC:B,N is 38%, assuming that the impurity level is 100% radiatively efficient. In ref. **[49]** Kelifi et al also studied the impurity photovoltaic (IPV) effect in a wide band gap GaAs solar cell doped with copper, containing three Cu acceptor impurity levels: copper level located at Ev+0.14 eV, second level located at Ev+0.40 eV and copper level at Ev+0.24 eV for investigating the role of more than one defect on PV cell based on IPV effect. They showed that when two levels are present in the band gap, the IPV effect is higher with only the deepest level present. They found also that the IPV effect gives an improvement in the short-circuit current density in the presence of A+B levels, but at the same time a decrease in the open-circuit voltage higher than in the presence of only the level B. This is due to the increase of recombination in the solar cell, which increases more drastically when the concentration of the defects is around the base layer doping (see figure **II- 18** and **II- 19**).

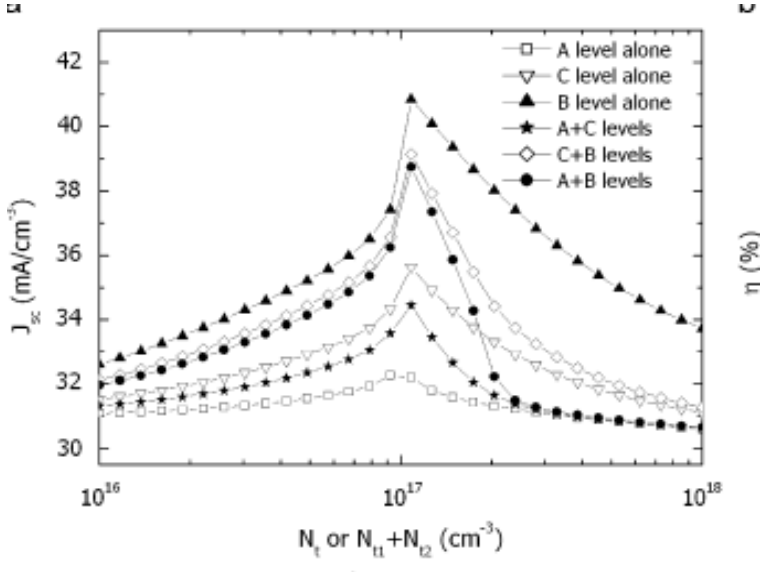

Figure II-18. Short circuit current density as a function of impurity concentration of an IPV GaAs cell with one or two IPV levels present. Calculated for a base doping density N_D = $10^{17}cm^{-3}$ **[49].**

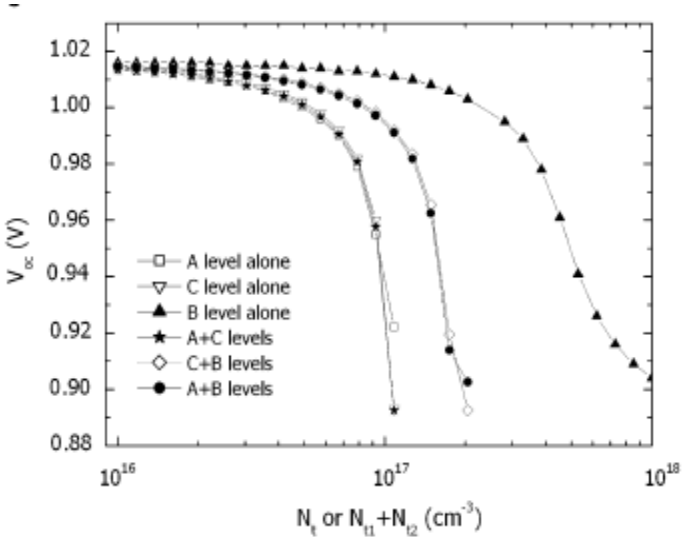

Figure II-19. Open circuit voltage as a function of impurity concentration of an IPV GaAs cell with one or two IPV levels present. Calculated for a base doping density N_D = $10^{17}cm^{-3}$ **[49].**

- **Effect of Light Trapping**

In chapter one, we described some techniques used for reduce optical and electrical losses in solar cells. As was mentioned in this chapter, the light trapping methods can reduce optical losses in solar cells. The degree of light trapping is adjusted by varying the internal reflection coefficients at the front and back of the cell R_b and R_f. The most previous works treated the IPV effect observed that the incorporation of IPV impurities into silicon or into another host material, together with the use of light trapping, leads to an increase in short-circuit current (see figure **II-20**). We will describe in chapter three the effectiveness of the optical confinement on silicon solar cells based on the IPV effect.

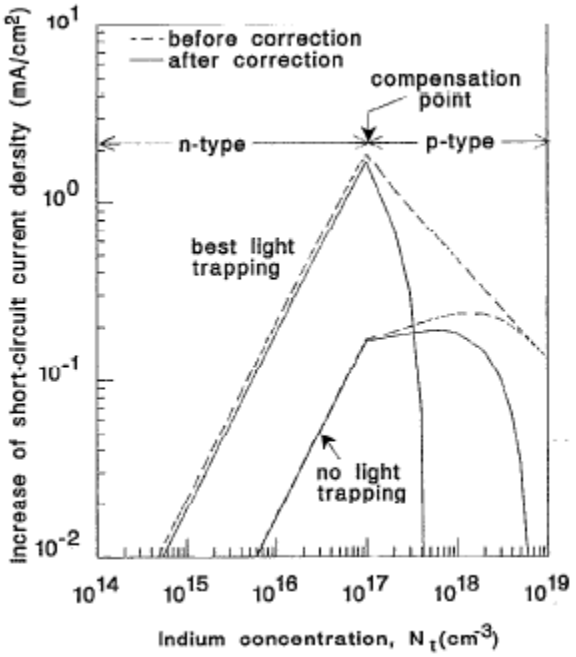

Figure II- 20. Short-circuit current improvement as a function of indium concentration for a fixed background donor concentration of 10^{17} cm^{-3}.
The effect of light trapping is included. [26]

II.5 Conclusion

This chapter summarised the main third generation concepts such as up-conversion, down-conversion, intermediate band solar cells, hot carrier cells, Multijunction cells and the impurity photovoltaic effect. These different new approaches, their advantages and limitations are described in this chapter.

REFERENCES

[1] Shockley and Queisser, Journal of Applied Physics, Volume 32 (March 1961), pp. 510-519

[2] M. A. Green, *Third Generation Photovoltaics: Ultra-High Efficiency at Low Cost*, Springer-Verlag, Berlin, (2003).

[3] R. Brendel, J.H. Werner, H.J. Queisser, Sol. Cells Mater. 41/42 (1996) 419–425.

[4] A. Luque, A. Mart!ı, Phys. Rev. Lett. 78 (1997) 5014–5017.

[5] S. Kolodinski, J.H. Werner, H.J. Queisser, Sol. Energy Mater. Sol. Cells 33 (1994) 275 285.

[6] H. Kasai, T. Sato, H. Matsumura, 26th PVSC, September 30–October 3, 1997, Anaheim, CA.

[7] H. Yoon, J. Granata, P. Hebert, R. R. King, C. M. Fetzer, P. Colter, K. M. Edmondson, D. Law, G. S. Kinsey, D. D. Krut, J. H. Ermer, M. S. Gillanders, and N. H. Karam, Prog. Photovoltaics 13, 133 (2005).

[8] A. Marti and A. Luque, Next Generation Photovoltaics: High Efficiency through Full Spectrum Utilization (Institute of Physics, Bristol, 2003).

[9] A. Luque and S. Hegedus, Handbook of Photovoltaic Science and Engineering (Wiley, Chichester, 2003).

[10] T. Takamoto, T. Agui, K. Kamimura, and M. Kaneiwa, in: Proceedings of the 3rd World Conference on Energy Conversion, Osaka, Japan 2003, Vol. 1, pp. 581–586.

[11] R. R. King, D. C. Law, K. M. Edmondson, C. Fetzer, G. S. Kinsey, H. Yoon, R. A. Sherif, and N. H. Karam, Appl. Phys. Lett. 90 183516 (2007).

[12] P. Wurfel, Physica E 14,18 (2002).

[13] Yang J, Banerjee A, Lord K, Guha S. In Proceedings of the 2ndWorld Conference on Photovoltaic Solar Energy Conversion, Vienna, 1998; p 387±390.

[14] G.F Brown and J. Wu, laser and photon Rev. 3,4(2009) 394-405.

[15] T. Trupke, M.A. Green and P. Wiirfel, J. Appl. Phys**. 92,** (2002), **41** 17.

[16] A. Shalav, B. S. Richards, T. Trupke, R.P Corkich, K.W Kramer, H. U. Gudel, MA Green 3rd word conf. o Photovoltaic energy conversion 2003 Osaka, Japan

[17] Saxena VN, Indian J. Pure Applied Physics 21(5) (1983). 306.

[18] T. Trupke, M. A. Green, P. Würfel, J Appl Phys 2002;92:1668.

[19] R.T. Ross and **A.J.** Norik, J. Appl. Phys. 53, 3318 **(**1 982).

[20] M. Green, Progress in Photovolr: Res. Appl. 9, 123 (2001).

[21] P. Würfel, Solar Energy Materials and Solar Cells 46, 1997, pp. 43-52.

[22] G. Conibeer, M. Green, R. Corkish, Y. Cho, E.-C. Cho, C.-W. Jiang, T. Fangsuwannarak, E. Pink, Y. Huang, T. Puzzer, T. Trupke, B. Richards, A. Shalav and K. Lin, Thin Solid Films 511-512, 2006, pp. 654-662.

[23] G.J. Conibeer C.-W. Jiang, D. König, S. Shrestha, T. Walsh and M.A. Green, Thin Solid Films 516, 2008, pp. 6968-6973.

[24] B. Berghoff, R. Rölver, B. Spangenberg, D. L. Bätzner and H. Kurz, Proc. of the 22nd European Photovoltaic Solar Energy Conference, 2007, pp. 571-574.

[25] A. S. Brown, M. A. Green, and R. P. Corkish, Physica E 14, 121 (2002).

[26] M.J. Keevers, M.A. Green, J. Appl. Phys. 75 (1994) 4022.

[27] A. Marti, L. Cuadra, and A. Luque, in: Proceedings of the 28th Photovoltaics Specialist Conference, Anchorage, AK, USA 2000, pp. 940–943

[28] A. J. Nozik, Physica E 14, 115 (2002).

[29] A. Marti, L. Cuadra, and A. Luque, IEEE Trans. Electron Devices 48, 2394 (2001).

[30] A. Marti, L. Cuadra, and A. Luque, Physica E 14, 150 (2002).

[31] L. Cuadra, A. Marti, and A. Luque, IEEE Trans. Electron Devices 51, 1002 (2004).

[32] A. Luque, A. Marti, N. Lopez, E. Antolin, E. Canovas, C. Stanley, C. Farmer, L. J. Caballero, L. Cuadra, and J. L. Balenzategui, Appl. Phys. Lett. 87, 083505 (2005).

[33] A. Luque, A. Marti, N. Lopez, E. Antolin, E. Canovas, C. Stanley, C. Farmer, and P. Diaz, J. Appl. Phys. 99, 094503 (2006).

[34] N. Lopez, A. Marti, A. Luque, C. Stanley, C. Farmer, an P. Diaz, J. Sol, Energy Eng. 129, 319 (2007).

[35] A. Marti, N. Lopez, E. Antolin, E. Canovas, A. Luque, C. R. Stanley, C. D. Farmer, and P. Diaz, Appl. Phys. Lett. 90, 233510 (2007).

[36] S. M. Hubbard, C. D. Cress, C. G. Bailey, R. P. Raffaelle, S. G. Bailey, and D. M. Wilt, Appl. Phys. Lett. 92, 123512 (2008).

[37] C. Tablero and P. Wahnon, Appl. Phys. Lett. 82, 151 (2003).

[38] J. J. Fernandez, C. Tablero, and P. Wahnon, J. Chem. Phys. 120, 10780 (2004).

[39] A. Marti, D. Fuertes Marron, and A. Luque, J. Appl. Phys. 103, 073706 (2008).

[40] M. Wolf, Proc. IRE 48, 1246 (1960).

[41] W. Shockley and H. J. Queisser, J. Appl. Phys. 32, 510 (1961).

[42] 0. Giittler and H. J. Queisser, Energy Convers. 10, 51 (1970).

[43] P. Wiirfel, Sol. Energy Mater. Sol. Cells 29, 403 (1993).

[44] M. Schmeits, A.A. Mani, J. Appl. Phys. 85 (1999) 2207.

[45] H. Kasai and H. Matsumura, Sol. Energy Mater. Sol. Cells **48**, 93 ~1997

[46] S.Zh. Karazhanov, J. Appl. Phys. 89 (2001) 4030.

[47] S. Khelifi, J. Verschraegen, M. Burgelman, A. Belghachi, Renew. Energ. 33 (2008) 293.

[48] G. Beaucarne, A.S. Brown, M.J. Keevers, R. Corkish, M.A. Green, Prog. Photovolt. Res. Appl. 10 (2002) 345

[49] S. Khelifi, M. Burgelman , J. Verschraegen and A. Belghach, Sol. Energy Mater. & Sol. Cells 92 (2008) 1559–1565.

[50] M. S. Saidov, *Geliotekhnika*, 2003, no. 3, pp. 3–6.

[51] J. Verschraegen1, S. Khelifi, M. Burgelman, A. belghachi, 21st European Photovoltaic Solar Energy Conference, 4-8 September 2006, Dresden, Germany.

Chapter Three

SCAPS Simulator, Results and Discussion

III.1 Introduction

This chapter consists of two main parts, the first part gives a detailed description of the Solar Cell Capacitance Simulator in one Dimension (SCAPS-1D) which is used to analyze and study the solar cell performances based on the impurity photovoltaic effect. The second part describes the solar cell structure, some physical parameters concerning both the impurity and the host material used in this study. This part also presents and discusses some results obtained using the Scaps 1D program.

III.2 Part I: SCAPS Simulator:

III.2.1 Principal Operations and Main Panels

Physically-based computer simulations of thin film photovoltaic devices have received more attention and become more and more mature over the past two decades since modelling of solar cells started in the early *80s* **[1-3].** A number of simulation packages such as *AMPS-1D*, *SCAPS-1D*, *PC-1D*, SimWindows, *ADEPT-F*, *AFORS-HET*, *ASPIN*, and *ASA* have been developed. These software programs have been written with a specific reason of modelling solar cells. They have different possibilities and limitations, but the basic principles are the same. A review of different simulation methods and their advantages and disadvantages is given in Ref. **[4].** In this work, we use the *SCAPS* simulator for our calculations.

SCAPS (a Solar Cell Capacitance Simulator) is a one dimensional solar cell simulation programme developed at the Department of Electronics and Information Systems (*ELIS*) of the University of Gent, Belgium **[5-6].** Several researchers have contributed to its development: Alex Niemegeers, Marc Burgelman, Koen Decock, Stefaan Degrave, and Johan Verschraegen. This programme is developed for cell structures of the CuInSe2 and the CdTe family. Recent developments make the programme now also applicable to crystalline solar cells (Si and GaAs family) and amorphous cells (a-Si and micromorphous Si).

Entering a new problem into **SCAPS** is directly forward (see **Figure III-1**). Up to seven layers can be added to the device and for each layer or contact all physical and electronic properties can be shown and changed inside a separate window.

SCAPS-1D runs on a personal computer (*PC*) under Microsoft Windows. The minimum system requirements are: *PC* at least *25 MHz 80386* (*33 MHz 80486* recommended minimum); Operating systems Windows *3.1*, Windows *3.11* or Windows *95* or higher; *VGA*

resolution video adapter or higher; Math coprocessor; *4 MB* of memory; free hard disk space equal to *2 MB*, plus the size of the installed files needed (about *2.5 MB*). A mouse is essential for convenient navigation through the program.

For our simulations, we used the *SCAPS-1D*, version *2802*, which was the latest version available at the time. In the last two version of this software (*SCAPE 2.7 and 2.8*) M. Burgelman et al introduced the impurity photovoltaic effect (IPV) and gradual solar cell. Among the advantages of this calculator is easy to interact with the simulator through numerous dialog boxes that appear during the use of *SCAPS* and the opportunity to study the influence of one or more than one parameter on solar cell performances, we only take profit of the batch option in *SCAPS*. We can vary until *9* parameters at once.

SCAPS program consists of several panels (or windows, or pages). The main panel is the "action panel". It allows setting the problem, to set the action list of required calculations, to execute the calculations, to navigate to other panels, to save and plot results, and to quit the program. In general, the following items(as described in Scaps Manuel) are available on the action panel (see **Figure III-1**):

- The definition of the working point.
- The definition of the action list.
- Setting the calculation mode: "**pause"** between calculations or not
- Setting the problem definition: button **"calculate new"**
- Carrying out calculations according to a new action list: button **"calculate next"** **"continue"** to calculate next item from action list, when **"pause"** is enabled
- **"stop"** to halt a calculation being carried out
- **"clear previous"** to clear previously calculated graphs
- **"graphs"** to activate the energy bands panel, from which in turn one can navigate to all other graphical panels (*IV*, *CV*, *Cf* and *QE*)
- **"save all"** to save the results of all calculations yet preformed in a text file; the data in the text file are separated by tabs, and can be cut and pasted in a spread sheet or graphical program
- **"Quit"** to quit from **SCAPS-1D**. This is the only correct way to leave **SCAPS**.

III.2.1.1 Define the working point

The working point specifies the parameters which are not varied in a measurement simulation, and which are relevant to that measurement. Thus:

- The temperature *T*: relevant for all measurements. Note: in *SCAPS*, only $N_C(T)$, $N_V(T)$ and the thermal voltage *kT* are the only variables which have an explicit temperature dependence;
- The voltage *V*: is discarded in *I-V* and *C-V* simulation. It is the dc-bias voltage in *C-f* simulation and in QE (λ) simulation. *SCAPS* always starts at 0 V, and proceeds at the working point voltage in a number of steps that we also should specify.
- The frequency *f*: is discarded in *I-V, QE* (λ) and *C-f* simulation. It is the frequency at which the *C-V* measurement is simulated.
- The illumination: is used for all measurements. For the *QE* (λ) measurement, it determines the bias light conditions. The basis settings are: dark or light, choice of the illuminated side, choice of the spectrum. A one sun *(= 1000 W/m2)* illumination with the 'air mass1.5, global' spectrum is the default, but we have a large choice of monochromatic light and spectra for our specialised simulations.

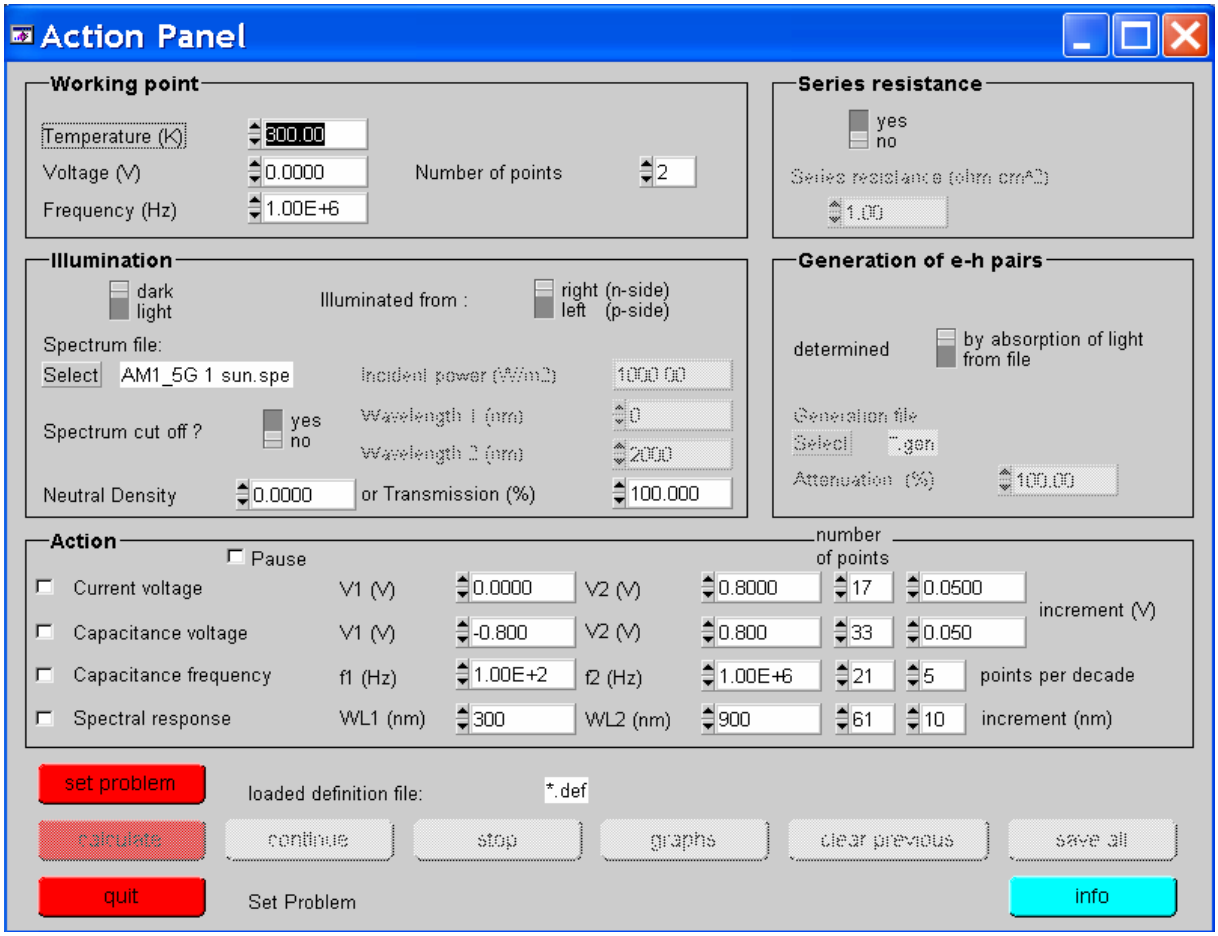

Figure III-1 Action panel window.

III.2.1.2 Select the Measurement(s) To Simulate

In the action-part of the Action Panel, we can select one or more of the following measurements to simulate: *I-V*, *C-V*, *C-f* and *QE* (λ). We can Adjust (if necessary) the start and end values of the argument, and the number of steps. Initially, we can do one simulation at a time, and use rather coarse steps: our computer and/or the *SCAPS* programme might be less fast than we hope, or our problem could be really tough.

III.2.1.3 Define the problem

To define the problem, thus the geometry, the materials and all properties of the solar cell, we click on "set problem" button. We find Solar Cell Definition Panel (figure III-2). In this window, we can define structures consisting of up to 9 layers. The first layer is the back contact; the last one is the front contact. The user can specify the properties of the intermediate semiconductor layers (max. 7). For each layer, up to three different SRH recombination centers (discrete or distributed in energy) can be defined, and for each interface up to three different interface recombination centers (discrete or distributed in energy).
Except for front and back contact, each layer contains the following semiconductor properties:

- Thickness (μm).
- Band gap (eV)
- Electron affinity (eV)
- Dielectric permittivity (relative)
- Conduction band effective density of states ($1/cm^3$)
- Valence band effective density of states ($1/cm^3$)
- Electron thermal velocity (cm/s)
- Hole thermal velocity (cm/s)
- Donor shallow density (N_D)
- Acceptor shallow density (N_A)

The optical absorption of the semiconductor layers can be taken from a user file. Examples of such user files are distributed with the program: *CdS.abs*, *CdTe.abs*, and *ZnO.abs*…..etc. we can add other absorption files for other relevant thin film materials. The SCAPS also proposes two constant values (A and B) for the absorption coefficient.

Front and Back Contact: The identification of each contact is made as follows:

- Electron and hole surface recombination velocities.
- Information about the metal work function.

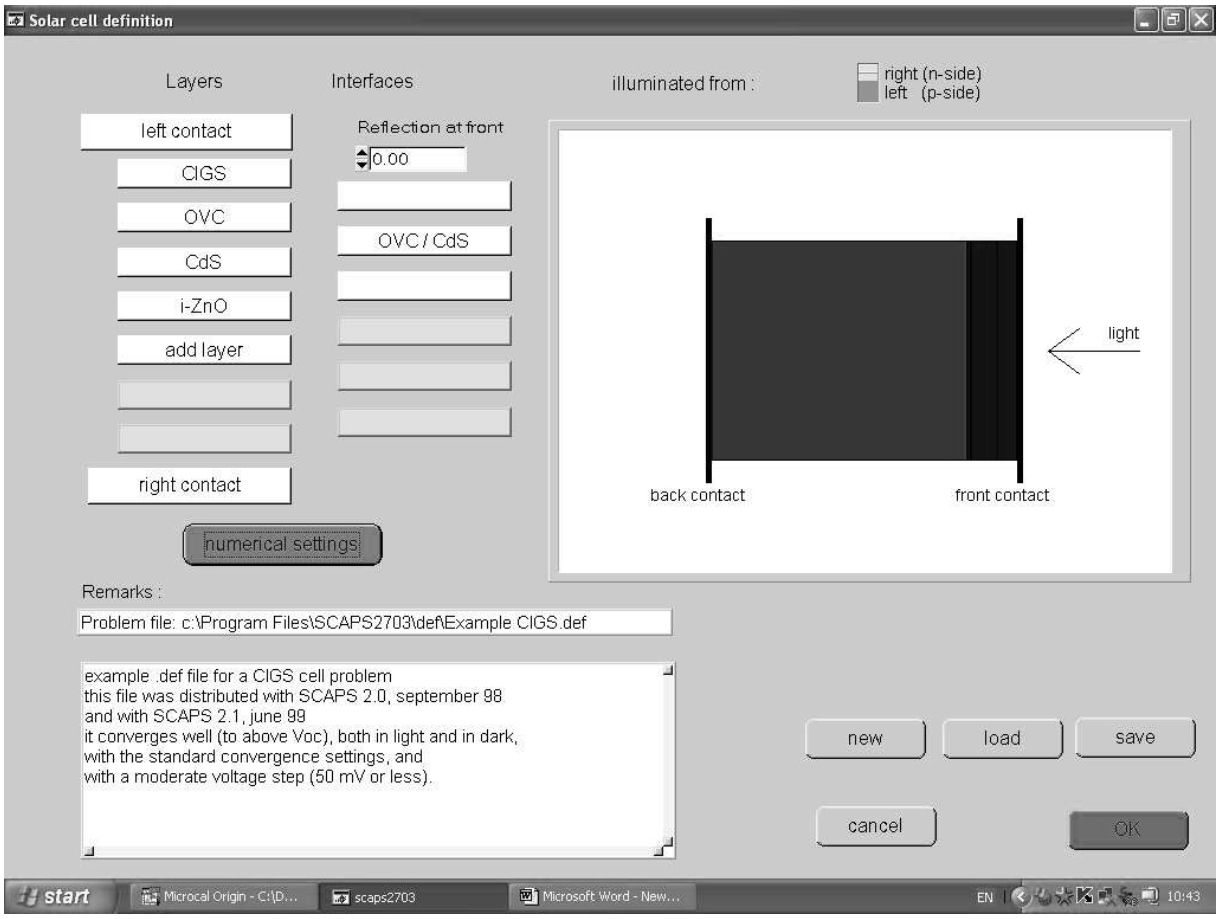

Figure III-2. Solar Cell Definition Panel: Window in SCAPS-1D for imputing all layers and interface parameters

III.2.2 General Remark on Defects and Recombination:

In a diode, current is converted from hole current at the p-contact to electron current at the n contact. This means that somewhere in the diode recombination must take place, even in the most ideal device. So the user must specify recombination somewhere, at least at one place (in a layer or at an interface).

Defects are the most important parameters for our study. In this software, defects are identified by the following parameters (see table I and II):

1. Position of Energy level in the gap.

2. Defect type (ie acceptor, donor or neutral).
3. Electron thermal capture cross section.
4. Hole thermal capture cross section.
5. Energetic distribution (single, uniform, cb tail….)
6. Reference for defect energy level (above *Ev* or bellow *Ec*).
7. Electron optical capture cross section.
8. Hole optical capture cross section.
9. Impurity defect concentration.

Name	Description	Value	Default	Units
Type	type of the defect	**donor** **acceptor** **neutral**	**neutral**	
Sigma_n	capture cross section for electrons	numeric	1.0E-15	cm^2
Sigma_p	capture cross section for holes	numeric	1.0E-15	cm^2
Energydistribution	type of the defect distribution	**single** **uniform** **cb tail** **vb tail** **gauss**	**single**	
Et	energy of the trap level with respect to the valence band	numeric	0.5	eV
Ekar	Characteristic energy	numeric	0	eV
Profile	spatial variation of defect density	**constant** **linear** **exponential**	**constant**	
Lkar	characteristic length	numeric	0.1	µm
Nleft	max. defect concentration to the left of the layer	numeric	1.0E+14	$/cm^3$ or $/cm^3.eV$

Table I Defects and Recombination Parameters

Energy Distribution	**single**	**Uniform**	**Valenceband** Tail	**Conductionband** tail	**Gauss**
Et	energy level	mean energy of the distribution	bottom of the tail (see energy axis)	top of the tail (see energy axis)	mean energy of the distribution
Ekar	no meaning	total width of the distribution	characteristic energy (see energy axis)	characteristic energy (see energy axis)	width of the distribution (see energy axis)
Nleft, Nright	density in /cm^3	constant density of the distribution in /cm^{3}eV	density of the distribution at E=**Et** in /cm^{3}eV	density of the distribution at E=**Et** in /cm^{3}eV	density of the distribution at E=**Et** in /cm^{3}eV

Table II Different Meanings of Some Parameters Concerning the Nature of Energy Distribution.

The optical capture cross sections for electrons and holes are either taken from a file or calculated analytically according to a model by Lucovsky **[7],** this model needs the input of the four parameters: refractive index n of the semiconductor, the effective mass m_n^* and m_p^* of the carriers, and the effective field ratio E_{eff}/E_0 which represents the ratio between the electric field at the impurity and the electric field of the incident wave **[7]**

To our information, *SCAPS* is the only solar cell simulator available that treats the *IPV* effect. This program has some limitations: we can input only three recombination mechanisms. One mechanism is needed to adjust the recombination and the open-circuit voltage to a realistic value and therefore only two *IPV* levels are available (Ref.49 chap.II)

III.2.3 Calculate and Display the simulated curves:

After introducing all the necessary data (layer properties, configuration of the solar cell), we Click the button "calculate" in the action panel. The Energy Bands Panel opens, and the calculations start. After calculation, *SCAPS* switches to the Energy band panel. In this window we can obtain our desired curves. We select for example the IV button in the energy band panel window we can obtain the *IV* curve (see **Figure III-3**). We do the same for quantum efficiency curve.

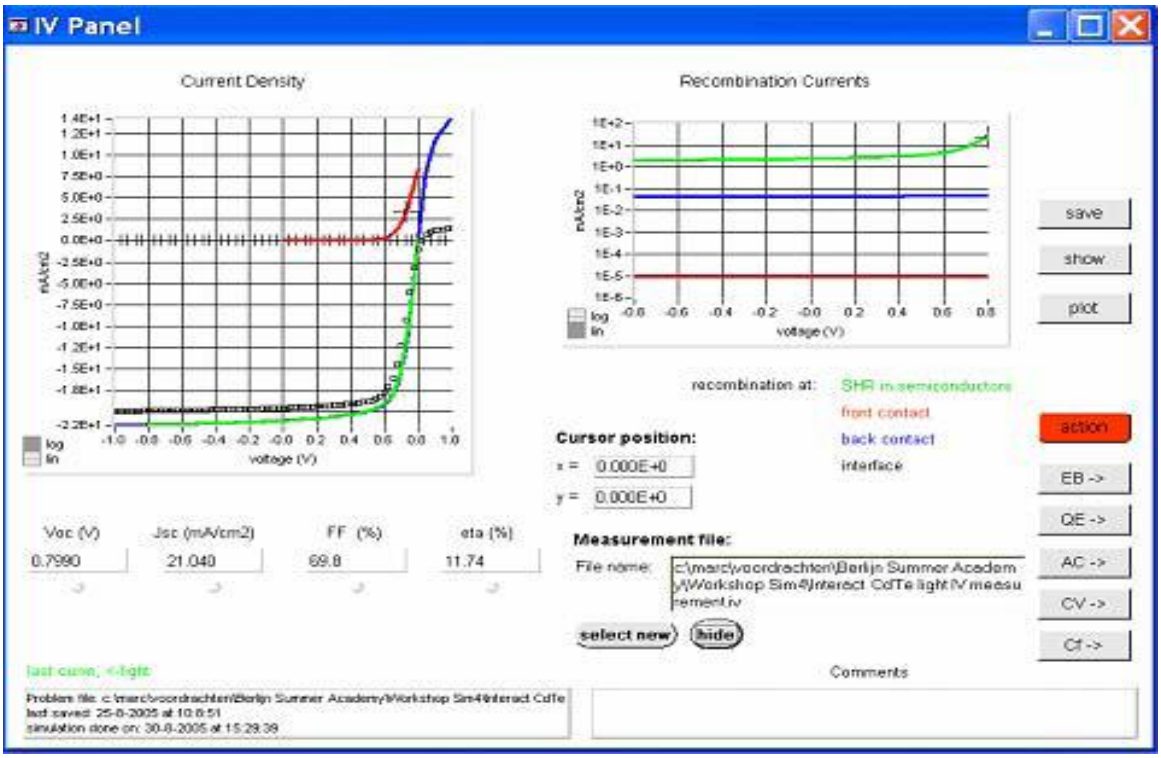

Figure III-3 *I-V* curve obtained using *SCAPS* simulator.

III.3 Part II: results and discussion

III.3.1 Introduction

As mentioned in chapter two, the impurity photovoltaic effect *(IPV)* is one of the third generation solar cells concepts. It aims to tackle the below band gap loss mechanism in the solar cell. The *IPV* effect is the idea of exploiting two step generations by means of impurity states in the forbidden band to exploit sub gap photons and, therefore improve solar cell performances. Indium is the most studied as an optically active impurity in silicon solar cells. The challenge of many researchers is to find a new appropriate impurity which helps them to enhance cell efficiency through *IPV* effect. In this thesis we choose sulphur as new IPV impurity and crystalline silicon as host material. This part presents and discusses our results obtained using the *Scaps 1D* program to calculate silicon solar cell performances. It presents also the goal of our study, solar cell structure, Lucovsky model and some physical parameters concerning the sulphur impurity and the host material used in this work.

III.3.2 Aim of the study

Silicon doped with Indium as an optically active impurity has been widely studied in the last few years but several attempts of researchers to develop more efficient solar cells based on the impurity photovoltaic effect have not yet been realised conclusively. The most important causes as mentioned in chapter two are the very strict requirements imposed on the impurity atoms and on the semiconductor host material. Therefore, their goal is to find an appropriate host material, suitable structure and impurities.

The purpose of this work is to study the *IPV* effect in crystalline silicon doped with sulphur as new IPV impurity. Wu et al **[8]** showed that the incorporation of structural defects and sulphur impurities into silicon lattice by surface microstructuring, most likely producing bands of impurity states in the band gap that can enhance photocarrier production in microstructured silicon at infrared wavelengths near and below the band gap. They concluded that the infrared absorptance of microstructured silicon most likely comes from the incorporation of sulphur into silicon lattice.

Keever et al **[9]** also showed experimentally that the infrared photoresponse of silicon solar cells can be improved by doping with optically active elements like Er, Ge, Si and S…etc. The subgap response of sulphur, silicon and germanium is enhanced but this enhancement is low compared with other elements like rare earth.

Kasai et al **[10]** studied theoretically the *IPV* effect in crystalline silicon. They found that there are strict energy ranges in the band gap of semiconductor where trap level could contribute to improve cell efficiency. Sulphur is an optically active impurity **[11]** which is known to introduce three donor levels into the forbidden band of silicon at 0.18, 0.37 and 0.52 eV below the conduction band **[12].** The solubility of sulphur in silicon is about 2.5×10^{17} cm^{-3} **[13]**. This work investigates numerically which of these three energy levels is responsible for the appearance of the *IPV* effect and proceeds to study the influence of the optical confinement on the performances of silicon solar cell based on *IPV* effect.

III.3.3 Silicon solar cell structure and physical parameters used in the simulation

The solar cell structure used to calculate solar cell performances, assumed as n^{+}-p-p^{+} junction(**Figure III-3**), consists of a thin n emitter ($0.3\mu m$) doped at 10^{18} cm^{-3}, a P base

region with thickness of $50\ \mu m$ and P^+ layer with thickness of 1 µm serving as back surface field (*BSF*). The doping of *P* and P^+ layers is fixed at $10^{17}\ cm^{-3}$ and $10^{18}\ cm^{-3}$ respectively.
The sulphur impurities were introduced into the base region. The front and rear surface recombination velocities are set to be $S_n = S_p = 10^4$ cm/s. Following Ref. **[14]** we considered the value $\sigma_n = 2\times10^{-13}\ cm^2$ for the electron capture cross section of sulphur in silicon. Unfortunately, we have found no experimental value for the hole capture cross section of sulphur in silicon (σ_p). In our simulation we assume $\sigma_p = 10^{-22}\ cm^2$.

SCAPS simulator developed at Elis, University of Gent **[6]** is used to calculate PV parameters under standard illumination (*AM1.5G, 100mW/cm², 300K*). The Lucovsky model was used to calculate the optical capture cross section of the impurities **[7].**
For our simulation, the main parameters characterizing silicon are summarized in **Table II**.

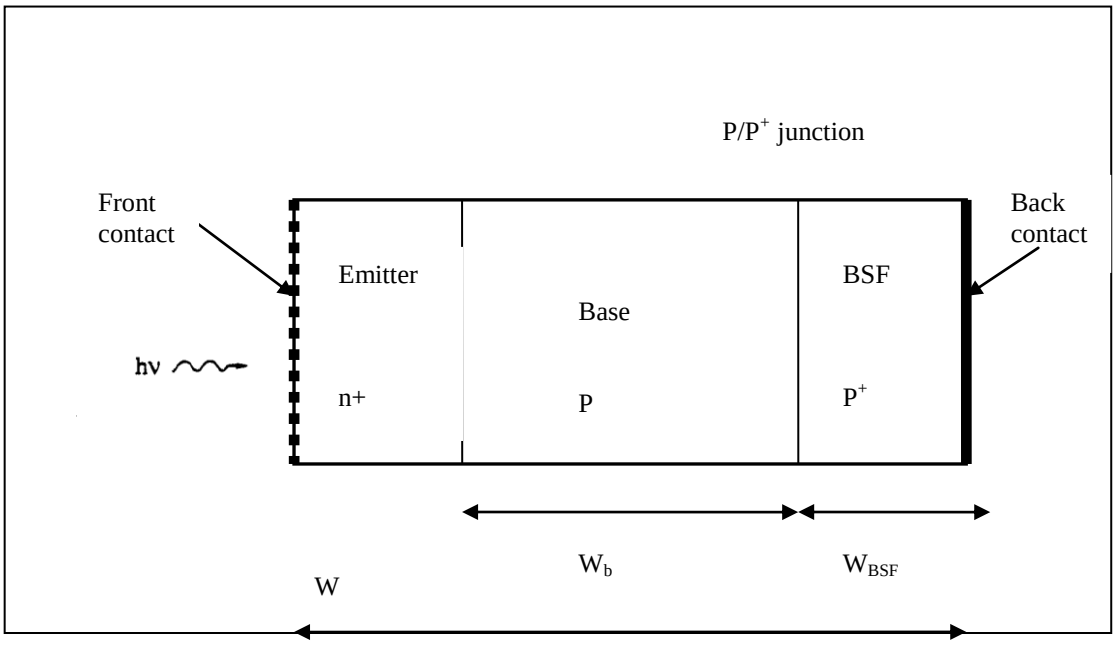

Figure III-3: P-type solar cell structure used in this study.

Property	Value
Band gap (eV)	**1.12**
Dielectric permittivity	**11.9**
Electron mobility (cm^2/Vs)	**1350**
Hole mobility (cm^2/Vs)	**480**
Conduction band effective density of states (cm^{-3})	**2.8×10^{19}**
Valence band effective density of states (cm^{-3})	**2.65×10^{19}**
Electron thermal velocity (cm/s)	**10^7**
Hole thermal velocity (cm/s)	**10^7**
Refractive index	**3.42**
Electron affinity (eV)	**4.05**
Effective mass of electron	**1.08**
Effective mass of hole	**0.55**

Table III. Main parameters used for the silicon solar cell **[15-16].**

III.3.4 Results and Discussion

The most important factor to realize *IPV* effect is the location of the energy levels of deep defects. Figure **III-4** shows the variation of the conversion efficiency as a function of the donor energy level of the impurity E_c-E_t. The impurity concentration is $3\times10^{16}\ cm^{-3}$. In this simulation, both front and back reflectances are taken close to unity. From this figure it is observed that the energy range where the *IPV* effect is able to contribute to an improvement of the best conversion efficiency of silicon solar cells is between 0.1 to 0.28 eV from the conduction band edge. Maximal conversion efficiency is found for an impurity energy level located at 0.28 eV below the conduction band. In the following, the base layer of our structure is incorporated by the Sulphur donor levels into the forbidden band, with their three impurity energy levels. Figure **(III-5)** shows that for the impurity level located at 0.18 eV below the conduction band, the short circuit current density J_{sc} (Figure **III-5(a))** and conversion efficiency η (Figure **III-5(b))** increase with increasing impurity concentration up to the value $N_t \approx N_a$ this due to the fact that sulphur level is fully empted, so sub bandgap photons can be absorbed by hole photoemission process from the valence band to the sulphur level. When Nt>Na the short circuit current and the efficiency decrease. The overcompensation of the sulphur impurity for the base doping makes electron photoemission from sulphur level to the

conduction band maximized. This reduces the photon flux available for the hole photoemission process from the valence band to the sulphur level and results in the decrease of the Jsc. We can conclude that for this sulphur level, the efficiency increases only when impurity concentration is low.

In practice, the maximum impurity concentration that can be introduced in silicon is fixed by the solid solubility of each doping species in this material. For this reason, to obtain an important *IPV* effect, the impurity concentration must not exceed maximum sulphur solubility in silicon. Another reason which makes the larger impurity concentration not usable is when the principle of *SRH* used here becomes no more valid due to the onset of degeneration and other heavy doping effects. Finally, when N_t exceeds the shallow doping concentration, the semiconductor is compensated and becomes *N* type.

In Figure **III-6**, we plot the open circuit voltage V_{oc} as a function of the impurity concentration N_t. For the energy level located at 0.18 eV below the conduction band, it is seen from this figure that V_{oc} decreases for larger values of sulphur concentration and remains constant when N_t is below the acceptor doping concentration. This effect is due to the particular choice of the structure *n+–p–p+*. This structure has an advantage to keep a high value for the built-in voltage and therefore, the open-circuit voltage is safeguarded. Concerning the impurity level located at 0.37 eV below the conduction band, the short circuit current density increases with impurity concentration and decreases when this parameter approaches the shallow acceptor concentration (Figure **III-7(a)).** The efficiency increases slightly with increasing *Nt* up to Nt $=2\times10^{16}$ cm^{-3}. Above this value the efficiency (Figure **III-7(b)**) and the open circuit voltage (Figure **III-6**) decrease with increasing Nt. This degradation is due to the increase of recombination in the solar cell.

For the last level, i.e. 0.52 eV below the conduction band, we observe a severe degradation of all photovoltaic parameters (see Figure **III-8(a),** (**III-8(b))** and (**III-6)),** this is due to the increase of the electron-hole recombination through the defects. The same result is observed in **[10]** where they showed that when E_t is located near the middle of the band gap, the impurity-traps act as recombination centers and therefore work only to degrade cell efficiency.

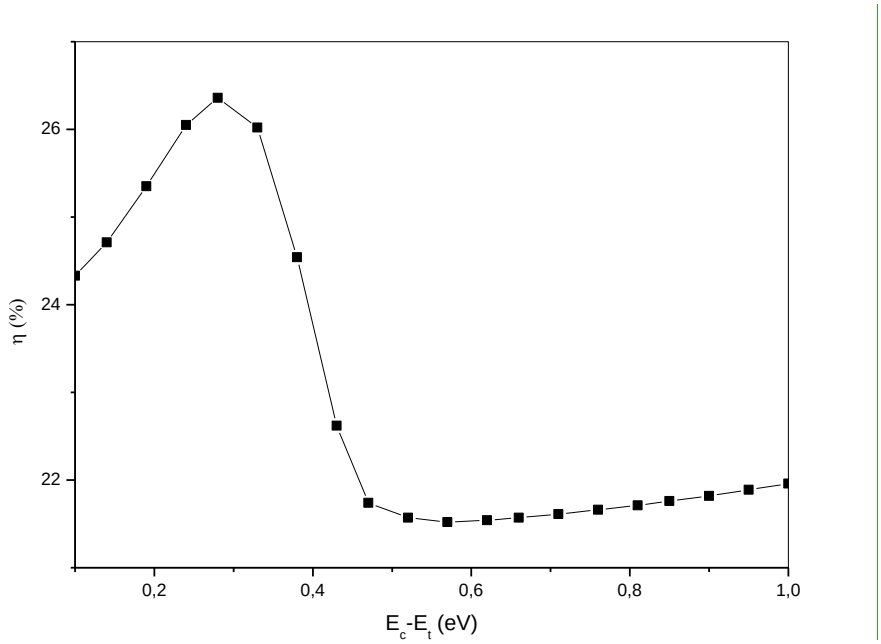

Figure III-4. Conversion efficiency for n+-p-p+ silicon solar cell as a function of energy level of Impurity E_c-E_t. (Base doping $N_a = 10^{17}$ cm^{-3}, base thickness 50 μm, density of optically active Sulphur impurities $N_t = 3\times10^{16}$cm^{-3}. Standard conditions: AM1.5G, 100 mW/cm^2, 300K).

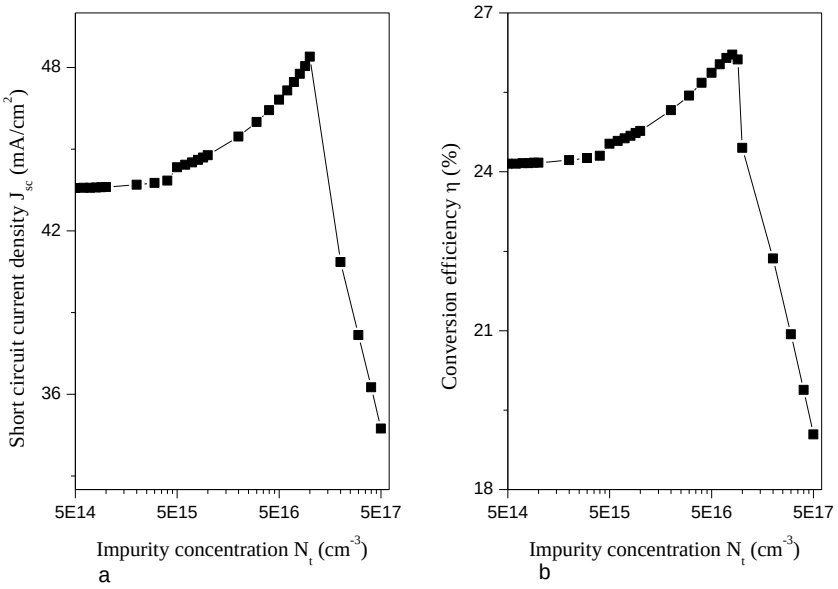

Figure III-5. Dependence of a) Short circuit current density J_{sc}, b) conversion efficiency η on concentration of the sulphur impurities in silicon solar cell for the energy level located at 0.18 eV below the conduction band. The internal reflections are set to $R_f = R_b = 0.999$.

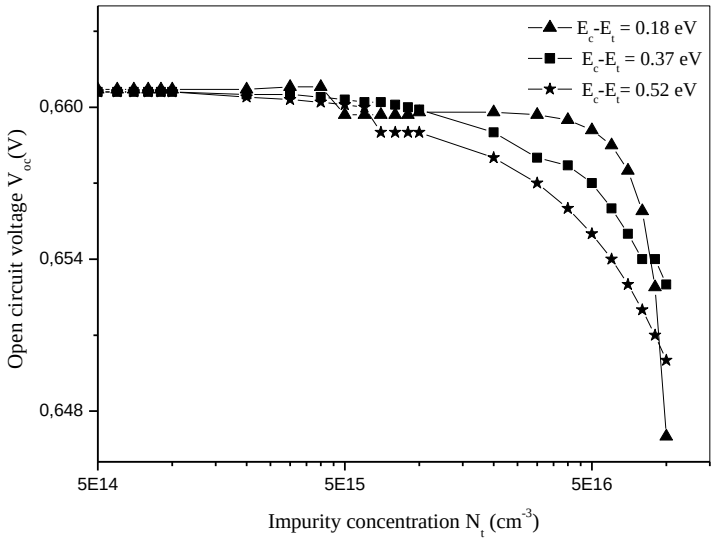

Figure III-6. Open circuit voltage V_{oc} as a function of impurity concentration N_t for the three sulphur energy levels.

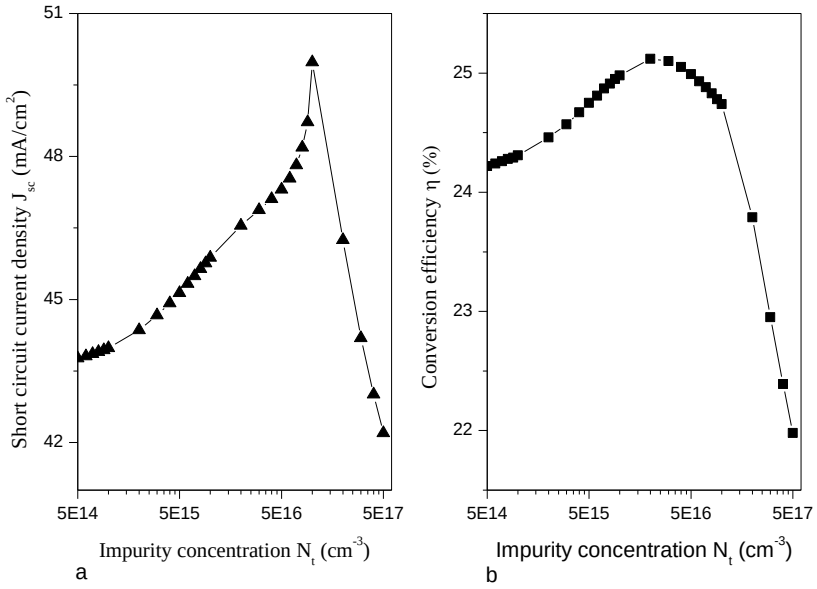

Figure III-7. Dependence of a) Short circuit current density J_{sc}, b) conversion efficiency η on concentration of the sulphur impurities in silicon solar cell for the energy level E_c-E_t = 0.37 eV. The internal reflections are set to $R_f = R_b$ =0.999.

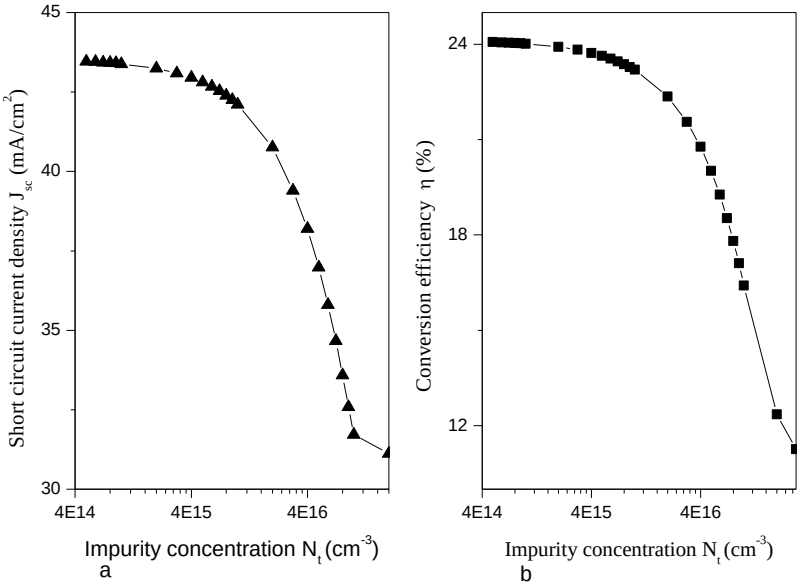

Figure III-8. Dependence of a) Short circuit current density J_{sc}, b) conversion efficiency η on sulphur impurity concentration in silicon solar cell for the energy level located at 0.52 eV below the conduction band. ($R_f = R_b = 0.999$).

The spectral response of a solar cell permits an examination of how photons of different wavelengths contribute to the short circuit current. The value of quantum efficiency of the simulated cell as a function of spectral wavelengths, for different values of sulphur concentration, is shown in **Figure III-9**.

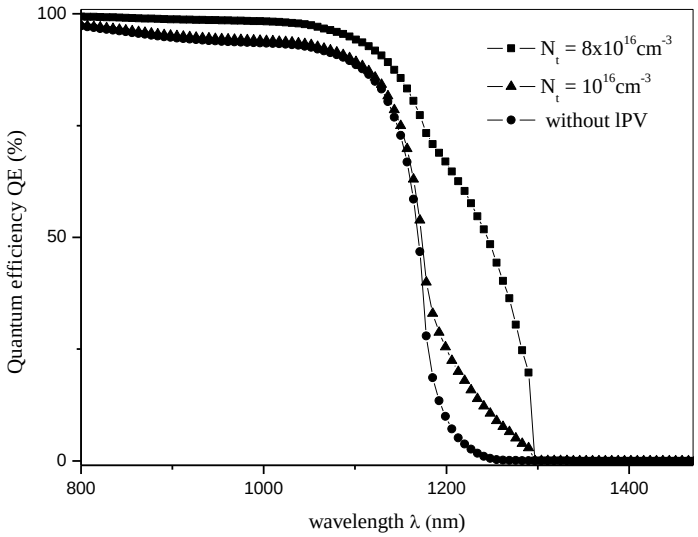

Figure III-9. Quantum efficiency *QE* of silicon solar cell with and without IPV effect for E_c-E_t = 0.18 eV. The internal reflections are $R_f = R_b = 0.999$.

It is observed that an extension of the infrared response is between 800 to about 1300 nm. This extension is due to an enhancement of a subband gap mechanism by sulphur doping.

In order to check the effectiveness of the optical confinement on our silicon solar cell parameters; in this last part, the focus is on what influence light trapping has on the solar cell performances. As mentioned above, the principle of the *IPV* effect is based on the inclusion of deep defects in the solar cell. These defects provide a multistep absorption mechanism for sub band gap photons to create electron-hole pairs. Thick silicon layer does not absorb efficiently the infrared light in one pass through the layer. This effect becomes more important as layers become thinner. This means that the sub band gap process is rather weak in silicon. However, silicon has a large refractive index around 3.42 **[16].** This high index enables the use of total internal reflection as a powerful way to let light realise multiple passes through the layer, enhancing the path length of rays and therefore increase the probability that an infrared photon is absorbed. This means, the best light trapping is required for enhance the potential of the *IPV* effect. In the *SCAPS* simulator, the internal reflection coefficients at the front and back of the solar cell (R_f and R_b) are used to characterise light trapping. The extreme values $R_f = R_b = 0$, representing the case of no optical confinement, and $R_f = R_b = 1$ representing the case of ideal optical confinement. For the study of the effect of light trapping on our solar cell performances, the back and front reflectance values are varied. In table III, it is found that a maximum efficiency of 27.45% is obtained for the perfect values $R_f = R_b = 0.9999$. For more realistic values of R_f and R_b ($R_f = 0.93$, $R_b = 0.97$), a maximum efficiency of only 22.66% is found. It can be concluded that to realize the benefit of the IPV effect, the silicon solar cell requires a good optical confinement.

R_f	R_b	V_{oc}(V)	J_{sc}(mA/cm^2)	η(%)
0.9999	*0.9999*	*0.662*	*49.45*	*27.45*
0.98	*0.98*	*0.658*	*42.59*	*23.57*
0.97	*0.97*	*0.658*	*41.97*	*23.18*
0.93	*0.97*	*0.657*	*41.09*	*22.66*

Table IV. Open-circuit voltages short-circuit current densities and energy conversion efficiencies for our silicon solar cells, as function of the back and front reflectances R_f and R_b. The S impurity concentration is $N_t = 8\times10^{16}$cm^{-3} and E_c-E_t = 0.18 eV.

III.4 Conclusion

In our study we used the Scaps 1D simulator. We present in part one of this chapter, the principal operations and the main panels which can help us to understand and use this simulator. In part two of this chapter, the influences of the defect parameters and light trapping on the sulphur doped silicon solar cell performances were investigated using *SCAPS* simulator. The results show that the *PV* parameters of solar cell are drastically reduced when E_t is located near the middle of the band gap. We found also that the incorporation of sulphur impurity in the base layer does increase the short circuit current density and efficiency when the carrier concentration is low, especially for sulphur impurity located at 0.18 eV below the conduction band. The *IPV* effect gives an extension of the infrared response of the solar cell between 800 to about 1300 nm due to the enhancement of the sub-band gap absorption mechanism. A good light trapping is very important to obtain a high solar cell performances based on the *IPV* effect.

REFERENCES

[1] H. Okamoto H. kida, S. Nonomura and Y.Hamakawa, *Solar Cells* **8**, 1983, pp. 317

[2] R. S. Crandall, *J. Appl. Phys.* **54**, 1983, pp. 7176

[3] P. Sichanugrist, M. Konagai, and K. Takahashi, *J. Appl. Phys*. **55**, 1984, pp. 1155

[4] M. Burgelman, J. Verschraegen, S. Degrave and P. Nollet, Modelling thin film PV devices Prog Photovoltaics **12**, 143 (2004).

[5] A. Niemegeers and M. Burgelman, in Proc. 25nd IEEE Photovoltaic Spec.Conf.,(1996) pp. 901

[6] M. Burgelman, P. Nollet and S. Degrave, *Thin Solid Films* **361**, 527 (2000).

[7] G. Lucovsky 1965 Solid State Commun. **3** 299

[8] C. Wu, C. H. Crouch, L. Zhao , and J E Carey 2001 Appl. Phys. Lett. **78** 1850-1852

[9] M J. Keevers, F. W. Saris, G. C. Zhang, J Zhao and M. A. Green , 13th Eur. Photovoltaic Sol. Energy Conf. 1995 Nice, France 1215

[10] H. Kasai and H. Matsumura, 1997 Sol. Energy Mater. Sol. Cells **48** 93-100.

[11] G. Davies 1983, *phys. rep*. **176** 83

[12] E. Schibli and A. G. Milnes, 1967 Review Paper

[13] C. Holm 1981 Doctoral Thesis, University München

[14] P. Migliorato, C. T. Elliott 1978 Solid-State Electronics 21 443-447.

[15] M. Burgelman, P. Nollet and S. Degrave 2000 Thin Solid Film **527** 361–362

[16] S. M. Sze and K. Ng. Kwok 2007 Physics of Semiconductor Devices, Wiley and Son, third edition.

[17] P. Wurfel 2005 Physics of Solar Cells From Principles to New Concepts, Wiley- VcH Velag GmbH & Co. KGaA

GENERAL CONCLUSION

The objective of the present work was to study the performances of silicon solar cells using the impurity photovoltaic effect. The idea of this concept is to introduce one or more impurity levels within the band gap of the host material. These impurities can help the solar cell to absorb sub-band gap photons, by this means increasing the short-circuit current (Jsc) and therefore increasing the conversion efficiency. In this work, we presented a numerical study of the IPV effect in sulphur-doped crystalline silicon solar cells with SCAPS simulator. We used for our calculation the Shockley Read Hall recombination model modified by M A Green and the Lucovsky model to obtain the values of the optical capture cross section of electrons and holes.

Sulphur is an optically active impurity, which is known to introduce three donor levels into the forbidden band of silicon at 0.18, 0.37 and 0.52 eV below the conduction band. Many attempts of researchers to develop more efficient solar cells using the IPVeffect have not yet been successful. The main reason is the very strict requirements imposed either on the impurity atoms or on semiconductor host material. The position of the impurity in the gap of the host material (silicon in our case) is an important factor in order to increase the conversion efficiency of a solar cell via the IPV. The purpose of this work was to establish what sulphur levels in silicon are responsible for the appearance of the IPV effect and investigate the conditions of its observation on our n+pp+ solar cell structure.

Simulation results for IPV effect on silicon doped with sulphur show an improvement of the short circuit current and the efficiency for sulphur energy levels located far from the middle of the band gap especially at Ec–Et=0.18 eV and the effect of IPV increases with increasing the sulphur concentration, when this concentration is less than the base doping density. For the level located in the middle of the band gap i.e. at 0.52 eV below the conduction band, we observed a severe degradation of all photovoltaic parameters due to an increase in the electron-hole recombination through the defects.

In this work, It is observed that an extension of the infrared response is between 800 and 1300 nm. This extension is due to an enhancement of a sub-band gap mechanism by sulphur doping. We confirmed the importance of optical confinement on the solar cells

performances. The perfect light trapping can maximize the optical path and increase optical absorption (infrared absorption). It is found that a maximum efficiency of 27.45% is obtained for the perfect values Rf=Rb=0.9999. For more realistic values of Rf and Rb , a maximum efficiency of only 22.66% is found. It can be concluded that to realize the benefit of the IPV effect, the silicon solar cell requires a good optical confinement.

ملخص

درسنا في هذه الأطروحة مميزات الخلايا الشمسية المعتمدة على السيلكو ن . لزيادة فعالية هذه الخلايا درسنا احد مفاهيم الجيل الثالث للخلايا الشمسية والمسمى فعل الشوائب الفوتوجهدية. قمنا بإدخال الكبريت كشائبة جديدة في قاعدة الخلية. استعملنا لحساب المميزات البرنامج" سكابس" قمنا بتغيير تركيز الكبريت ووضع الشائبة في النطاق الممنوع وكذا محاصرة الضوء لزيادة امتصاص الضوء في المجال تحت الأحمر. النتائج المتحصل عليها تبين تحسن في فعالية الخلايا المدروسة وخاصة بالنسبة للشائبة الموجودة في المستوي 0.18الكترون فولت تحت مستوى عصابة التوصيل عند التركيز الضعيف ومحاصرة الضوء المثالية

الكلمات المفاتيح

فعل الشوائب الفوتوجهدية ، مميزات الخلايا الشمسية المعتمدة على السيلكون، البرنامج سكابس

Resumé

Nous avons étudié dans cette thèse les caractéristiques des cellules solaires à base de de silicium. Pour améliorer le rendement des cellules photovoltaïques, nous avons étudié un concept de la troisième génération des cellules solaires nommé '' impurity photovoltaic effect''. Nous avons introduit le soufre comme une nouvelle impureté dans la base du composant afin d'augmenter le courant de court circuit et par conséquent le rendement de conversion. Nous avons utilisé pour le calcul de ses caractéristiques le simulateur Scaps. La structure utilisée dans cette étude est la structure n+pp+. Nous avons varié quelques paramètres comme la concentration de ces impuretés et la position des niveaux énergétiques dans le gap. Nous avons varié aussi les coefficients de réflexion interne pour augmenter l'absorption de la lumière dans la région IR. L'incorporation du soufre comme IPV impureté dans le gap fait augmenter le photocourant et le rendement de conversion des cellules étudiées, particulièrement pour le niveau énergétique Ec-Et=0.18eV et pour un piégeage idéal et une faible concentration du soufre.

Mots clés :

Effet des impuretés photovoltaïques ; performances des cellules solaires au silicium ; simulateur SCAPS.

Summary

In this thesis we study one of the third generation solar cells called impurity photovoltaic effect in order to improve silicon solar cells performances .We investigate numerically the potential of the IPV effect in silicon solar cell doped with sulphur as novel IPV impurity. We study the influence of light trapping and certain impurity parameters like impurity concentration and position in the gap on the silicon solar cell performances. (Short circuit current density *Jsc*, open circuit voltage *Voc*, conversion efficiency η and quantum efficiency *QE*). The results show that the *PV* parameters of silicon solar cells are drastically reduced when E_t is located near the middle of the band gap. We found also that the incorporation of sulphur impurity in the base layer does increase the short circuit current density and efficiency when the carrier concentration is low, especially for sulphur impurity located at 0.18 eV below the conduction band. The *IPV* effect gives an extension of the infrared response of the solar cell between 800 to about 1300 nm due to the enhancement of the sub-band gap absorption mechanism. A good light trapping is very important to obtain a high solar cell performances based on the *IPV* effect.

Keywords

Impurity photovoltaic effect, silicon solar cells performances, SCAPS Simulator.